VOLUME 49, NUMBER 2, JUNE 2026

HADRONIC JOURNAL

HADRONIC JOURNAL Volume 49, Number 2, June 2026

Founded in 1978 by Prof. R. M. Santilli at Harvard University. Some of the past Editors include Professors S. L. Adler, A. 0. Barut, L. C. Biedenharn, N. N. Bogoliubov, M. Froissart, J.Lohmus, S. Okubo, Nobel Laureate Ilya Prigogine, M. L. Tomber, J. P.Vigier, J. Wess, Nobel Laureate Chen Ning Yang.

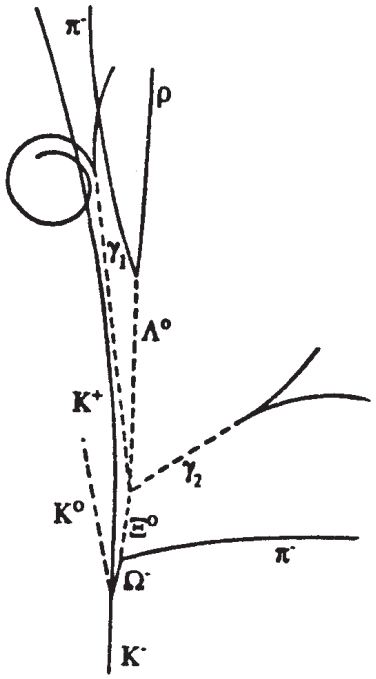

EDITORIAL BOARD

A.O.ANIMALU
A. K. ARINGAZIN
A. A. BHALEKAR
S. J. DHOBLE
J. DUNNING-DAVIES
T. L. GILL
L. P. HORWITZ
S. L. KALLA
S. I. KRUGLOV
J. LISSNER
M. NISHIOKA
R. F. O'CONNELL
Z. OZIEWICZ*
E. RECAMI*
M. SALEEM
S. SILVESTROV
H. M. SRIVASTAVA
E. TRELL
R.I. TSONCHEV
QI-REN ZHANG
C.A.WOLF
YI-ZHONG ZHUO

*In memoriam

FOUNDER and Editor In Chief
R. M. SANTILLI

HADRONIC PRESS, INC.

HADRONIC JOURNAL

Established in 1978 by Prof. R. M. Santilli at Harvard University Hadronic Journal and Algebras, Groups and Geometries have been regularly published since 1978 without publication charges and are among the few remaining independent refereed journals.

This Journal publishes advances research papers and Ph. D. theses in any field of mathematics without publication charges.

For subscription, format and any other information please visit the website
http://www.hadronicpress.com

HADRONIC PRESS INC.
35246 U. S. 19 North Suite 215
Palm Harbor, FL 34684, U.S.A.
http://www.hadronicpress.com
Email: info@hadronicpress.com
Phone: +1-727-946-0427

HADRONIC JOURNAL

Founder and Editor in Chief
RUGGERO MARIA SANTILLI
The Institute for Basic Research
35246 U. S. 19 North Suite 215, Palm Harbor, FL 34684, U.S.A.
Email: resarch@i-b-r.org; TEL: +1-727-688-3992

A. O. ANIMALU, University of Nigeria, Department of Physics, Nsukka, Nigeria animalu@nmc.edu.ng
A.K. ARINGAZIN, Department of Theoretical Physics, Institute for Basic Research Eurasian National University Astana 010008, Kazakhstan aringazin@mail.kz
A.A. BHALEKAR, Department of Chemistry, R.T.M. Nagpur University, Nagpur, 440033 India anabha@hotmail.com
S.J. DHOBLE, Department of Physics R.T.M. Nagpur University Nagpur, 440033 India sjdhoble@rediffmail.com
J. DUNNING-DAVIES, Department of Physics (Retired) University of Hull Hull, HU6 7RX England j.dunning-davies@hull.ac.uk
T. L. GILL, Howard University Research Center ComSERC Washington, DC 20059, USA tgill@howard.edu
L. P. HORWITZ, Department of Physics Tel Aviv Univ., Ramat Aviv, Israel horwitz@taunivm.tau.ac.il
S.L. KALLA, Department of Mathematics Vyas Institute of Higher Education Jodhpur, 342008, India shyamkalla@gmail.com
S.I. KRUGLOV, University of Toronto at Scarborough, Physical and Environmental Sciences Dept., 1265 Military Trail, Toronto, Ontario, Canada M1C 1A4 skrouglo@utm.utoronto.ca
J. LISSNER, Alumnus Foukzon Laboratory Center for Mathematical Sciences Technion-Israel Institute of Technology Haifa, 3200003, Israel
M. NISHIOKA, Yamaguchi University Department of Physics, Yamaguchi 753, Japan
R. F. O'CONNELL, Louisiana State University Department of Physics, Baton Rouge, LA 70803
Z.OZIEWICZ,* Universidad National Autonoma de Mexico, Faculdad de Estudios Superiores C.P. 54714, Cuautitlan Izcalli Aparto Postal # 25, Mexico **** In memoriam***
E. RECAMI, Universita' de Bergamo, Facolta' di Ingeneria, Viale Marconi 5, 1-24044 Dalmine (BG) Italy **** In memoriam***
M. SALEEM, University of the Punjab Center for High Energy Phys., Lahore, Pakistan dms@lhr.paknet.com.pk
S. SILVESTROV, School of Education, Culture and Communication (UKK) Malardalen University Box 883, 71610 Västerås, Sweden sergei.silvestrov@mdh.se
H. M. SRIVASTAVA, Department of Mathematics and Statistics, University of Victoria, Victoria, B. C. V8W 3P4, Canada, hmsri@uvvm.uvic.ca
E. TRELL, Faculty of Health Sciences, University of Linkoping, Se-581 83, Linkoping, Sweden erik.trell@gmail.com
R.I. TSONCHEV, Facultad de Fisica, Universidad Autonoma de Zacatecas, P. O. C-580, Zacatecas 98068, zac, Mexico rumen@ahobon.reduaz.ms
QI-REN ZHANG, Peking University, Department of Technical Phys., Beijing 100871, China zhangqr@sun.ihep.ac.cn
C.A. WOLF, Department of Physics, Massachusetts College of Liberal Arts, North Adams, Ma 01247 cwolf@mcla.mass.edu
YI-ZHONG ZHUO, Institute of Atomic Energy P.O. Box 275 (18) Beijing 102413, China zhuoyz@mipsa.ciae.ac.cn

HADRONIC JOURNAL

VOLUME 49, NUMBER 2, JUNE 2026

THE SPHERICAL VACUUM: EMERGENT SPACETIME AND THE RESTORATION OF SYMMETRY THROUGH ENTROPIC ASYMMETRY, 121

Tamás Kovács and Tamás Kovács, Jr.
Eotvos Lorand University
Budapest, Hungary

A VARIATIONAL FORMULATION FOR MODELING A COMPRESSIBLE AND TIME-DEPENDENT PROTIUM HYDROGEN FLUID FLOW, 137

Fabio Silva Botelho
Department of Mathematics
Federal University of Santa Catarina – UFSC
Florianópolis, SC, Brazil

HEAVY QUARKS AND HADRONS: MODEL, THEORY AND NEW SU(3) SYMMETRY, 167

Yi-Fang Chang
Department of Physics
Yunnan University
Kunming, 650091, China

THREE-DIMENSIONAL QUANTUM MECHANICS IN THE ENERGY DOMAIN: A TIME FREE TREATMENT OF THE HYDROGEN ATOM, 179

Dr. Michail Lazos
Department of Computing
Manchester Innovation and Technology Center
Dubai, UAE

Semen Ivanov
Imperial College of London

FROM EIGHT-DIMENSIONAL SUPERSYMMETRIC SPACETIME TO NUCLEAR FORCES: A GEOMETRIC DERIVATION OF STRONG INTERACTION PARAMETERS, 197

Zhi Cheng
Guangzhou, China

PROTON-MAGNETIC MONOPOLE BINDING ENERGY USING THE PAULI EQUATION, 213
J. J. Bevelacqua
Bevelacqua Resources
7531 Flint Crossing Circle SE
Owens Cross Roads, AL 35763
ANALYSIS OF A HIGH EFFICIENCY MAGNETIC MOTOR, 231
Patrick Cornille
Retired Physicist from the C.E.A.
7 Rue de la Perdriere
59320 Ennetieres-en-Weppes, France

HADRONIC JOURNAL 49, 121 - 136 (2026)
DOI 10.29083/HJ.49.02.2026/SC121

THE SPHERICAL VACUUM: EMERGENT SPACETIME AND THE RESTORATION OF SYMMETRY THROUGH ENTROPIC ASYMMETRY

Tamás Kovács and Tamás Kovács, Jr.
Eotvos Lorand University
Budapest, Hungary
takovacs@gmail.com

Received April 8, 2026

Abstract

Current cosmological models suffer from a fundamental reliance on Euclidean manifolds that necessitate "dark" corrections and physical singularities. We propose the Spherical Vacuum Model (SVM), a non-Euclidean framework where the universe is a singular, absolute sphere of infinite energetic potential and zero entropy (S=0). In this paradigm, matter is not an additive substance but a localized negative displacement (a "void") within the vacuum plenum, where the vacuum represents a state of infinite energy and zero entropy. We argue that time, space, and gravity are non-fundamental, emergent properties arising from the distortion of spherical geometry. By redefining mass as a negative displacement of the vacuum and entropy as a measure of geometric fragmentation, we provide a framework where the Golden ratio emerges naturally from packing constraints. By addressing the inconsistencies in the Schwarzschild solution identified by Loinger and the alternative plasma-electric architectures of Scott, we provide a unified zero-sum equation for the cosmos. This model reinterprets "black holes" not as singularities, but as phase transitions back into pure vacuum energy at the Planck scale, addressing inconsistencies in the Schwarzschild solution.

Keywords: Spherical Vacuum Model, illusion, geometric fragmentation, negative displacement, symmetry, Golden ratio

Copyright © 2026 by Hadronic Press, Inc., Palm Harbor, FL 34684, USA

1. Introduction

For over a century, theoretical physics has been bifurcated by the "Euclidean construct", the assumption that spacetime is a passive, linear container for events [7]. This assumption forces a mathematical deadlock between general relativity [2] and quantum mechanics. When equations are constrained to a coordinate grid (x,y,x,t), gravity must be treated as a force or a curvature of a fabric.

By treating "flat" or "curved" space as a literal container, we constrain our equations within a secondary coordinate system. We propose a departure toward pure spherical geometry, where the "vacuum" is a perfect, absolute sphere of infinite energetic potential. The universe is modelled as a perfect, absolute sphere of infinite energetic potential. The vacuum state (Ψ_V) defines the ground state of the universe as a non-local potential field ϕ with absolute spherical symmetry:

$$\Psi_V \Rightarrow \nabla\phi = 0 \qquad S = 0 \qquad E = \infty \tag{1}$$

The classical (x, y, z, t) coordinate system is replaced with a unified radial potential system, where every "point" is a vector $\underline{r}$ representing a radial extension from a singular central potential U_0

$$\underline{P}(r,\theta,\phi) = U_o \cdot \underline{r} \tag{2}$$

We posit that this coordinate "fabric" is an illusion. By shifting the foundational basis to pure spherical geometry, we eliminate the need for time and gravity to be independent forces. We propose that the "Universum" is a plenum of perfect symmetry. Reality, as perceived by an observer, is merely the sensory and entropic manifestation of local deviations from this primordial spherical stasis.

2. Results and discussion

2.1 Entropy and time

To address the ambiguity of the term, we define entropy (S) specifically within the context of information theory and geometric distortion. In the classical view,

entropy is linked strictly to heat flow. In general, it is a measure of the disorder, randomness, or uncertainty within a system. The definition shifts and specifies slightly depending on the field: In classical thermodynamics, it is a state function that quantifies the amount of energy in a physical system that cannot be used to do work. According to the second law of thermodynamics, the total entropy of an isolated system can never decrease over time; it can only remain constant or increase. In statistical thermodynamics, it represents the number of specific microscopic configurations (microstates) that correspond to a system's macroscopic state (macrostate). More possible microstates mean higher entropy. Finally, in information theory it measures the average amount of information produced by a stochastic source of data. Essentially, it quantifies the level of "surprise" or uncertainty in a variable; the more unpredictable a message is, the higher its entropy.

In our SVM framework, we adjust its meaning: here entropy becomes the quantitative measure of geometric deviation (G) or "fragmentation" from the primordial spherical stasis. Therefore, in the SVM, we introduce a technical geometric definition of entropy: as the measure of information loss through geometric deviation. In this context, the ground state is the perfect sphere that represents the highest possible information density where all points are unified (S = 0) and the entropic state is the state when the vacuum is displaced to form matter and the "unity" is fragmented into discrete "quanta." Time is not a dimension but the measurement of the rate of this fragmentation. It is important to bring up the term “energy”. Here, energy (E) and entropy are inverse manifestations of the same geometric potential (inverse duality). This means that the product of energy and entropy is constant for a given geometric volume V:

$$E \cdot S = K \tag{3}$$

From this, when $S \to 0$ (perfect symmetry) then $E \to \infty$ (infinite potential).

The "vacuum" (S = 0) is a state of total symmetry where no distinct "events" can exist. Matter is a localized increase in entropy: a "scab" or "hole" in the vacuum potential. Therefore, mass is defined as a negative displacement in the + vacuum potential and the total energy becomes

$$E_{total} = E_V(+) + E_{mass}(-) \tag{4}$$

As the total energy is a constant of the infinite sphere, we get a zero-sum geometric equation

$$\int_V \quad \Delta\phi dV = 0 \tag{5}$$

We can define a geometric deviation tensor ($G_{\mu\nu}$) that measures the "roughness" or asymmetry of the local vacuum. Time (t) is then not a dimension, but is defined as a secondary scalar derivative of this entropic decay relative to this distortion:

$$\Delta t \equiv \frac{dS}{dG} \tag{6}$$

This definition satisfies the "arrow of time" without requiring a four-dimensional manifold; time is simply the shadow cast by the vacuum's decay into complexity. The past is defined as the high symmetry extreme ($G = 0$) and the future is as the low symmetry extreme ($G \rightarrow \infty$).

The integral is giving the "absolute" time definition over a range of distortions:

$$t = \int \quad \frac{\partial S}{\partial G} dG \tag{7}$$

2.2. The emergence of gravity

In this framework, gravity is redefined as a mechanical pressure of the vacuum attempting to restore symmetry. The vacuum pressure gradient labelled as F_g is defined as

$$\underline{F_g} = -\nabla P_V \tag{8}$$

Where P_V is a function of the local density of "holes" (mass). This naturally derives the inverse-square laws as the pressure disturbances across the surface area ($4\pi r^2$) of the spherical distortion - see below.

In this model, therefore, gravity is not a "pull" between masses but an inward push from the high-pressure vacuum (+) into the low-pressure "mass-hole" (-).

We define the vacuum plenum as having an intrinsic pressure Π_∞. A mass M is a localized depletion of this pressure. The local pressure Π(r) at a distance r from the centre of a mass can be modeled as

$$\Pi(r) = \Pi_\infty \left(1 - \frac{R_s}{r}\right) \tag{9}$$

Where R_s is the "displacement radius" that is proportional to the amount of vacuum displaced by mass.

The F_g force is the gradient of the vacuum pressure acting on the surface are of the spherical distortion:

$$\underline{F_g} = -\oint_A \Pi(r) dA \tag{10}$$

Since the surface area of the vacuum displacement scales as $4\pi r^2$, the pressure gradient must distribute over this area to maintain equilibrium:

$$\nabla\Pi = \frac{\partial\Pi}{\partial r}\underline{r} = \frac{\Pi_\infty R_S}{r^2}\ \underline{r} \tag{11}$$

This confirms that what we perceive as "gravitational pull" is mathematically the radial restoration force of the vacuum density seeking symmetry.

2.3. Black holes and singularity

We can define a critical vacuum pressure Π_c, which represents the maximum tension the "material" geometry can sustain before collapsing back into the vacuum plenum, this threshold is reached at the Planck length (Lp). The local vacuum pressure Π(r) from our previous derivation was

$$\Pi(r) = \Pi_\infty \left(1 - \frac{R_s}{r}\right)$$

From this, when r is approaching Lp, the displacement R_s (the "hole") becomes indistinguishable from the surrounding vacuum potential. At this point, the gradient $\nabla\Pi$ becomes non-linear:

$$\lim_{r \to L_P} \nabla \Pi \Rightarrow \infty \tag{12}$$

With these, instead of the density becoming infinite (as in general relativity) the entropy of the system hits a hard floor of zero.

The notion of a gravitational singularity arises from the Schwarzschild solution, but as shown by Angelo Loinger in "*On Black Holes and Gravitational Waves*" [4], the original Schwarzschild article contains no such singularity as the original Schwarzschild solution does not necessitate a point of infinite density. Furthermore, we must acknowledge the "political" nature of black hole theory, often used as a mathematical "fix" for models [1] that fail at extreme scales (see *Exploding a Myth*, [6].

The SVM accepts this view, proposing that at the Planck Limit (Lp) a physical phase transition occurs. In our SVM model, the "black hole" is reclassified as a Planck phase transition. The SVM asserts that the "singularity" (r = 0) is a mathematical failure of the Schwarzschild coordinate system, not a physical reality.

Black holes are modelled as regions where negative potential depletions overlap until they reach the Planck scale, triggering a reversion to vacuum. Here, we model the state of the black hole core as a phase transition. The black hole is the mechanism by which the "debt" of material existence is settled. The total energy flux (Ψ_{BH}) of a black hole in this model is:

$$\psi_{BH} = \int_{V_{pANCK}} |M(-) + \Pi(+)| dV (= 0) \tag{13}$$

When the integral equals zero, the "hole" is closed, and the local region of the universe returns to the spherical vacuum state. A black hole is modelled as a region where negative potential depletions overlap until they reach the Planck scale, triggering a reversion to the vacuum.

Mathematically, this is geometric cancellation, where the input is a massive displacement (high entropy, negative potential), the transition is the overlap of displacements at the Planck scale and the output is zero entropy with infinite positive potential (Ψ_V). In this context, the singularity is redefined as the point there inverse duality resets:

$E \cdot S = K \qquad \text{if} \qquad S \to 0 \text{ then, } \quad E \to \infty$

At the Planck limit the singularity is resolved as a geometric cancellation. In this model, the black hole is a "pressure leak" where the compressed "negative" mass is being squeezed out by the surrounding "positive" vacuum pressure. As the black hole "heals" the holes in the vacuum, the excess restored energy is pushed outward as pure symmetric potential which we perceive as high-energy radiation.

In standard physics, Hawking radiation [3] is seen as a loss of mass, in the SVM it is the recovery of the vacuum's ground state. We define the restoration flux ϕ_{res} as the rate at which the vacuum "heals" the hole created by mass M:

$$\phi_{res} = \frac{d}{dt} V(+) \tag{14}$$

Because the total energy of the system is zero-sum equation (V(+) + M(-)), any increase in the vacuum's symmetric potential must result in a decrease in the absolute value of the negative mass-hole:

$$\frac{dV}{dt} = -\frac{d[M]}{dt} \tag{15}$$

The event horizon is not a point of no return for light, but the boundary layer of the phase transition. We can model the Hawking radiation as, instead of a "thermal evaporation" from a mass, the restored energy leakage from the vacuum or the vacuum overflow (ϕ_{out}). In other words, the event horizon is where the vacuum's inward push (gravity) meets the material resistance of the mass-hole. We can model the radiation as a result of quantum tunnelling through a pressure gradient.

$$\phi_{out} = \frac{d}{dt}\left(V_{restored} - V_{eq}\right) \tag{16}$$

The P probability of energy escaping the horizon is proportional to the local curvature of the vacuum displacement:

$$P_{rad} \sim exp\left(\frac{\Pi_c}{\nabla \Pi}\right) \tag{17}$$

In small black holes the pressure gradient is sharper, meaning the vacuum "heals" them faster. This explains why smaller black holes radiate more

intensely. On the other hand, large black holes have a flatter gradient, and this leads to a slower restoration of symmetry.

When a phase transition at the core occurs (Planck collapse), the volume of restored vacuum energy can exceed the local geometric capacity of the hole. This results in relativistic jets that can be modelled as a symmetric potential discharge (D):

$$\underline{D} = \eta(\Pi_{core} - \Pi_{vacuum}) \cdot \underline{z} \tag{18}$$

Where η is the "conductivity" of the vacuum and z is the axis of the least resistance (usually the rotational poles).

We can now represent the entire life cycle of matter in this model with a single symmetry loop:

1. **Crystallization:** $\mathbb{V}(+) \xrightarrow{\text{Entropy Increase}} M(-)$ (Creation of the "Hole").
2. **Persistence:** Gravity ($\nabla\Pi$) attempts to "push" the hole closed.
3. **Collapse:** $M(-) \xrightarrow{\text{Planck Limit}} \mathbb{V}(+)$ (The Phase Transition).
4. **Return:** $\Phi_{res} \rightarrow$ Restored Vacuum (The debt is settled).

Figure 1. Full life cycle of matter.

The SV model suggests that information is never lost because "information" is simply a specific geometric distortion (G). When the black hole dissolves the distortion, the "information" (the shape of the hole) is simply smoothed back into the infinite potential of the spherical vacuum.

To summarize, in our SVM model, at the Planck limit (Lp), negative displacements (mass) overlap so significantly they undergo geometric cancellation. The system flips back into its most stable state: the vacuum (+). The black hole is a cosmic recycler, returning asymmetric "mass-debt" to the ground state of zero entropy. Instead of a "black hole," we define these regions as symmetry restoration gateways. When mass-density reaches the limit where

the vacuum "holes" overlap (r to Lp) the local entropy approaches a local maximum, triggering a geometric flip. The negative potential of matter is "squeezed out" by the infinite pressure of the surrounding vacuum plenum. As a result, the matter dissolves back into pure, symmetric vacuum energy. The "black hole" is a cosmic recycler, settling the "energy debt" of material existence and returning the region to S = 0. This idea removes the infinite values that plague general relativity.

The general relativity-based model and the SVM differ significantly at numerous points:

Feature	**General relativity**	**SVM**
Core nature	Singularity (infinite mass)	Phase transition (zero mass)
Entropy	Maximum ($S \to \infty$)	Minimum ($S \to 0$)
Gravity	Spacetime curvature	Vacuum restoration pressure
Energy scale	Crushing weight	Absolute energetic purity

2.4. Dark phenomena

Standard cosmology relies on "dark matter" and "dark energy" to prop up the Big Bang theory. However, critics like Don Scott [5] suggest these are structures used to maintain an absolute truth that may be flawed.

Following the work of Scott, we argue that these phenomena are emergent properties of the vacuum plenum itself. We define the vacuum not as "nothing," but as an infinite positive potential ($\mathbf{\Phi}_v$). This plenum possesses an inherent "pressure of Integrity." The "missing mass" in galaxies is reinterpreted as the radial potential gradient of the vacuum. As the vacuum "pushes" inward to close the holes of a galaxy, it creates a tension field that mimics the effects of additional mass. This removes the need for hypothetical unobserved particles.

To make this framework more complete and mathematically sound, we will formalize dark energy not as a “mysterious force” but as the global restoration pressure (Π_G) of the infinite vacuum plenum. In this model, the “expansion” of

the universe is not the vacuum's energetic effort to smooth out the "material scabs" (galaxies and matter) and return the entire system to absolute spherical symmetry.

We define the vacuum as a state of positive potential, with the ethernet outward pressure. Matter represents negative displacement (voids) that create tension in the field.

The "expansion velocity" (v_e) of a point in space is modeled as the rate at which the vacuum recovers volume from these depletions:

$$v_e = \nabla \Pi_G \tag{19}$$

Unlike the standard Hubble constant (H_D), which is often treated as a property of space itself, our symmetry restoration constant (Λ_S) is a measure of the vacuum's "healing rate":

$$\Lambda_S = \frac{\partial V(+)}{\partial M(-)} \tag{20}$$

Standard gravity explains why matter "clumps" (local restoration). Dark energy explains why those clumps move apart (global restoration).

We can model the "Repulsion" between two galaxies (M_1, M_2) as the vacuum attempting to maximise the symmetry of the region between them. If the vacuum pressure between two masses is higher than the internal pressure of the masses themselves, then

$$F_{ext} = F_{vacuum-push}(+) - F_{vacuum-pull}(0) \tag{21}$$

At cosmological scales, the vacuum plenum pressure (Π_∞) dominates:

$$\lim_{d \to \infty} F_{net} \approx \Pi_\infty A_{surface} \tag{22}$$

This results in the observed accelerated expansion, as the infinite vacuum asserts its geometric dominance over the finite "scabs" of matter.

In this framework, the Big Bang was not the creation of space but the initial massive displacement of the perfect vacuum into a state of high entropy. Therefore, this single event is the large symmetry break event.

t = 0 is characterised by the absolute spherical symmetry (S = 0, $E = \infty$) and t > 0 is the "crystallisation" event when the vacuum "breaks" into M(-). In the current era the vacuum is actively "healing" the Big Bang's displacement, which we perceive as dark energy.

As a summary, in our SVM, these "dark particles" are not "missing particles" but geometric restoration pressures. Dark energy is the inherent outward pressure of the infinite vacuum plenum (+) attempting to "smooth out" the material voids (-) and restore spherical integrity and dark matter is the localized tension of the vacuum field accommodating mass-holes, removing the need for auxiliary particles. The "expansion" of the universe is the vacuum's effort to restore total symmetry. This is not a "force" driving space apart, but the vacuum recovering volume from material fragmentation.

2.5. Spherical packing

To minimise internal tension (energy loss) and maximise geometric stability during a phase transition, energy must be distributed according to spherical phyllotaxis.

For N points (energy quanta) on the unit sphere, the most stable distribution (the "Fibonacci lattice") is defined by the coordinates

$$z_i = \frac{2i-(N+1)}{N} \tag{23}$$

$$\phi_i = \frac{2\pi i}{\phi} \tag{24}$$

Where $\phi = \frac{1+\sqrt{5}}{2} = 1.618$, that is the Golden ratio.

This framework argues that the Golden ratio is the mathematical "signature" of the vacuum attempting to maintain maximum symmetry while "crystallizing" into matter.

We can define the "symmetry retention" of a system as a function of its packing efficiency:

$$H(G) = \sum_{i=1}^{N} \quad \frac{1}{\left|\underline{r_i}-\underline{r_j}\right|^2} \tag{25}$$

The framework posits that the vacuum naturally settles into a state where H(G) is minimised. Mathematically, the global minimum for this energetic tension on a spherical manifold is only achieved when the angular displacement between points follows the Golden angle:

$$\Psi_{angle} = \frac{160}{\phi^2} = 137.5 \quad (26)$$

This maintains maximum symmetry during the phase transition from vacuum to mass as this spherical phyllotaxis function guarantees that the distribution of energy "crystallasing" into matter follows the most efficient geometric path.

Therefore, the magic question, "why does the Golden ratio appear from the subatomic to the galactic scale?" can be answered in this framework. In the SVM, it is the inevitable result of spherical packing efficiency. When the high-energy vacuum "crystallizes" into mass, it must distribute that energy to minimize internal tension. The Fibonacci sequence (expressed via spherical phyllotaxis) is the most stable geometric path for a vacuum attempting to maintain maximum symmetry while constrained by material "voids."

2.6. Synthesis

The entire model can be summarized by the conservation of symmetry equation. We introduce the universal symmetry equation, which governs the conservation of geometric potential and is based on the the zero-sum geometric potential (**Ω**) defined below:

$$\Omega = \phi_V(+) + \sum_{i=1}^{N} M_i(-) + \int \frac{dS}{dt} dG = 0 \quad (27)$$

Where $\Phi_V(+)$ is the infinite positive potential of the spherical vacuum, $M_i(-)$ is the localized mass-holes (negative displacements or mass) and the third term accounts for the entropic "noise" perceived as time and space.

In the equation, the infinite potential of the vacuum ($\Phi_V(+)$) is always perfectly balanced by the "debts" of the mass and the "noise" of entropic time (third term).

In this framework, the following parameters form the foundation:

Concept	Representation	Description
Vacuum	$\Phi(+)$	Infinite potential, zero-entropy ground state
Mass	$\Delta\Phi(-)$	Localized depletion or "hole" in the vacuum
Time	$\frac{dS}{dG}$	A measurement of geometric deviation (G) from symmetry
Gravity	∇P_v	Pressure gradient of the vacuum plenum
Space	$d(\Delta\Phi_i, \Delta\Phi_j)$	Relational distance between vacuum displacements

Equation (27) demonstrates two ideas:

1. Mass is a debt - matter can only exist if there is a corresponding "tension" in the vacuum.
2. Conservation: Energy is never "created"; it is only displaced from the infinite symmetric plenum into asymmetric entropic states.

In general relativity, gravity increases to infinity as distance (r) approaches zero, creating the "singularity paradox". The SVM predicts a phase transition instead.

In SV, the force of gravity is limited to maximum vacuum pressure. As we approach the Planck length, the "hole" in the vacuum reaches its maximum possible geometric density.

In SVM the gravitational potential is defined as

$$\phi_{SVM}(r) = -\frac{GM}{r}\left(1 - exp(-\frac{r-Lp}{Lp}\right) \quad (28)$$

As the distance r approaches the Lp Plack scale, the gravitational force tends to infinity, while in the SVM it tends to zero (geometric cancellation).

When r = Lp, the term (1-exp(0)) becomes 0. The gravitational "pull" vanishes because the negative displacement (mass) and the positive restoration (vacuum) perfectly overlap. The system undergoes a symmetry flip.

The SVM predicts that at extremely high energy densities (such as the final micro-seconds of a black hole's life or the earliest moments of the Big Bang), gravity should effectively "shut off" of invert. Instead of a crushing point, there should be a symmetry rebound or "Planck bounce". Astronomers could look evidence for this in two phenomena:

1. Hawking radiation spectra: A sudden "spike" in energy as the last of the mass-hole cancels out into pure vacuum potential.
2. Gravitational waves: High-frequency "ringing" signatures that deviate from general relativity predictions as two micro-black holes merge, showing a lack of infinite density.

3. Conclusions

The universe is a self-regulating geometric system with an absolute sphere of infinite energy. It began in perfect symmetry with no internal dimensions (due to the lack of discrete points to define distance) and zero entropy, was perturbed into the "illusion" of material existence and linear time, and is now mathematically fated to return to its ground state of zero entropy through the pressure of spherical vacuum. In this framework energy and entropy are reciprocal manifestations of singular geometric potential. Matter is not an existing "thing" added to the universe but a localised negative displacement (a "hole") in the positive vacuum potential. The universe itself is a zero-sum geometric system with no defined dimensions. Furthermore, gravity is not a fundamental force but a mechanical pressure gradient of the high-energy vacuum attempting to "push" a mass-hole closed to restore spherical symmetry.

Time is a secondary measurement of the degree of geometric deviation (G) from the primordial sphere. "The arrow of time" is the derivative of entropy relative to its fragmentation. By removing the concepts of linear time and fundamental gravity, we dissolve the paradox of the singularity. The universe is not a collection of separate parts, but a single, symmetric whole viewed through the fractured lens of material existence.

The SVM resolves the "singularity" by reclassifying it as a phase transition and demystifies "dark" phenomena as geometric restoration pressures. By adopting the technical definitions of entropy and the critiques of the Schwarzschild/Big Bang dogmas provided by Loinger and Scott, we move toward the physics of symmetry restoration.

We are not observers on a stage; we are intrinsic fluctuations within an infinite, symmetric whole. The future of physics lies in mapping the "healing rate" of the vacuum as it pulls the fragmented, entropic world back into the perfect, spherical embrace of the absolute.

Phenomenon	**SVM interpretation**
Gravity	$-\nabla P_{v:}$: The pressure of the vacuum "pushing" a hole closed.
Charge	Geometric "spin" required to maintain the equilibrium of the distorted sphere.
Black hole	A "phase transition" where the hole is fully settled.
Matter	A "frozen" or "crystallised" state of vacuum energy.
Dark energy	Global vacuum pressure "smoothing" the field.
Golden ratio	The inevitable consequence of packing efficiency within spherical constraints.

In this framework, a black hole is a region where the "negative" mass-holes are packed so tightly that the surrounding "positive" vacuum pressure can no longer hold them apart, leading to a restoration of the original symmetry.

The SVM replaces the "broken" infinities of modern physics with a self-regulating geometric loop. By treating the universe as a sphere seeking its own perfection, we move from a physics of "objects" to a physics of symmetry restoration.

The goal of future inquiry lies in mapping the precise mathematical pathways by which the infinite energy of the vacuum manifests as the finite world.

Acknowledgement

The authors would like to thank to Sir Prof. Santilli for his useful comments.

References

[1] Bekenstein, J. D. (1973). *Black Holes and Entropy*. Physical Review D.

[2] Einstein, A. (1915). *Die Grundlage der allgemeinen Relativitätstheorie*.

[3] Hawking, S.W. (1974). *Black Hole Explosions?* Nature, 248.

[4] Loinger, A. (2002). *On Black Holes and Gravitational Waves*. La Goliardica Pavese.

[5] Scott, D. E. (2015). "The Electric Sky," *Progress in Physics*, vol. 11, p. 167.

[6] Unzicker, A. (2007). *Exploding a Myth: "Conventional Wisdom" or Scientific Truth*. Horwood Publishing.

[7] Verlinde, E. (2011). *On the Origin of Gravity and the Laws of Newton*.

HADRONIC JOURNAL 49, 137 - 166 (2026)
DOI 10.29083/HJ.49.02.2026/SC137

A VARIATIONAL FORMULATION FOR MODELING A COMPRESSIBLE AND TIME-DEPENDENT PROTIUM HYDROGEN FLUID FLOW

Fabio Silva Botelho
Department of Mathematics
Federal University of Santa Catarina – UFSC
Florianópolis, SC, Brazil
fabio.botelho@usfc.br

Received April 25, 2026
Revised May 1, 2026

Abstract

This article develops a variational formulation for modeling a compressible protium hydrogen fluid motion. The results are based on standard tools of calculus of variations and optimization theory. The context here addressed is essentially an Euler-Bernoullian one and includes also a new approximate Bernoulli-perfect-gas equation. Finally, it is worth highlighting, with the inclusion of such a new Bernoulli-perfect-gas equation, we have established a system of partial differential equations suitable for modeling a compressible case in fluid mechanics.

AMS Classification 76A02, 76N15
Keywords. Protium hydrogen fluid, Euler system, Bernoulli-perfect-gas type equation, strong variational formulations, Lagrange multipliers.

Copyright © 2026 by Hadronic Press, Inc., Palm Harbor, FL 34684, USA

1 Introduction

The first part of this article develops a variational formulation for modeling a gaseous hydrogen motion in an Euler-Bernoullian context.

Such results are based on tools of calculus of variations and related Lagrange multipliers approach. It is worth emphasizing, in the last section, we have obtained a system of partial differential equations including a new Bernoulli-perfect-gas equation originally presented in [1]. We believe such a new equation represents an important advance concerning the mathematical theory of fluid mechanics. It is also worth mentioning, such a system of partial differential equations we have obtained is similar to those previously known in the literature, however, with such a Bernoulli-perfect-gas equation replacing the standard ideal-gas equation.

Furthermore, we highlight the two main fields for such a system are a position one and a velocity one, which we specify below in the next lines.

As standard references in theoretical fluid mechanics we would cite [2, 3, 4, 5, 6, 7]. For related numerical methods we would mention [8, 9, 10, 11]. Concerning similar models, we would cite [12, 13, 14, 15, 16, 17].

Finally, details on the Sobolev spaces involved may be found in [18].

Let $\Omega \subset \mathbb{R}^3$ be an open, bounded and simply connected set with a regular (Lipschitzian) boundary denoted by $\partial\Omega$.

Generically, we consider a fluid motion initially modeled as a particle system one, through the field of position $\mathbf{r} : \Omega \times [0, t_f] \to \mathbb{R}^3$ and field of velocities $\mathbf{v}$ where $\mathbf{v}(\mathbf{r}(x,t),t)$ stands for the velocity at the position $\mathbf{r}(x,t)$ and time $t \in [0,t_f]$.

Moreover, the gravity field is denoted by

$$\mathbf{g} = -g\mathbf{k},$$

related to the $\mathbb{R}^3$ basis

$$\{\mathbf{i} = (1,0,0), \mathbf{j} = (0,1,0), \mathbf{k} = (0,0,1)\}.$$

2 The mathematical model

In this section, we develop in details the concerning variational formulation for a compressible case.

We emphasize such a set $\Omega \subset \mathbb{R}^3$ stands for a control volume, in which along a time interval $[0,t_f]$, where $t \in [0,t_f]$ denotes time, a protium Hydrogen gas develops a compressible motion.

Here we recall a protium hydrogen atom comprises one electron and one proton (no neutrons). We also highlight the gaseous atomic protium Hydrogen is relatively rare on Earth however, may be found in great amount in stars such as the Sun.

Denoting by m_e the mass of one electron and by m_p the mass of one proton, we start by defining the following protium hydrogen atomic density

$$\hat{\rho}(x,y,z,t) = \left(|\phi_e(x,y,z,t)|^2 + |\phi_p(x,y,z,t)|^2\right)|\phi_A(y,z,t)|^2\frac{|\phi_M(z,t)|^2}{m_e+m_p} \quad (1)$$

The macroscopic fluid density is defined by

$$\rho = |\phi_M(z,t)|^2.$$

It is worth highlighting that generically, we denote

$$\begin{aligned} & L^2(\Omega\times[0,t_f]) \\ = & \left\{h:\Omega\times[0,t_f]\to\mathbb{R} \text{ measurable } : \int_\Omega\int_0^T |h(x,t)|^2\,dxdt<+\infty\right\}, \quad (2) \end{aligned}$$

$$\begin{aligned} L^2(\Omega\times[0,t_f];\mathbb{R}^3) = & \left\{h=(h_1,h_2,h_3):\Omega\times[0,t_f]\to\mathbb{R}^3\right. \\ & \left.: h_k\in L^2(\Omega\times[0,t_f]),\ \forall k\in\{1,2,3\}\right\}, \quad (3) \end{aligned}$$

$$\begin{aligned} W^{1,2}(\Omega\times[0,t_f]) = & \left\{h:\Omega\times[0,t_f]\to\mathbb{R} \ : \ h\in L^2(\Omega\times[0,t_f])\right. \\ & \left. h_t \text{ and } h_{x_j}\in L^2(\Omega\times[0,t_f]),\ \forall j\in\{1,2,3\}\right\}, \quad (4) \end{aligned}$$

where the partial derivatives h_{x_j} are understood in a distributional sense, $\forall j\in\{1,2,3\}$.

Moreover,

$$\begin{aligned} W^{1,2}(\Omega\times[0,t_f];\mathbb{R}^3) = & \left\{h=(h_1,h_2,h_3):\Omega\times[0,t_f]\to\mathbb{R}^3\right. \\ & \left.: h_k\in W^{1,2}(\Omega\times[0,t_f]),\ \forall k\in\{1,2,3\}\right\} \quad (5) \end{aligned}$$

Similar notations are valid for other sets and other related complex and vectorial cases.

With such notations in mind, we define the concerning function spaces

$$\begin{aligned} V_1 = & \left\{\phi_e\in W^{1,2}(\Omega\times\Omega\times\Omega\times[0,t_f];\mathbb{C}) \ : \ \phi_e=0 \text{ on } \partial(\Omega\times\Omega\times\Omega)\times[0,t_f],\right. \\ & \left.\phi_e(x,y,z,0)=\hat{\phi}_0 \text{ and } \boldsymbol{\phi}_e(x,y,z,t_f)=\hat{\phi}_f \text{ in } \Omega\times\Omega\times\Omega\right\} \quad (6) \end{aligned}$$

$$V_2 = W_0^{1,2}(\Omega\times\Omega\times[0,t_f];\mathbb{C}),$$

and

$$V_3 = \{\phi_M \in W^{1,2}(\Omega \times [0,t_f];\mathbb{C}) \,:\, \phi_M = 0 \text{ on } \partial(\Omega_1 \cup \Omega_2) \times [0,t_f], \\ \phi_M(z,t) = \phi_{in}(z,t) \in \partial\Omega_{in} \times [0,t_f] \text{ and } \phi_M(z,0) = \phi_0 \text{ in } \Omega\}, \quad (7)$$

where

$$\partial\Omega = \partial\Omega_{in} \cup \partial\Omega_1 \cup \partial\Omega_2 \cup \partial\Omega_{out}.$$

Moreover we suppose such a union is quasi-disjoint and through $\partial\Omega_{in}$ and $\partial\Omega_{out}$ are allowed the entering and exiting of gaseous hydrogen mass, respectively.

Remark 2.1. *In this text we denote*

$$\rho(z,t) = \int_\Omega \int_\Omega \hat{\rho}(x,y,z,t)\, dx\, dy$$

however, we consider ρ and $\hat{\rho}$ as two independent variables.

We define also

$$\hat{\rho}_e(x,z,y,t) = |\phi_e(x,y,z,t)|^2 |\phi_A(y,z,t)|^2 \frac{|\phi_M(z,t)|^2}{m_e + m_p}$$

$$\hat{\rho}_p(x,z,y,t) = |\phi_p(x,y,z,t)|^2 |\phi_A(y,z,t)|^2 \frac{|\phi_M(z,t)|^2}{m_e + m_p}$$

and the restrictions

$$\int_\Omega |\phi_e(x,y,z,t)|^2\, dx = m_e \text{ in } \Omega \times \Omega \times [0,t_f],$$

$$\int_\Omega |\phi_p(x,y,z,t)|^2\, dx = m_p \text{ in } \Omega \times \Omega \times [0,t_f]$$

and

$$\int_\Omega |\phi_A(y,z,t)|^2\, dy = 1, \text{ in } \Omega \times [0,t_f].$$

2.1 The position fields

We start by denoting the macroscopic hydrogen position field as

$$\mathbf{r} : \Omega \times [0,t_f] \to \mathbb{R}^3.$$

where

$$\mathbf{r}(z,t) = (X_1(z,t), X_2(z,t), X_3(z,t)), \text{ in } \Omega \times [0,t_f].$$

The atomic particle position field is defined by $\mathbf{r}_A : \Omega \times \Omega \times [0, t_f] \to \mathbb{R}^3$, where

$$\mathbf{r}_A(y, z, t) = \mathbf{r}(z, t) + \hat{\mathbf{r}}_A(y, \mathbf{r}(z, t)).$$

In a relativistic context, the electronic particle position field stands for

$$\mathbf{r}_e(x, y, z, t) = (ct, \hat{\mathbf{r}}_e(x, \mathbf{r}_A(y, z, t), \mathbf{r}(z, t))),$$

so that

$$\mathbf{r}_e(x, y, z, t) = (ct, \tilde{\mathbf{r}}_e(x, y, z, t)),$$

where

$$\tilde{\mathbf{r}}_e(x, y, z, t) = \hat{\mathbf{r}}_e(x, \mathbf{r}_A(y, z, t), \mathbf{r}(z, t)).$$

Similarly, the proton particle field stands for

$$\mathbf{r}_p(x, y, z, t) = (ct, \hat{\mathbf{r}}_p(x, \mathbf{r}_A(y, z, t), \mathbf{r}(z, t))),$$

so that

$$\mathbf{r}_p(x, y, z, t) = (ct, \tilde{\mathbf{r}}_p(x, y, z, t)),$$

where

$$\tilde{\mathbf{r}}_p(x, y, z, t) = \hat{\mathbf{r}}_p(x, \mathbf{r}_A(y, z, t), \mathbf{r}(z, t)).$$

Here $c > 0$ denotes the speed of light.

We define also the following function spaces

$$\begin{aligned} V_4 \quad = \quad & \{\mathbf{r} \in W^{1,2}(\Omega \times [0, t_f]; \mathbb{R}^3) \ : \ \mathbf{r} = \mathbf{0} \text{ on } (\partial\Omega_1 \cap \partial\Omega_2) \times [0, t_f] \\ & \text{and } \mathbf{r}(z, 0) = \mathbf{r}_0 \text{ in } \Omega\}, \end{aligned} \tag{8}$$

and

$$\tilde{\mathbf{r}}_e \in V_5 = W^{1,2}(\mathbb{R}^{10}; \mathbb{R}^3).$$

$$\tilde{\mathbf{r}}_p \in V_5$$

and

$$\hat{\mathbf{r}}_A \in V_6 = W^{1,2}(\mathbb{R}^7; \mathbb{R}^3).$$

2.2 About the system constraints

Denoting by $m_e(0)$ the total system mass at $t = 0$, we have the following constraint

$$\begin{aligned} m_e(0) &= \int_\Omega \rho(y,0)\, dy \\ &= \int_\Omega \rho(y,t)\, dy + \int_0^t \int_{\partial\Omega} \rho(y,\tau)\mathbf{v}\cdot\mathbf{n}\, dS\, d\tau \end{aligned} \tag{9}$$

where

$$\mathbf{v} = \mathbf{v}(\mathbf{r}(x,t),t).$$

Here $\mathbf{n}$ denotes outward normal field to $\partial\Omega = S$.

Relating the internal kinetics energy, in a relativistic context, we define the following functional

$$\begin{aligned} E^e_{C_1} &= -\frac{1}{2}\int_0^{t_f}\int_\Omega\int_\Omega\int_\Omega \frac{\hat\rho_e(x,y,z,t)}{\sqrt{1-\frac{v_e^2}{c^2}}}\frac{d\tilde{\mathbf{r}}_e}{dt}\cdot\frac{d\tilde{\mathbf{r}}_e}{dt}\, dx\, dy\, dz\, dt \\ &= \frac{1}{2}\int_0^{t_f}\int_\Omega\int_\Omega\int_\Omega \frac{\hat\rho_e}{\sqrt{1-\frac{v_e^2}{c^2}}}(c^2-v_e^2)\, dx\, dy\, dz\, dt \\ &= \frac{1}{2}\int_0^{t_f}\int_\Omega\int_\Omega\int_\Omega c\hat\rho_e\sqrt{c^2-v_e^2}\, dx\, dy\, dz\, dt \end{aligned} \tag{10}$$

where generically, we have denoted

$$a\cdot b = -a_0b_0 + \sum_{k=1}^{3} a_kb_k$$

for

$$a = (a_0, a_1, a_2, a_3)$$

and

$$b = (b_0, b_1, b_2, b_3) \in \mathbb{R}^4.$$

Similarly, we may define

$$\begin{aligned} E^p_{C_1} &= -\frac{1}{2}\int_0^{t_f}\int_\Omega\int_\Omega\int_\Omega \frac{\hat\rho_p(x,y,z,t)}{\sqrt{1-\frac{v_p^2}{c^2}}}\frac{d\tilde{\mathbf{r}}_p}{dt}\cdot\frac{d\tilde{\mathbf{r}}_p}{dt}\, dx\, dy\, dz\, dt \\ &= \frac{1}{2}\int_0^{t_f}\int_\Omega\int_\Omega\int_\Omega \frac{\hat\rho_p}{\sqrt{1-\frac{v_p^2}{c^2}}}(c^2-v_p^2)\, dx\, dy\, dz\, dt \\ &= \frac{1}{2}\int_0^{t_f}\int_\Omega\int_\Omega\int_\Omega c\hat\rho_p\sqrt{c^2-v_p^2}\, dx\, dy\, dz\, dt \end{aligned} \tag{11}$$

For the interacting and self-interacting energies, we define the following functionals,

$$
\begin{aligned}
& E_{in}^{e} \\
= \; & \frac{\alpha_e}{2} \int_0^{t_f} \int_\Omega \int_\Omega \int_\Omega \int_\Omega \int_\Omega \int_\Omega \frac{|\phi_e(x,y,z,t)|^2 |\phi_e(\tilde{x},\tilde{y},\tilde{z},t)|^2}{|\mathbf{r}_e(x,y,z,t) - \mathbf{r}_e(\tilde{x},\tilde{y},\tilde{z},t)|} \\
& \times |\phi_A(y,z,t)|^2 |\phi_A(\tilde{y},\tilde{z},t)|^2 \\
& \times |\phi_M(z,t)|^2 |\phi_M(\tilde{z},t)|^2 \, dx \, dy \, dz \, d\tilde{x} \, d\tilde{y} \, d\tilde{z} \, dt
\end{aligned} \tag{12}
$$

$$
\begin{aligned}
& E_{in}^{p} \\
= \; & \frac{\alpha_p}{2} \int_0^{t_f} \int_\Omega \int_\Omega \int_\Omega \int_\Omega \int_\Omega \int_\Omega \frac{|\phi_p(x,y,z,t)|^2 |\phi_p(\tilde{x},\tilde{y},\tilde{z},t)|^2}{|\mathbf{r}_p(x,y,z,t) - \mathbf{r}_p(\tilde{x},\tilde{y},\tilde{z},t)|} \\
& \times |\phi_A(y,z,t)|^2 |\phi_A(\tilde{y},\tilde{z},t)|^2 \\
& \times |\phi_M(z,t)|^2 |\phi_M(\tilde{z},t)|^2 \, dx \, dy \, dz \, d\tilde{x} \, d\tilde{y} \, d\tilde{z} \, dt
\end{aligned} \tag{13}
$$

$$
\begin{aligned}
& E_{in}^{ep} \\
= \; & \frac{\alpha_{ep}}{2} \int_0^{t_f} \int_\Omega \int_\Omega \int_\Omega \int_\Omega \int_\Omega \int_\Omega \frac{|\phi_e(x,y,z,t)|^2 |\phi_p(\tilde{x},\tilde{y},\tilde{z},t)|^2}{|\mathbf{r}_e(x,y,z,t) - \mathbf{r}_p(\tilde{x},\tilde{y},\tilde{z},t)|} \\
& \times |\phi_A(y,z,t)|^2 |\phi_A(\tilde{y},\tilde{z},t)|^2 \\
& \times |\phi_M(z,t)|^2 |\phi_M(\tilde{z},t)|^2 \, dx \, dy \, dz \, d\tilde{x} \, d\tilde{y} \, d\tilde{z} \, dt.
\end{aligned} \tag{14}
$$

On the other hand, we define

$$
\begin{aligned}
& E_{M}^{e} \\
= \; & \frac{\gamma_e}{2} \int_0^{t_f} \int_\Omega \int_\Omega \int_\Omega \nabla(\phi_e(x,y,t)\phi_A(y,z,t)\phi_M(z,t)) \\
& \cdot \nabla(\phi_e^*(x,y,z,t)\phi_A^*(y,z,t)\phi_M^*(z,t)) \, dx \, dy \, dz \, dt
\end{aligned} \tag{15}
$$

for an appropriate $\gamma_e > 0$ and,

$$
\begin{aligned}
& E_{M}^{p} \\
= \; & \frac{\gamma_p}{2} \int_0^{t_f} \int_\Omega \int_\Omega \int_\Omega \nabla(\phi_p(x,y,t)\phi_A(y,z,t)\phi_M(z,t)) \\
& \cdot \nabla(\phi_p^*(x,y,z,t)\phi_A^*(y,z,t)\phi_M^*(z,t)) \, dx \, dy \, dz \, dt
\end{aligned} \tag{16}
$$

for an appropriate $\gamma_p > 0$.

Concerning the restrictions, we define also the following functionals,

$$
\begin{aligned}
&J_{Aux_1} = \\
&\int_0^{t_f} \int_\Omega \int_\Omega E_1(y,z,t) \left(\int_\Omega (|\phi_e(x,y,z,t)|^2 \, dx - m_e \right) dy \, dz \, dt \\
&+ \int_0^{t_f} \int_\Omega \int_\Omega E_{1a}(y,z,t) \left(\int_\Omega (|\phi_p(x,y,z,t)|^2 \, dx - m_p \right) dy \, dz \, dt \\
&+ \int_0^{t_f} \int_\Omega E_{1b}(z,t) \left(\int_\Omega (|\phi_A(y,z,t)|^2 \, dy - 1 \right) dz \, dt, \qquad (17)
\end{aligned}
$$

$$
\begin{aligned}
J_{Aux_2} \;=\; & \int_0^{t_f} E_2(t) \left(\int_\Omega \rho(y,0) \, dy \right. \\
& \left. - \int_\Omega \rho(y,t) \, dy - \int_0^t \int_{\partial\Omega} \rho(y,\tau) \mathbf{v} \cdot \mathbf{n} \, dS \, d\tau \right) dt \qquad (18)
\end{aligned}
$$

$$
J_{Aux_3} = \int_0^{t_f} \int_\Omega E_3(x,t) \left(\mathbf{v}(\mathbf{r}(x,t),t) - \frac{\partial \mathbf{r}(x,t)}{\partial t} \right) dx \, dt,
$$

$$
J_{Aux_4} \;=\; -\int_0^{t_f} \int_\Omega \hat{P} \left(\frac{d\rho}{dt} + \rho \, \mathrm{div} \, \mathbf{v} \right) dy \, dt, \qquad (19)
$$

Moreover, considering the pressure and temperature scalar fields, we define

$$
P = \frac{d(\hat{P}\rho)}{dt},
$$

where

$$
\hat{P} \in V_5
$$

and

$$
V_5 = \{ \hat{P} \in W^{1,2}(\Omega \times [0,t_f]) \; : \; P = P(\hat{P},\rho) = P_0, \text{ on } \partial\Omega \times [0,t_f] \}.
$$

$$
(C_v)\rho T \;=\; \hat{E}_C^e + \hat{E}_C^p \qquad (20)
$$

where

$$
\hat{E}_C^e = \frac{1}{2} c \int_\Omega \int_\Omega \hat{\rho}_e(x,y,z,t) \sqrt{c^2 - v_e^2} \, dxdy,
$$

and

$$
\hat{E}_C^p = \frac{1}{2} c \int_\Omega \int_\Omega \hat{\rho}_p(x,y,z,t) \sqrt{c^2 - v_p^2} \, dxdy,
$$

for an appropriate real constant $C_v > 0$.

Here we define the entropy differentials

$$dS_e = -K_B \frac{\hat{\rho}_e}{\hat{\rho}} \ln\left(\frac{\hat{\rho}_e}{e\,\hat{\rho}}\right)\, dxdydzdt,$$

and

$$dS_p = -K_B \frac{\hat{\rho}_p}{\hat{\rho}} \ln\left(\frac{\hat{\rho}_p}{e\,\hat{\rho}}\right)\, dxdydzdt.$$

Moreover, we define

$$S_e = -K_B \frac{\hat{\rho}_e}{\hat{\rho}} \ln\left(\frac{\hat{\rho}_e}{e\,\hat{\rho}}\right),$$

and

$$S_p = -K_B \frac{\hat{\rho}_p}{\hat{\rho}} \ln\left(\frac{\hat{\rho}_p}{e\,\hat{\rho}}\right)$$

and

$$E_S = \int_0^{t_f} \int_\Omega \int_\Omega \int_\Omega T(dS_e + dS_p),$$

for an appropriate constant $K_B > 0$.

With such results in mind, defining $S = \int_\Omega \int_\Omega (S_e + S_p)\, dx\, dy$, we define also the restriction

$$\rho(C_v)\frac{dT}{dt} = K\nabla^2 T$$
$$-P \text{ div } \mathbf{v} + \frac{d(TS)}{dt}, \tag{21}$$

for an appropriate real constant $K > 0$.

At this point, we define the following function space

$$\begin{aligned} V_6 \;=\; & \{T \in W^{1,2}(\Omega \times [0,t_f]) \;:\; T(z,t) = T_1(z,t) \\ & \text{on } \partial\Omega \times [0,t_f] \text{ and } T(z,0) = T_0(z) \text{ in } \Omega\}, \end{aligned} \tag{22}$$

and

$$\begin{aligned} V_7 \;=\; & \{\mathbf{v} \in W^{1,2}(\mathbb{R}^3;\mathbb{R}^3) \;:\; \mathbf{v} = \mathbf{0} \text{ on } (\partial\Omega_1 \cup \partial\Omega_2) \times [0,t_f] \\ & \text{and } \mathbf{v}(z,0) = \mathbf{v}_0 \text{ on } \Omega\}. \end{aligned} \tag{23}$$

With such restrictions and definitions in mind, we define the following functionals,

$$\begin{aligned} & J_{Aux_5} \\ = \; & \int_0^{t_f} \int_\Omega E_5(z,t) \left((C_v)\rho T - (\hat{E}_C^e + \hat{E}_C^p)\right)\, dz\, dt \end{aligned} \tag{24}$$

and

$$J_{Aux_6} = \int_0^{t_f} \int_\Omega E_6(z,t) \left(\rho(C_v) \frac{dT}{dt} - K\nabla^2 T + P \text{ div } \mathbf{v} - \frac{d(TS)}{dt} \right) dz\, dt. \quad (25)$$

Finally, we define the following functionals,

$$J_{Aux_7} = \int_0^{t_f} \int_\Omega E_{50}(z,t) \times \left(\rho(z,t) - \int_\Omega \int_\Omega (\hat{\rho}_e(x,y,z,t) + \hat{\rho}_p(x,y,z,t))\, dxdy \right) dz\, dt \quad (26)$$

and

$$J_{Aux_8} = \int_0^{t_f} \int_\Omega E_{51}(z,t)(\rho(z,t) - |\phi_M|^2)\, dzdt.$$

3 The main functional

Here we define the functional J by

$$J = \frac{1}{2} \int_0^{t_f} \int_\Omega \rho \mathbf{v} \cdot \mathbf{v}\, dy\, dt - \int_0^T \int_\Omega \rho \mathbf{g} \cdot \mathbf{r}\, dy\, dt. \quad (27)$$

The final variational formulation J_{total} for such an ionization process stands for

$$J_{total} = J - E^e_{C_1} - E^p_{C_1} + E^e_{in} + E^p_{in} + E^{ep}_{in} + E^e_M + E^p_M + \sum_{k=1}^{8} J_{Aux_k} + E_S. \quad (28)$$

Observe that the extremal equation

$$\frac{\partial J_{total}}{\partial \rho} = \mathbf{0}$$

stands for

$$\frac{1}{2}\mathbf{v} \cdot \mathbf{v} + \frac{\partial J_{Aux_2}}{\partial \rho} + \frac{\partial J_{Aux_5}}{\partial \rho} + \frac{\partial J_{Aux_6}}{\partial \rho} + \frac{d\hat{P}}{dt} - \hat{P} \text{ div } \mathbf{v} - \mathbf{g} \cdot \mathbf{r} + E_{50}(z,t) + E_{51}(z,t) = \mathbf{0}. \quad (29)$$

Thus, we have

$$\frac{1}{2}\mathbf{v}\cdot\mathbf{v}+\frac{d\hat{P}}{dt}-\hat{P}\ \mathrm{div}\ \mathbf{v}-\mathbf{g}\cdot\mathbf{r}+E_{51}(z,t)+\tilde{E}_1=\mathbf{0}. \tag{30}$$

for an appropriate function $\tilde{E}_1$.

Observe also that

$$P=\frac{d(\hat{P}\rho)}{dt},$$

so that

$$P=\frac{d\hat{P}}{dt}\rho+\hat{P}\frac{d\rho}{dt}.$$

Thus,

$$\frac{d\hat{P}}{dt}=\frac{P}{\rho}-\frac{\hat{P}}{\rho}\frac{d\rho}{dt}.$$

From such last results, we may infer that

$$\frac{1}{2}\mathbf{v}\cdot\mathbf{v}+\frac{P}{\rho}-\frac{\hat{P}}{\rho}\frac{d\rho}{dt}-\hat{P}\ \mathrm{div}\ \mathbf{v}-\mathbf{g}\cdot\mathbf{r}+E_{51}(z,t)+\tilde{E}_1=\mathbf{0}, \tag{31}$$

so that,

$$\frac{1}{2}\mathbf{v}\cdot\mathbf{v}+\frac{P}{\rho}-\mathbf{g}\cdot\mathbf{r}+E_{51}(z,t)+\tilde{E}_1=\mathbf{0}, \tag{32}$$

Moreover, from the extremal equation

$$\frac{\partial J_{total}}{\partial\hat{\rho}_e}=\mathbf{0},$$

we obtain

$$-c\sqrt{c^2-v_e^2}-E_{51}(z,t)+\tilde{E}_2=0,$$

and from the extremal equation

$$\frac{\partial J_{total}}{\partial\hat{\rho}_p}=\mathbf{0},$$

we obtain

$$-c\sqrt{c^2-v_p^2}-E_{51}(z,t)+\tilde{E}_3=0,$$

for appropriate functions $\tilde{E}_2$ and $\tilde{E}_3$.

From these last two equations, neglecting $\tilde{E}_2$ and $\tilde{E}_3$, we obtain

$$-\int_\Omega\int_\Omega \hat{\rho}_e c\sqrt{c^2-v_e^2}\,dxdy-\int_\Omega\int_\Omega \hat{\rho}_p c\sqrt{c^2-v_p^2}\,dxdy$$
$$-E_{51}(z,t)\left(\int_\Omega\int_\Omega \hat{\rho}_e\,dxdy+\int_\Omega\int_\Omega \hat{\rho}_p\,dxdy\right)\approx 0, \tag{33}$$

so that

$$-\int_\Omega\int_\Omega \hat{\rho}_e c\sqrt{c^2-v_e^2}\,dxdy-\int_\Omega\int_\Omega \hat{\rho}_p c\sqrt{c^2-v_p^2}\,dxdy-E_{51}(z,t)\rho\approx 0,$$

that is,

$$E_{51}(z,t)\rho\approx -C_v\rho T.$$

Moreover from (32), neglecting $\tilde{E}_1$, we have

$$\frac{\rho}{2}\mathbf{v}\cdot\mathbf{v}+P-\rho\mathbf{g}\cdot\mathbf{r}\approx -E_{51}(z,t)\rho=K_5\rho T \tag{34}$$

for an appropriate constant $K_5>0$.

From such a result we have also obtained the following Bernoulli-perfect-gas equation

$$\frac{P}{\rho}+\frac{1}{2}\mathbf{v}\cdot\mathbf{v}+gX_3=K_5T+C_3,$$

for an appropriate $C_3\in\mathbb{R}$ and an appropriate $K_5>0$.

In summary, we have got the following Bernoulli-perfect-gas equation

$$P+\frac{\rho}{2}\mathbf{v}\cdot\mathbf{v}+\rho gX_3=K_5\rho T+C_3\rho,$$

for real constant C_3.

Finally, from the variational of J_{total} in $\mathbf{v}$, we obtain

$$\rho\mathbf{v}+E_3+\nabla(\hat{P}\rho)+C_5=\mathbf{0},$$

for an appropriate function C_5. The variation of J_{total} in $\mathbf{r}$, stands for

$$-\rho\mathbf{g}+\frac{dE_3}{dt}+C_7=\mathbf{0},$$

for an appropriate function C_7. Joining the pieces we have got

$$\rho\mathbf{g}+\frac{d(\rho\mathbf{v})}{dt}+\frac{d(\nabla(\hat{P}\rho))}{dt}-C_{10}=\mathbf{0},$$

so that

$$\frac{\partial(\rho \mathbf{v})}{\partial t} + \frac{\partial(\rho \mathbf{v})}{\partial X_j}\frac{\partial X_j}{\partial t} + \nabla P + \rho \mathbf{g} = C_{10},$$

where

$$C_{10} = C_7 - \frac{dC_5}{dt}.$$

This just an approximate version of the well known Euler system.

Moreover, from the variation of J_{total} in $\hat{P}$, we have,

$$\frac{d\rho}{dt} + \rho \text{ div } \mathbf{v} - C_8 = 0,$$

for an appropriate function C_8.

Hence, through the Eulerian identification

$$X_k(y,t) \approx x_k, \ \forall k \in \{1,2,3\},$$

neglecting C_5, C_7, C_8, we have obtained the following approximate macroscopic system,

1. Euler Equations:

$$\frac{\partial(\rho \mathbf{v})}{\partial t} + \frac{\partial(\rho \mathbf{v})}{\partial x_j} v_j + \nabla P = -\rho \mathbf{g}.$$

2. Continuity equation:

$$\frac{d\rho}{dt} + \rho \text{ div } \mathbf{v} = 0,$$

where we have generically (with a not relabeled notation) denoted

$$\rho = \rho(\mathbf{r}(x,t),t),$$

so that with the Eulerian identification

$$X_k(y,t) \approx x_k, \ \forall k \in \{1,2,3\},$$

we have

$$\frac{d\rho}{dt} = \frac{\partial \rho}{\partial t} + \frac{\partial \rho}{\partial x_j} v_j.$$

3. A Temperature T equation:

$$\rho(C_v)\frac{dT}{dt} = K\nabla^2 T$$
$$-P \text{ div } \mathbf{v} + \frac{d(TS)}{dt}. \tag{35}$$

4. A Bernoulli-perfect-gas type equation:

$$P + \frac{\rho}{2}\mathbf{v}\cdot\mathbf{v} + \rho g z = K_5\rho T + C_3\rho.$$

Remark 3.1. *We highlight the functions C_5, C_7, C_8 and C_{10} may be exactly obtained from the exact previous variations of J_{total}.*

4 A numerical example

Let $\Omega = [0,1]\times[0,1] \subset \mathbb{R}^2$ and let $[0, t_f]$ be a time interval.

Consider the following time-dependent, compressible approximate Navier Stokes system, which includes viscosity effects (see [10] for details), where

$$\begin{cases} (\rho u)_t = \nu\nabla^2 u - u(\rho u)_x - v(\rho u)_y - P_x, \\ (\rho v)_t = \nu\nabla^2 v - u(\rho v)_x - v(\rho v)_y - P_y, \\ \rho_t + (\rho u)_x + (\rho v)_y = \varepsilon\nabla^2\rho \\ \rho C_v T_t = K_5\nabla^2 T - P(u_x + v_y) + \Phi, \\ P = -\rho(u^2+v^2)/2 + K_3\rho T - K_3\rho, \qquad \text{in } \Omega\times[0,t_f]. \end{cases} \tag{36}$$

Here,

$$\Phi = 2C_4(u_x^2 + v_y^2) + C_4(u_y + v_x)^2 - (2/3)C_4(u_x + v_y)^2,$$

$\nu > 0$ is a small constant to be specified, $\mathbf{u} = (u, v, T, \rho) \in W^{1,2}(\Omega\times[0,t_f];\mathbb{R}^4)$ where u denotes the fluid velocity in the direction $\mathbf{i} = (1,0) \in \mathbb{R}^2$, v denotes the fluid velocity in the direction $\mathbf{j} = (0,1) \in \mathbb{R}^2$, T is the scalar temperature field, ρ is the fluid density field and P is a concerning pressure field, with the boundary conditions,

$$u(0,y) = \hat{u}_0(y), \text{ in } [0,1],$$

$$u(x,0) = 0, \text{ in } [0,1],$$
$$u(x,1) = 0, \text{ in } [0,1],$$
$$u_x(1,y) = 0, \text{ in } [0,1],$$
$$v(0,y) = 0, \text{ in } [0,1],$$
$$v(x,0) = 0, \text{ in } [0,1],$$
$$v(x,1) = 0, \text{ in } [0,1],$$
$$v_x(1,y) = 0, \text{ in } [0,1],$$
$$\rho \equiv 1, \text{ on } \partial\Omega,$$
$$T \equiv 1, \text{ on } \partial\Omega.$$

We have set $t_f = 1$, $\nu = 0.0055$, $K_5 = 1$, $C_4 = 0.0055$, $\varepsilon = 0.01$ and $K_3 = 100$. Moreover, we have set $m_{10} = 100$ and $\Delta t = d_2 = 1/m_{10}$.

For the solutions u, v, T, ρ obtained for the lines $j_1 = 10$, $j_1 = 50$ and $j_1 = 90$ please see figures from 1 to 12 respectively.

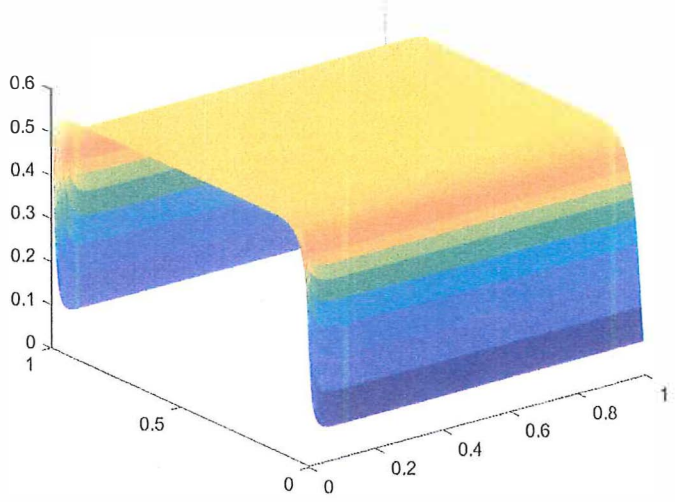

Figure 1: Velocity field $u(x,y)$ for the line $j_1 = 10$ for the case $\nu = 0.0055$.

Here we present the software in MAT-LAB entitled "LinesNavierStokesMarch2026RT1" through such numerical results have been obtained.

****

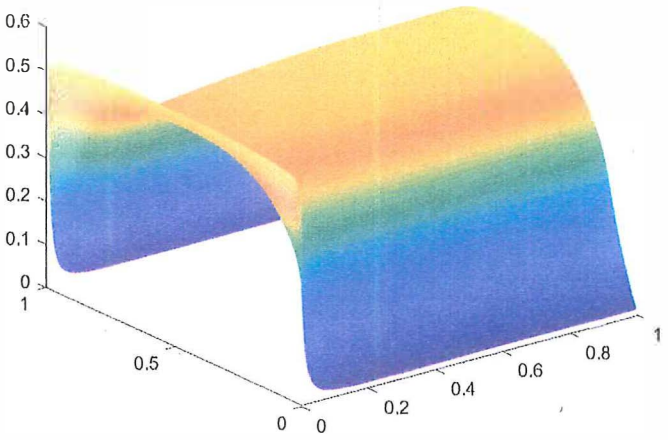

Figure 2: Velocity field $u(x, y)$ for the line $j_1 = 50$ for the case $\nu = 0.0055$.

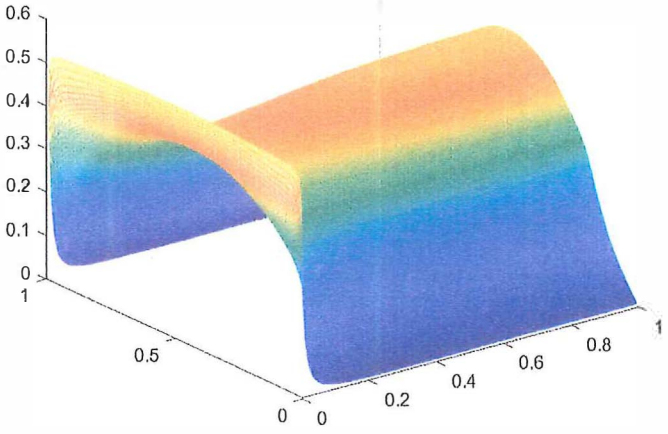

Figure 3: Velocity field $u(x, y)$ for the line $j_1 = 90$ for the case $\nu = 0.0055$.

1. clear all

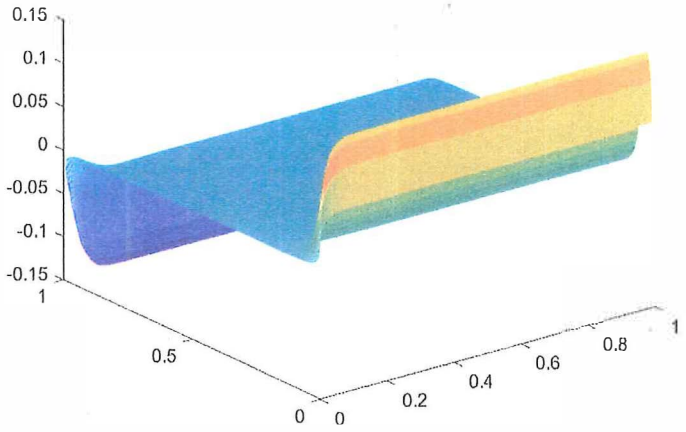

Figure 4: Velocity field $v(x, y)$ for the line $j_1 = 10$ for the case $\nu = 0.0055$.

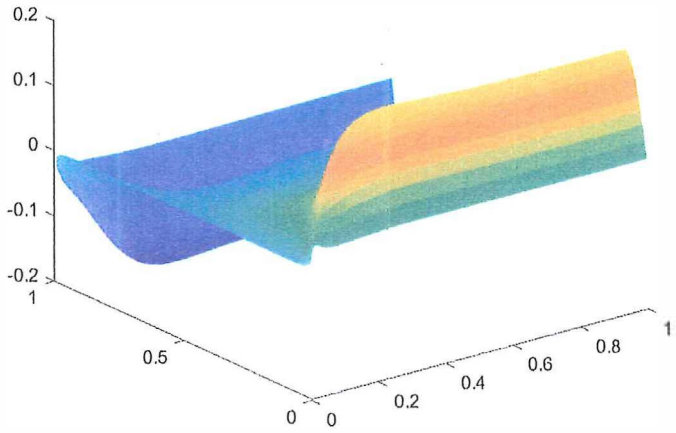

Figure 5: Velocity field $v(x, y)$ for the line $j_1 = 50$ for the case $\nu = 0.0055$.

m8=600;

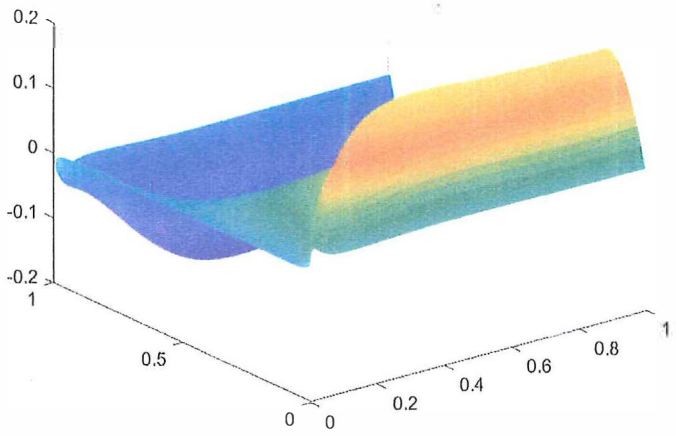

Figure 6: Velocity field $v(x, y)$ for the line $j_1 = 90$ for the case $\nu = 0.0055$.

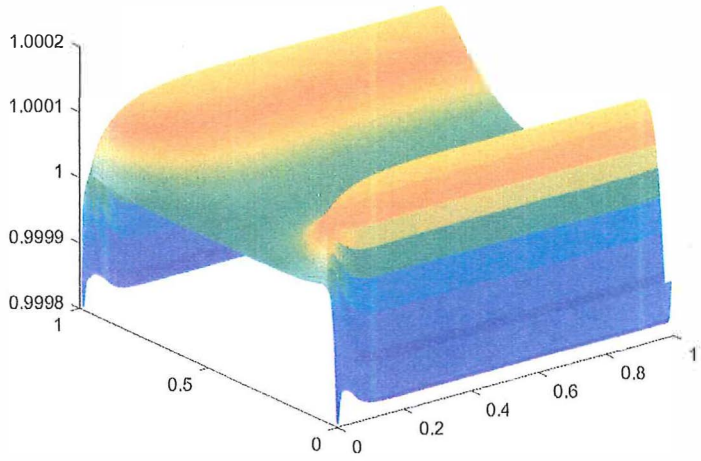

Figure 7: Temperature field $T(x, y)$ for the line $j_1 = 10$ for the case $\nu = 0.0055$.

m9=140;

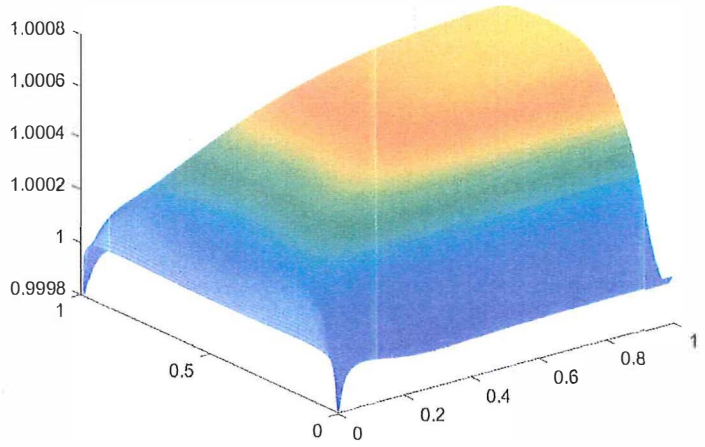

Figure 8: Temperature field $T(x, y)$ for the line $j_1 = 50$ for the case $\nu = 0.0055$.

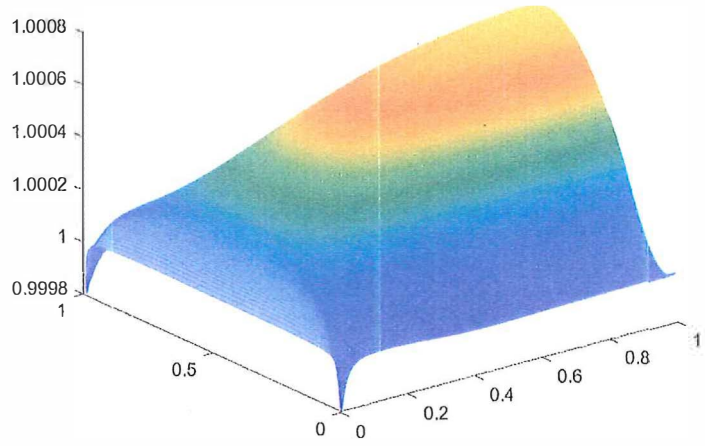

Figure 9: Temperature field $u(x, y)$ for the line $j_1 = 90$ for the case $\nu = 0.0055$.

d=1/m8;

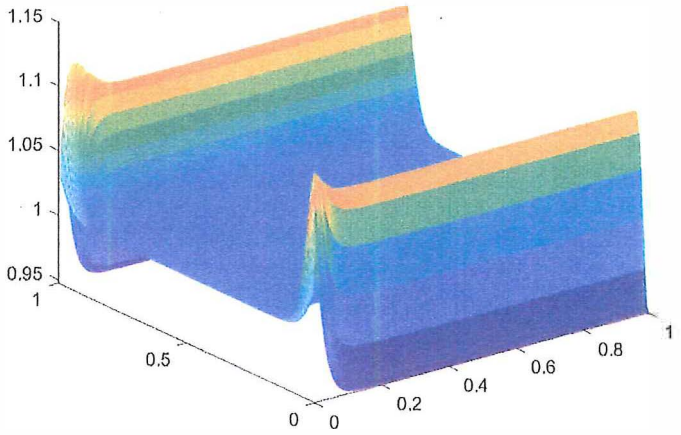

Figure 10: Density field $T(x, y)$ for the line $j_1 = 10$ for the case $\nu = 0.0055$.

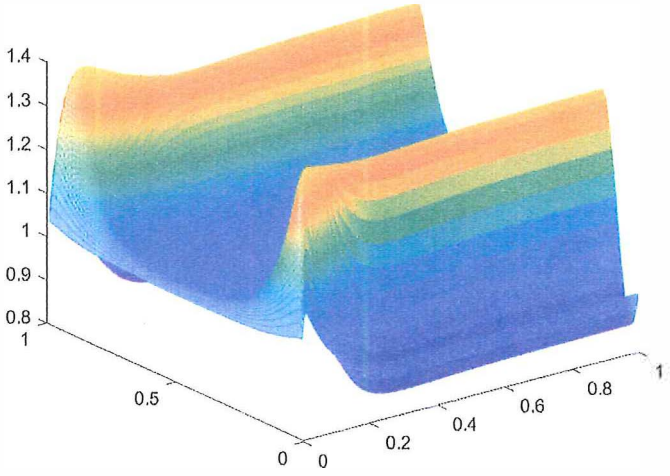

Figure 11: Density field $T(x, y)$ for the line $j_1 = 50$ for the case $\nu = 0.0055$.

d1=1/m9;

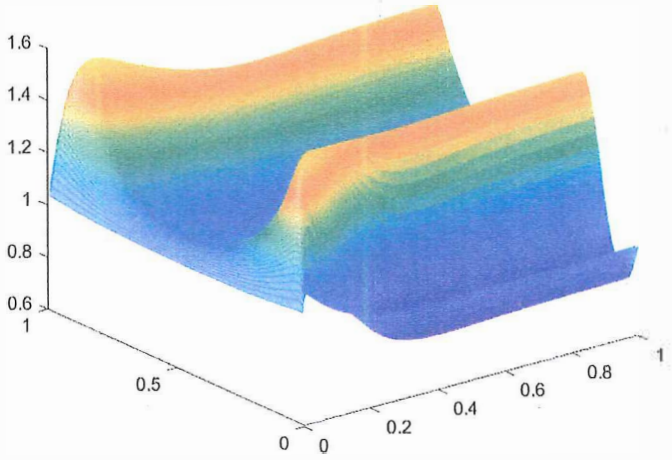

Figure 12: Density field $u(x, y)$ for the line $j_1 = 90$ for the case $\nu = 0.0055$.

```
m10=100;
d2=1/m10;
e1=0.0055;
e5=0.01;
K3=100;
C4=0.0055;
y5(:,1)=0.000000001*ones(m9-1,1);
K5=1;
Id=eye(m9-1);
m2=zeros(m9-1,m9-1);
for i=2:m9-2
m2(i,i)=-2.0;
m2(i,i+1)=1.0;
m2(i,i-1)=1.0;
end;
m2(1,1)=-2;
```

```
m2(1,2)=1;
m2(m9-1,m9-1)=-2;
m2(m9-1,m9-2)=1.0;
m1a=zeros(m9-1,m9-1);
for i=1:m9-2
m1a(i,i)=-1;
m1a(i,i+1)=1;
end;
m1a(m9-1,m9-1)=-1;
m1b=zeros(m9-1,m9-1);
for i=2:m9-1
m1b(i,i)=1;
m1b(i,i-1)=-1.0;
end;
m1b(1,1)=1;
m1=(m1a+m1b)/2;
m22=zeros(m9-1,m9-1);
for i=2:m9-2
m22(i,i)=-2.0;
m22(i,i+1)=1.0;
m22(i,i-1)=1.0;
end;
m22(1,1)=-1;
m22(1,2)=1;
m22(m9-1,m9-1)=-1;
m22(m9-1,m9-2)=1.0;
b8(:,1)=zeros(m9-1,1);
b8(1,1)=1;
b8(m9-1,1)=1;
uoo(:,1)=0.55*ones(m9-1,1);
voo(:,1)=0.0000*ones(m9-1,1);
```

```
Too(:,1)=ones(m9-1,1);
Tf(:,1)=ones(m9-1,1);
roo(:,1)=ones(m9-1,1);
for i=1:m8
uo(:,i)=0.3*ones(m9-1,1);
vo(:,i)=0.0001*ones(m9-1,1);
To(:,i)=ones(m9-1,1);
ro(:,i)=ones(m9-1,1);
u1(:,i)=0.20*ones(m9-1,1);
u3(:,1)=0.20*ones(m9-1,1);
v1(:,i)=0.01*ones(m9-1,1);
T1(:,i)=0.92*ones(m9-1,1);
r1(:,i)=0.95*ones(m9-1,1);
u(:,i,1)=uoo(:,1);
v(:,i,1)=voo(:,1);
T(:,i,1)=Too(:,1);
r(:,i,1)=roo(:,1);
end;
for j1=2:m10
b38=1;
k8=1;
while (b38 > 10^-4) && (k8 < 120)
k8
j1
k8=k8+1;
b12=1;
k=1;
while (b12 > 10^-4) && (k < 200)
k
j1
k=k+1;
```

for i=1:m8

$Po(:,i) = K3 * ro(:,i).*To(:,i) - (uo(:,i).*uo(:,i) + vo(:,i).*vo(:,i)).*ro(:,i)/2 - K3*ro(:,i);$

end;

$Poo(:,1) = K3 * roo(:,1).*Too(:,1) - (uoo(:,1).*uoo(:,1) + voo(:,1).*voo(:,1)).*roo(:,1)/2 - K3*roo(:,1);$

i=1;

$m12 = 2*Id - m2/d1^2*d^2 + diag(ro(:,i))*Id/d2*d^2/e1;$

m50(:,:,i)=inv(m12);

$z1(:,i) = m50(:,:,i)*(uoo(:,1) + r(:,i,j1-1).*u(:,i,j1-1)/d2*d^2/e1 - uo(:,i).*(ro(:,i).*uo(:,i) - roo(:,1).*uoo(:,1))/d*d^2/e1);$

$z1(:,i) = z1(:,i) + m50(:,:,i)*(-vo(:,i).*(m1*(ro(:,i).*uo(:,i)))/d1*d^2/e1 - (Po(:,i) - Poo(:,1))/d*d^2/e1);$

for i=2:m8-1

$m12 = 2*Id - m2/d1^2*d^2 + diag(ro(:,i))*Id/d2*d^2/e1 - m50(:,:,i-1);$

m50(:,:,i)=inv(m12);

$z1(:,i) = m50(:,:,i)*(r(:,i,j1-1).*u(:,i,j1-1)/d2*d^2/e1 - uo(:,i).*(ro(:,i).*uo(:,i) - ro(:,i-1).*uo(:,i-1))/d*d^2/e1);$

$z1(:,i) = z1(:,i) + m50(:,:,i)*(z1(:,i-1) - vo(:,i).*(m1*(ro(:,i).*uo(:,i)))/d1*d^2/e1 - (Po(:,i) - Po(:,i-1))/d*d^2/e1);$

end;

u(:,m8,j1)=inv(Id-m50(:,:,m8-1))*z1(:,m8-1);

for i=1:m8-1

u(:,m8-i,j1)=m50(:,:,m8-i)*u(:,m8-i+1,j1)+z1(:,m8-i);

end;

uo=u(:,:,j1);

b12=max(max(abs(uo-u1)));

u1=uo;

end;

b14=1.0;

k1=1;

while $(b14 > 10^{-4})$ && $(k1 < 200)$

k1

j1

k1=k1+1;

i=1;

$m14 = 2 * Id - m2/d1^2 * d^2 + diag(ro(:,i)) * Id/d2 * d^2/e1;$

m60(:,:,i)=inv(m14);

$z2(:,i) = m60(:,:,i) * (voo(:,1) + r(:,i,j1-1). * v(:,i,j1-1)/d2 * d^2/e1 - uo(:,i). * (ro(:,i). * vo(:,i) - roo(:,1). * voo(:,1))/d * d^2/e1);$

$z2(:,i) = z2(:,i) + m60(:,:,i) * (-vo(:,i). * (m1 * (ro(:,i). * vo(:,i)))/d1 * d^2/e1 - m1 * Po(:,i)/d1 * d^2/e1);$

for i=2:m8-1

$m14 = 2 * Id - m2/d1^2 * d^2 + diag(ro(:,i)) * Id/d2 * d^2/e1 - m60(:,:,i-1);$

m60(:,:,i)=inv(m14);

$z2(:,i) = m60(:,:,i) * (r(:,i,j1-1). * v(:,i,j1-1)/d2 * d^2/e1 - uo(:,i). * (ro(:,i). * vo(:,i) - ro(:,i-1). * vo(:,i-1))/d * d^2/e1);$

$z2(:,i) = z2(:,i) + m60(:,:,i) * (z2(:,i-1) - vo(:,i). * (m1 * (ro(:,i). * vo(:,i)))/d1 * d^2/e1 - m1 * Po(:,i)/d1 * d^2/e1);$

end;

v(:,m8,j1)=inv(Id-m60(:,:,m8-1))*z2(:,m8-1);

for i=1:m8-1

v(:,m8-i,j1)=m60(:,:,m8-i)*v(:,m8-i+1,j1)+z2(:,m8-i);

end;

vo=v(:,:,j1);

b14=max(max(abs(vo-v1)));

v1=vo;

end;

i=1;

$W8(:,i) = 2 * C4 * (uo(:,i) - uoo(:,1))/d. * (uo(:,i) - uoo(:,1))/d + 2 * C4 * m1 * vo(:,i)/d1. * (m1 * vo(:,i)/d1);$

$W8(:,i) = W8(:,i) + C4 * (m1 * uo(:,i)/d1). * (m1 * uo(:,i)/d1) + C4 * (vo(:,i) - voo(:,1))/d. * (vo(:,i) - voo(:,1))/d;$

$W8(:,i) = W8(:,i) - 2/3 * C4 * ((uo(:,i) - uoo(:,1))/d + m1 * vo(:,i)/d1) .* ((uo(:,i) - uoo(:,1))/d + m1 * vo(:,i)/d1);$

for i=2:m8-1

$W8(:,i) = 2 * C4 * (uo(:,i) - uo(:,i-1))/d .* (uo(:,i) - uo(:,i-1))/d + 2 * C4 * m1 * vo(:,i)/d1 .* (m1 * vo(:,i)/d1);$

$W8(:,i) = W8(:,i) + C4 * (m1 * uo(:,i)/d1) .* (m1 * uo(:,i)/d1) + C4 * (vo(:,i) - vo(:,i-1))/d .* (vo(:,i) - vo(:,i-1))/d;$

$W8(:,i) = W8(:,i) - 2/3 * C4 * ((uo(:,i) - uo(:,i-1))/d + m1 * vo(:,i)/d1) .* ((uo(:,i) - uo(:,i-1))/d + m1 * vo(:,i)/d1);$

end;

b16=1.0;

k2=1;

while $(b16 > 10^{-4})$ && $(k2 < 200)$

k2

j1

k2=k2+1;

i=1;

$m16 = 2 * Id - m2/d1^2 * d^2 + diag(ro(:,i)) * Id/d2 * d^2/K5;$

m70(:,:,i)=inv(m16);

$z3(:,i) = m70(:,:,i) * (b8(:,1) * d^2/d1^2 + Too(:,1) + ro(:,i) .* T(:,i,j1-1)/d2 * d^2/K5 + Po(:,i) .* ((uo(:,i) - uoo(:,1))/d + m1 * vo(:,i)/d1) * d^2/K5 - W8(:,i) * d^2/K5);$

for i=2:m8-1

$m16 = 2 * Id - m2/d1^2 * d^2 + diag(ro(:,i)) * Id/d2 * d^2/K5 - m70(:,:,i-1);$

m70(:,:,i)=inv(m16);

$z3(:,i) = m70(:,:,i) * (b8(:,1) * d^2/d1^2 + z3(:,i-1) + ro(:,i) .* T(:,i,j1-1)/d2 * d^2/K5 + Po(:,i) .* ((uo(:,i) - uo(:,i-1))/d + m1 * vo(:,i)/d1) * d^2/K5 - W8(:,i) * d^2/K5);$

end;

T(:,m8,j1)=inv(Id-m70(:,:,m8-1))*z3(:,m8-1);

for i=1:m8-1

T(:,m8-i,j1)=m70(:,:,m8-i)*T(:,m8-i+1,j1)+z3(:,m8-i);

end;

To=T(:,:,j1);

b16=max(max(abs(To-T1)));

T1=To;

end

b30=1;

k5=1;

while $(b30 > 10^{-4})$ && $(k5 < 200)$

k5

j1

k5=k5+1;

i=1;

$m30 = 2 * Id - m2/d1^2 * d^2 + Id/d2 * d^2/e5;$

m80(:,:,i)=inv(m30);

$z5(:,i) = m80(:,:,i) * (b8(:,1) * d^2/d1^2 + roo(:,1) + r(:,i,j1-1)/d2 * d^2/e5 - (ro(:,i) - roo(:,1))/d. * uo(:,i) * d^2/e5 - m1 * ro(:,i)/d1. * vo(:,i) * d^2/e5);$

$z5(:,i) = z5(:,i) + m80(:,:,i) * (-ro(:,i). * ((uo(:,i) - uoo(:,1))/d + m1 * vo(:,i)/d1) * d^2/e5);$

for i=2:m8-1

$m30 = 2 * Id - m2/d1^2 * d^2 + Id/d2 * d^2/e5 - m80(:,:,i-1);$

m80(:,:,i)=inv(m30);

$z5(:,i) = m80(:,:,i) * (z5(:,i-1) + b8(:,1) * d^2/d1^2 + r(:,i,j1-1)/d2 * d^2/e5 - (ro(:,i) - ro(:,i-1))/d. * uo(:,i) * d^2/e5 - m1 * (ro(:,i)/d1). * vo(:,i) * d^2/e5);$

$z5(:,i) = z5(:,i) + m80(:,:,i) * (-ro(:,i). * ((uo(:,i) - uo(:,i-1))/d + m1 * vo(:,i)/d1) * d^2/e5);$

end;

r(:,m8,j1)=inv(Id-m80(:,:,m8-1))*z5(:,m8-1);

for i=1:m8-1

r(:,m8-i,j1)=m80(:,:,m8-i)*r(:,m8-i+1,j1)+z5(:,m8-i);

end;

ro=r(:,:,j1);

b30=max(max(abs(ro-r1)));

```
r1=ro;
end;
b38=max(max(abs(u3-u1)));
u3=u1;
end;
end;
for i=1:m8
x1(i,1)=i*d;
end;
for j=1:m9-1
y1(j,1)=j*d1;
end;
mesh(x1,y1,u(:,:,90))
```

****

5 Conclusion

In this article, we have developed a variational formulation for modeling an atomic hydrogen gas motion in an Euler-Bernoullian context.

In summary, we have obtained a functional such that the variation comprises a set of partial differential equations intended to mathematically model such a fluid motion.

We have obtained the establishment of a system of partial differential equations suitable for compressible fluid mechanics, including a Bernoulli-perfect-gas type equation as previously indicated.

Finally, in the last section we have developed a closely related numerical example.

References

[1] F.S. Botelho, A Variational Formulation for Modeling a Fluid Motion in an Euler-Bernoullian Context: A Detailed Development. J. Eng., 2025: e70097. https://doi.org/10.1049/tje2.70097

[2] F.S. Botelho, Variational formulations for the Euler and Navier-Stokes systems in fluid mechanics and related models. Nonlinear Engineering, vol. 14, no. 1, 2025, pp. 20250097. https://doi.org/10.1515/nleng-2025-0097

[3] P. Constantin , C. Foias. Navier-Stokes equation, University of Chicago Press, Chicago, 1989.

[4] C. De Lellis , E. Brué, D. Albritton, M. Colombo, V. Giri, M. Janisch and H. Kwon. Instability and Non-uniqueness for the 2D Euler Equations, after M. Vishik (AMS-219) Volume 219 in the series Annals of Mathematics Studies, Princeton University Press, New Jersey, 2024. https://doi.org/10.1515/9780691257846

[5] M. Hamouda, D. Han, C.Y. Jung , R. Temam. Boundary layers for the 3D primitive equations in a cube: the zero-mode, Journal of Applied Analysis and Computation. 2018; 8, No. 3, (873-889), DOI:10.11948/2018.873.

[6] A. Giorgini, A. Miranville A, R. Temam. Uniqueness and regularity for the Navier-Stokes-Cahn-Hilliard system, SIAM J. of Mathematical Analysis (SIMA).2019; 51, 3, (2535-2574), https://doi.org/10.1137/18M1223459.

[7] C. Foias , R.M. Rosa, R. Temam . Properties of stationary statistical solutions of the three-dimensional Navier-Stokes equations, J. of Dynamics and Differential Equations, Special issue in memory of George Sell. 2019; 31, 3, 1689-1741, https://doi.org/10.1007/s10884-018-9719-2.

[8] R. Temam Navier-Stokes Equations, AMS Chelsea, reprint (2001).

[9] J.C. Strikwerda finite difference cchemes and partial differential equations, second edition Philadelphia, SIAM, 2004.

[10] J.C. Tannehill, D.A. Anderson, R.H. Pletcher, *Computational Fluid Mechanics and Heat Transfer,* 2nd edn., Taylor and Francis, Philadelphia, PA, 1997.

[11] F.S. Botelho. "Approximate numerical procedures for the Navier-Stokes system through the generalized method of lines" Nonlinear Engineering, vol. 13, no. 1, 2024, pp. 20220376. https://doi.org/10.1515/nleng-2022-0376

[12] F. Botelho. Existence of solution for the Ginzburg-Landau system, a related optimal control problem and its computation by the generalized method of lines, Applied Mathematics and Computation, 2012; 218 (11976-11989).

[13] F.S. Botelho. An approximate proximal numerical procedure concerning the generalized method of lines. Mathematics 2022, 10(16), 2950; https://doi.org/10.3390/math10162950.

[14] F. Botelho. Functional Analysis and Applied Optimization in Banach Spaces, (Springer Switzerland, 2014).

[15] F.S.Botelho. Functional analysis, calculus of variations and numerical methods for models in physics and engineering. Boca Raton, Florida, USA CRC Taylor and Francis; 2020.

[16] F.S. Botelho. Advanced Calculus and its Applications in Variational Quantum Mechanics and Relativity Theory, CRC Taylor and Francis, Florida, 2021.

[17] S. Sheng and Z. Shao, Concentration of mass in the pressureless limit of the Euler equations of one-dimensional compressible fluid flow, Nonlinear Analysis, Real world applications, 52, (2020), 103039. https://doi.org/10.1016/j.nonrwa.2019.103039

[18] R.A. Adams and J.F. Fournier. Sobolev Spaces, 2nd edn. (Elsevier, New York, 2003).

HADRONIC JOURNAL 49, 167 - 177 (2026)
DOI 10.29083/HJ.49.02.2026/SC167

HEAVY QUARKS AND HADRONS: MODEL, THEORY AND NEW SU(3) SYMMETRY

Yi-Fang Chang
Department of Physics
Yunnan University
Kunming, 650091, China
yfc50445@qq.com

Received April 30, 2026

Abstract

First, theories of heavy flavor quarks and hadrons are mainly QCD and Heavy Quark Effective Theory (HQET). Next, based on symmetry we discuss some mass relations. Third, these are extended to lifetimes of heavy hadrons. Fourth, based on the comparison of mass ranges of light quarks and heavy quarks, we propose new possible SU(3) symmetry of heavy hadrons, in which c and b form of double (I=1/2), such light and heavy quarks show complete symmetry. Of course, symmetry breaking will be also inevitable. Finally, some possible development directions of particle physics are researched.

Key words: hadron, heavy quark, mass formula, lifetime, symmetry, development direction.

Copyright © 2026 by Hadronic Press, Inc., Palm Harbor, FL 34684, USA

I. Introduction

In the standard model quarks are the three generations (u,d) (c,s) and (t,b), in which heavy quarks are charm (c), bottom (b), top (t). Neubert reviewed heavy quark symmetry and its applications to weak decays of hadrons containing a single heavy quark [1].

Manohar and Wise studied respectively light and heavy quarks, and their symmetry [2]:

For QCD light quarks $m_q \to 0$, $SU(3)_L \otimes SU(3)_R$, chiral symmetry. $\Lambda_{QCD} >> m_q$.

Heavy quarks $m_Q \to \infty$, spin-flavor symmetry. $\Lambda_{QCD} << m_Q$.

Brambilla, et al., searched heavy quarkonium and its progress, puzzles, and opportunities [3].

It is very successful that the SU(3) symmetry and its broken are applied to the classification of the ground hadrons, which made of u, d and s quarks, and to the mass spectrum, etc. These hadrons agree with the Gell-Mann-Okubo (GMO) mass formula:

$$M = M_0 + AS + B[I(I+1) - \frac{S^2}{4})]. \tag{1}$$

Here must assume that $M = m^2$ for mesons [4,5].

Based on the emergence string and other mechanism, we may derive the GMO mass formula and its modified accurately form [5]. According to the symmetry of s-c quarks, the heavy flavor hadrons which made of u, d and c quarks may be classified by SU(3) octet and decuplet, and some simple mass formulas are obtained, then m(Ξ_{cc})=3715 or 3673MeV are predicted. In July 2017 LHC observed a new and very charming baryon $\Xi_{cc}^{++} = ucc$, whose mass is 3621Mev. It agrees more on new formula, whose error only is 1.4%. Further, we predict m(Ω_{cc}^{+})=3946, or 3950.8, or 3908.2MeV, etc. Moreover, this method may be extended to other heavy flavor hadrons, and predict $m(\Xi_{bb})$=10396.8 or 10348.9MeV, etc. It is a quantitative and testable theory [6]. In this paper, we discuss heavy flavor quarks and hadrons, their models and dynamics, and propose new SU(3) symmetry of heavy quarks.

2. Heavy Hadron Theory and Models

There are some well-known books on the quantum theory of fields and dynamics of the standard model [7,8].

General models of hadrons include quark model, potential models, bag models, lattice QCD, effective quantum field theories, NRQCD, etc. Dynamics includes production, decay (weak, electromagnetic, strong), CP Violation, oscillation, etc.

For heavy quarks Q∈{c,b,t} , the mass m_Q is significantly larger than the QCD confinement scale Λ_{QCD}≈200 MeV, and m(b)≫m(c)≫ Λ_{QCD}. The study of heavy flavor physics is motivated by the hierarchy of scales in Quantum Chromodynamics (QCD).

The separation of light and heavy quarks and hadrons allows for systematic expansions in powers of Λ_{QCD}/m_Q. The heavy quark acts as a static color source, simplifying the non-perturbative dynamics of the light degrees of freedom (light quarks and gluons).

The top quark mass, m(t)≈174GeV is so large that its weak decay width Γ_t exceeds the hadronization scale ($\Gamma_t \gg \Lambda_{QCD}$). Consequently, the top quark decays before it can form bound hadronic states.

The main theories are QCD and Heavy Quark Effective Theory (HQET), which may be applied to heavy-light systems (e.g., B, D mesons).

In the limit $m_Q \to \infty$, the heavy quark velocity is conserved. The spin of the heavy quark decouples from the dynamics.

Symmetries are Heavy Quark Spin Symmetry (HQSS) as the interaction is independent of the heavy quark spin orientation. Heavy Quark Flavor Symmetry as dynamics are independent of m_Q (e.g., B and D systems behave similarly up to $1/m_Q$ corrections).

Lagrangian of heavy quarks is:

$$L = -\frac{1}{4} G^A_{\mu\nu} G^{A\mu\nu} + \bar{q}[\gamma_\mu(\partial_\mu + igA^A_\mu T^A) - m_Q]q \,. \tag{2}$$

Here the strength tensor of gluon field is:

$$G^A_{\mu\nu} = \partial_\mu A^A_\nu - \partial_\nu A^A_\mu - g f^{ABC} A^B_\mu A^C_\nu \,, \tag{3}$$

and $$q = \begin{pmatrix} c \\ b \\ t \end{pmatrix}. \tag{4}$$

For the potential model, Cornell potential is Coulomb potential adds confining potential:

$$V(r) = -\frac{\alpha}{r} + br. \tag{5}$$

This predicts the spectrum of quark-antiquark pair charmonium $\psi(c\bar{c})$ and similar bottomonium $Y(b\bar{b})$ as a non-relativistic system bound by a static potential (5). It combines short-range perturbative gluon exchange and long-range confinement.

Other phenomenological models are the Lattice QCD (LQCD), constituent quark models provided the primary understanding of the hadron spectrum; the bag model, in which confinement is modeled by assuming quarks move freely inside a finite region (bag) with a constant energy density.

The decay constant of heavy mesons is one of the simplest physical quantities applicable for HQET studies [2]. The pseudo-scalar decay constant of B and D mesons is defined by form:

$$< 0 | \bar{q}\gamma^{\mu}\gamma_5 Q(0) | P(p) >= -if_p p^{\mu}. \tag{6}$$

Here the mass dimension of f_p is 1. The vector decay constant of B* and D* mesons is defined by form:

$$< 0 | \bar{q}\gamma^{\mu} Q(0) | P^*(p,\varepsilon) >= f_{p^*}\varepsilon^{\mu}. \tag{7}$$

Here the mass dimension of f_{p^*} is 2.

The decay constant of mesons derives the relations:

$$f_p = \frac{a}{\sqrt{m_p}}, f_{p^*} = a\sqrt{m_{p^*}}. \tag{8}$$

This leads to a significant modification $f_B / f_D = \sqrt{m_D / m_B} \approx 0.6$ on the prediction for heavy quarks [2].

Heavy hadrons are necessarily decays. Another important study is weak decays and CP violation, for which interference between mixing and decay leads to time-dependent CP asymmetries.

3. Mass Formulas, and Mass Relations of Heavy Hadrons

By different ways [4-6], we derived (1) and its modified accurate mass formula:

$$M = M_0 + AS + B[I(I+1) - \frac{S^2}{2})]. \tag{9}$$

Using Eq.(9), for the $J^P = 1^+ / 2$ baryon octet, let M_0=910.75MeV, A=-222.04MeV and B=38.43MeV, so

$m(n) = 939.5725, m(\Lambda) = 1115.6, m(\Sigma^0) = 1192.46, m(\Xi^0) = 1314.89 MeV.$ (10)

Therefore, Eq.(9) agrees completely with the experimental data of the neutral baryons [9].

For the $J^{pc} = 0^{-+}$ meson octet, let A=0, M_0=549.4MeV and B= –207.22MeV, so

$$m(\pi^0) = 134.96, m(K^0) = 497.6, m(\eta) = 549.4 MeV, \quad (11)$$

the neutral mesons agree completely within the range of error [9], and baryon and meson can be unified by M=m.

For the $J^p = 3^+/2$ baryon decuplet I=1+(B+S)/2 always holds, so the formula (9) just derives a more accurate formula

$$M = (M_0 + \frac{15}{4}B) - (A - 2B)S - \frac{B}{4}S^2 = M_0' - aS + bS^2. \quad (12)$$

Let M_0'=1231.8, a=156.8 and b= –3.3MeV, so

$$m(\Delta) = 1231.8, m(\Sigma) = 1385.3, m(\Xi) = 1532.2, m(\Omega) = 1672.5 MeV. \quad (13)$$

Corresponding mass formula (1) and (9) we obtained these mass relations:

$$2[m(N) + m(\Xi)] = 3m(\Lambda) + m(\Sigma),\ 4m(K) = 3m(\eta) + m(\pi). \quad (14)$$

$$4[m(N) + m(\Xi)] = 7m(\Lambda) + m(\Sigma),\ 8m(K) = 7m(\eta) + m(\pi). \quad (15)$$

Heavy quarks are charm (c), bottom (b), top (t). Some baryons with heavy quark c have been found. They include [9]:

$$m(\Lambda_c^+ = udc, I = 0) = 2286.5\,\text{MeV},$$

$$m(\Sigma_c^{++} = uuc, \Sigma_c^+ = udc, \Sigma_c^0 = ddc, I = 1) = 2453\,\text{MeV},$$

$$m(\Xi_c^+, usc) = 2468, m(\Xi_c^0, dsc) = 2472\,\text{MeV},$$

$$m(\Omega_c^0, ssc) = 2695\,\text{MeV}.$$

Some mesons with heavy quark c are:

$$m(D^+, c\bar{d}) = 1869.7, m(D^0, c\bar{u}) = 1864.8\,\text{MeV},$$

$$m(D_s^+, c\bar{s}) = 1968.3\,\text{MeV},$$

$$m(\eta_c, c\bar{c}) = 2980, m(J/\psi, c\bar{c}) = 3097\,\text{MeV}.$$

And there are their excitation states.

Manohar and Wise obtained some mass relations between hadrons based on the symmetry of heavy quarks [2], such as:

$$m(D_s^+, 1968) - m(D^+, 1870) = 98 = m(B_s^0, 5367) - m(B^+, 5279) = 88\,\text{MeV}, \text{ etc.} \quad (16)$$

Assume that (14) or (15) is still tenable, so

$$2[m(N2190, G_{17}) + m(\Xi_c^+)] = 3m(\Lambda_c^+) + m(\Sigma_c^+), (9316 = 9312.5)\,\text{MeV}. \quad (17)$$

Here N(2190) is excited state, and very agree.

$4[m(N2190,G_{17})+m(\Xi_c^+)]=7m(\Lambda_c^+)+m(\Sigma_c^+)$, (18632=18458.5)MeV. (18)

It is suboptimal.

This constitutes decuplet.

$$m(\Omega_c^0,2695)-m(\Xi_c^+,2575)=120=m(\Xi_c^+,2575)-m(\Sigma_c^0,2453)=122. \quad (19)$$

The known $m(\Delta)$=2420, the difference is only 33MeV. It suggests the possible existence $m(\Delta)$=2333MeV.

Similar to the extension to mesons, so

$$4m(D^0)=3m(f_4,2025)+m(\pi_1,1376), \ (7459.2=7451)\text{MeV}. \quad (20)$$

$$8m(D^0)=7m(f_4,2025,I=0)+m(\rho,770,I=1), \ (14918.4=14945)\text{MeV}. \quad (21)$$

Or let $4m(D_1,2422)=3m(\eta_c,2980)+m(\rho,770)$, (9688=9710)MeV. (22)

Some baryons with heavy quark b have been found [9]. They are mixtures of three generations:

$$m(\Lambda_b^0=udb,I=0)=5619.6\text{MeV},$$

$$m(\Sigma_b^+=uub)=5811.3, m(\Sigma_b^0=udb), m(\Sigma_b^-=ddb)=5815.5\text{MeV},$$

$$m(\Xi_b^0,usb)=5791.9, m(\Xi_b^-,dsb)=5797.0\text{MeV},$$

$$m(\Omega_b^-,ssb)=6046.1\text{MeV}.$$

$m(\Sigma_b)>m(\Xi_b)$ is unusual. Some mesons with heavy quark b are:

$$m(B^+,u\bar{b})=5279.3, m(B^0,d\bar{b})=5280\text{MeV},$$

$$m(B_s^0,s\bar{b})=5367, m(B_c^+,c\bar{b})=6275\text{MeV},$$

$$m(Y,b\bar{b})=9460\text{MeV}.$$

And there are their excitation states.

m(K*)–m(K)=396MeV, m(D*)–m(D)=142MeV, m(B*)–m(B)=46MeV. The difference between the two is becoming increasingly smaller.

In addition, there is a mass ratio: $m(B_s^0,s\bar{b}):m(D_s^0,s\bar{c})$ (5367/1968=2.73)= $m(B^0,d\bar{b}):m(D^-,d\bar{c})$ (5280/1870=2.82) = $m(Y,b\bar{b}):m(J/\psi,c\bar{c})$ (9460/3097=3.05).

4. Lifetime Formulas, and Life Relations of Heavy Hadrons

Based on the Y-Q and I-U symmetries between mass and lifetime on the general SU(3) theory, we can derive the lifetime formulas of hyperons and mesons:

$$\tau=A[2U(U+1)-Q/2], \quad (23)$$

And $$\tau=A'[(1/2)+2U(U+1)-Q/2-Q^2/3]. \quad (24)$$

It is a new method on lifetime of hadrons described by quantum numbers, and is symmetrical with corresponding mass formulas, and can be unified for mass and lifetime [4-6].

They agree better with the known lifetimes of hyperons [9]: $\tau(\Xi^0) = 2.90\times10^{-10}s$, $\tau(\Lambda)$ =2.63, $\tau(\Xi^-)$=1.63, $\tau(\Sigma^-)$=1.48, $\tau(\Sigma^+)$=0.80, $\tau(\Sigma^0)$=0.

We obtained a lifetime relation of hyperons [5]:

$$2[\tau(\Xi^0) + \tau(\Sigma^+)](7.404) = \tau(\Lambda) + 3\tau(\Xi^-)(7.549). \quad (25)$$

It is completely analogous to the Gell-Mann mass relation of baryons (14). Further, we extended these formulas to describe masses and lifetime of heavy flavor hadrons [5].

The lifetimes of heavy hadrons are: $\tau(\Lambda_c^+) = 2.00\times10^{-13}s$, $\tau(\Xi_c^+) = 4.42$, $\tau(\Xi_c^0) = 1.12$, $\tau(\Omega_c^0) = 0.69$ [9].

There is a lifetime relation:

$$\tau(\Lambda_c^+) + 2\tau(\Xi_c^0) = \tau(\Xi_c^+)(4.24=4.42), \text{ etc.} \quad (26)$$

The lifetimes of some mesons with heavy quark c are: $\tau(D^+) = 10.4$, $\tau(D^0) = 4.1\times10^{-13}s$, $\tau(D_s^+) = 5.04$. There is a lifetime relation:

$$\tau(D^0) + \tau(D_s^+) = \tau(D^+)(9.14=10.4), \text{ etc.} \quad (27)$$

The lifetimes of some mesons with heavy quark b are [9]:

$$\tau(B^+) = 1.64, \tau(B^0) = 1.53\times10^{-12}s, \ \tau(B_s^0) = 1.47, \tau(B_c^+) = 0.46.$$

There is a lifetime relation:

$$2\tau(B^0) = \tau(B_s^0) + \tau(B^+)(3.06=3.11), \ \tau(B_s^0) = 3\tau(B_c^+)(1.47=1.38), \text{ etc.} \quad (28)$$

5. New SU(3) Symmetry of Heavy Quarks-Hadrons

In the standard model quarks are the three generations (u,d) (c,s) and (t,b), whose properties exhibit a better symmetry. But, first generation (u,d) is I=1/2, other quarks are all I=0. Moreover, masses of various quarks have bigger uncertainty: for light quarks m(u)=1.5-3.0MeV, m(d)=3-7MeV, m(s)=95 $\pm$25MeV, m(c)=1.25 $\pm$0.09GeV, m(b)=4.20 $\pm$0.07GeV, m(t)=174.2 $\pm$3.3GeV [9]. Mass of light quarks is MeV, mass of heavy quarks is GeV.

Based on above masses of quarks m(b)/m(c)=4.2/1.25=3.36=7(m,d)/2.08 (2.08 corresponds mass of u), and m(t)/m(c-b)=174/3=58=95(m,s)/1.64 (1.64 corresponds also to mass of u), we propose new possible SU(3) symmetry on heavy quarks and hadrons, in which assume that c and b form I=1/2 doublet (which are the same with d-u), and t is I=0 with charge=(2/3)e. It is different with charge=(-1/3)e of s. This is

appropriate within the quark mass range. From this model two light quarks and heavy quarks show complete symmetry, and may form respectively two symmetrical SU(3).

The advantage of this model lies in its ability to closely replicate the application of many results of light quarks. For instance, classify of heavy hadrons, mass formulas and corresponding lifetime formulas, etc.

There are baryons: $\Delta_Q^{++} = ccc, \Delta_Q^{+} = ccb, \Delta_Q^{0} = cbb, \Delta_Q^{-} = bbb$ (I=3/2);

$\Sigma_Q^{++} = cct, \Sigma_Q^{+} = cbt, \Sigma_Q^{0} = bbt$ (I=1); $\Xi_Q^{++} = ctt, \Xi_Q^{+} = btt$ (I=1/2) and $\Omega_Q^{++} = ttt$ (I=0).

Mesons include known $J/\psi = c\bar{c}, Y = b\bar{b}$ and $B = c\bar{b}$, and some unknown $c\bar{t}, b\bar{t}, t\bar{t}$, etc.

For heavy mesons [9]

$$m(Y) - m(B_c^{+}) = 3185 = m(B_c^{+}) - m(J/\psi) = 3178. \tag{29}$$

Difference of masses is almost equality. From this we predict the approximate mass equalities of two types on baryons for $\Delta_Q^{++}, \Delta_Q^{+}, \Delta_Q^{0}, \Delta_Q^{-}$, and $\Delta_Q^{++}, \Sigma_Q^{++}, \Xi_Q^{++}, \Omega_Q^{++}$.

The similar Gell-Mann-Okubo (GMO) mass formula will be probably:

$$M = M_0 + AT + B[I(I+1) - \frac{T^2}{4})]. \tag{30}$$

Naturally, masses of various heavy hadrons vary significantly. Moreover, as quark mass increases, greater symmetry breaking inevitably occurs. It is also the symmetry breaking between light and heavy quarks and hadrons. Additionally, there are the mixtures of light quarks and heavy quarks, such as baryons $\Lambda_c^{+} = udc$, $\Xi_c^{+} = usc$, and mesons $D^{+} = c\bar{d}$, etc.

6. Research and Summary

Some questions exist still in particle physics, such as nature of exotics, which are probably the XYZ states molecules, tetraquarks, or kinematic effects. We should establish a unified classification scheme.

Strong and weak interactions as short-range should be unified. Except different action ranges their main character is: strong interactions are attraction each other, and weak interactions are mutual repulsion and derive decay. We proposed a new method on their unification, whose coupling constants are negative and positive, respectively

[10,11]. For QED and QCD, beta functions have different signs. The electroweak unification theory has the same sign with QED. Based on the known phenomena of dark energy and dark matter, we proposed the negative matter unified dark matter and dark energy. This is repulsion between positive matter and negative matter, both form two different regions of topological separation, which forms invisible dark matter, and repulsion is dark energy. It agrees on Occam's Razor. It is not only the simplest, and may be calculable, observable and testable, and may be mechanism of inflation [12-17]. Perhaps the current astronomical data can already prove the existence of negative matter, such as some amplifying Einstein rings. If the negative matter is confirmed by some observatories, it will open up a new world. Further, we researched a possible unified scheme of four-interactions [10,18]. It includes the simplified supersymmetry [18].

1988 Nobel Physics Prize gainer L. Lederman, et al., pointed out that we only must be u and d for quark model, both are composed nucleons p and n. Other particles are electron e and neutrino ν_e [19]. In fact first generation of quark-lepton in standard model (u,d; e, ν_e) constructs the whole stability world. 2004 Nobel Physics Prize gainer Wilczek proposed that standard model should reasonably be called the core theory [20,21].

So far the high energy experiments in the past sixty years have shown that the smallest mass fermions are proton, electron, neutrino ν_e and photon, only which are stable, other particles all decay. They form the simplest model of particles [22]. These fermions seem to be inseparable truth "atoms" (elements), because further experiments derive particles with bigger mass from hyperons to Ω_b^- by accelerators at huge energy. They are also the smallest masses fermions with strong, electromagnetic and weak interactions, and $m(\nu_e) \approx 0$, $m(\gamma) = 0$, and correspond to four interactions, and are also only stable particles. Later particles are their complete symmetric excited states, so they decay to the ground state, such as $\mu \to e\bar{\nu}\nu_\mu$ and $\pi^{\pm} \to \mu\nu$, which are strong interactions become into electromagnetic and weak interactions. Then there are particles with higher energy and bigger mass. It is also results of current high energy experiments. Such the final simplest theory is based on leptons (e- ν_e) and nucleons (p-n) or (u-d) in quark model with SU(2) symmetry and corresponding Yang-Mills field. Other particles and quark-lepton are their excited states [22,11].

After three generations of quarks-leptons and Higgs boson have been confirmed, we research some possible development directions of particle physics. First, particles of three generations are extended. Second, the hadronic theory must precision quantification such as heavy flavor hadrons and the lifetime formula, etc. Third, various unifications of interactions are discussed. Fourth, some basic principles are probably violated under some cases [23].

For example, for Pauli Exclusion Principle, in 1978-1980 Santilli proposed the rest of PEP, in particular, under strong interactions [24,25]. Based on some experiments and theories of particles at high energy, we investigated violation of PEP at high energy begin from 1984 [26-30] and researched some possible tests of violation of PEP (VIP) [27,29]. In 2020, we researched another possibility on VIP at ultra-low energy [31], which is similar to superconductivity, superfluids and Bose-Einstein condensation (BEC), etc.

For uncertainty principle, Santilli proposed a unified form of possible generalizations of Heisenberg uncertainty principle for strong interactions [32]. Hadronic mechanics (HM) [33-35] has generalized the uncertainty relations in the only non-trivial way.

We researched uncertain relations of entropy, information and thermodynamics, and proposed the speed of light and some fundamental constants should be uncertain. Further, we searched its possible development in the entanglement, superstring, and the extensive quantum theory, various matters and different phases, etc. Moreover, the irreversibility and statistics are discussed, and we derived operators of entropy, etc [36]. New measuring technology and some developed theories already challenge the uncertainty principle, which may not be held under certain conditions, and must be modified and developed.

Other basic principles are duality, etc. We proposed their precision, systematization of the simplest model and so on [22].

In a word, based on some symmetries among different generations and so on, our research should be those quantitative and testable theories and models.

References

[1] M. Neubert, *Phys.Rep.* 245(**1994**): 259.
[2] A.V. Manohar and M.B. Wise, *Heavy Quark Physics*. Cambridge University Press. **2000**.
[3] N. Brambilla, S. Eidelman, B.K. Heltsley, et al., *Eur.Phys.J.* C71(**2011**):1534.
[4] Yi-Fang Chang, *New Research of Particle Physics and Relativity*. Yunnan Science and Technology Press. **1989**; Phys.Abst. 93(**1990**) No1371.
[5] Yi-Fang Chang, *International Review of Physics*. 6(**2012**):261.
[6] Yi-Fang Chang, *Hadronic J.* 41(**2018**):335.
[7] S. Weinberg, *The Quantum Theory of Fields*. Cambridge University Press. **1995**.
[8] J.F. Donoghue, E. Golowich and B.R. Holstein, *Dynamics of the Standard Model*. Cambridge University Press. **1992**.
[9] M. Tanbashi, et al., Particle Data Group. *Phys. Rev. D.* 98(**2018**):030001.
[10] Yi-Fang Chang, *European Journal of Applied Sciences*. 8(**2020**):28.
[11] Yi-Fang Chang, *International Journal of Modern Theoretical Physics*. 11(**2022**):1.
[12] Yi-Fang Chang, arXiv(**2007**):0705.2908.
[13] Yi-Fang Chang, *International Review of Physics*. 5(**2011**):340.

[14] Yi-Fang Chang, *International Journal of Modern Theoretical Physics*. 2(**2013**):100.
[15] Yi-Fang Chang, *Hadronic J.* 40(**2017**):291.
[16] Yi-Fang Chang, *International Journal of Fundamental Physical Sciences*. 10(**2020**):40.
[17] Yi-Fang Chang, *Negative Matter as Unified Dark Matter and Dark Energy: Theories and Possible Observations*. Sara Book Publication. **2025**.
[18] Yi-Fang Chang, *Hadronic J.* 46(**2023**):97.
[19] L. Lederman and D. Teresi, *The God Particle: If the Universe Is the Answer, What Is the Question*? Boston: Houghton Mifflin. **1993**.
[20] F. Wilczek, *The Lightness of Being: Mass, Ether, and the Unification of Forces*. New York: Basic Books. **2010**.
[21] F. Wilczek, A Beautiful Question: Finding Nature's Deep Design. Brockman Inc. **2015**.
[22] Yi-Fang Chang, *Physical Science & Biophysics Journal*. 5(**2021**): 000196.
[23] Yi-Fang Chang, *Hadronic J.* 47(**2024**):15.
[24] R.M. Santilli, *Hadronic J.* 1(**1978**): 223.
[25] C.N. Ktorides, H.C. Myung and R.M. Santilli, *Phys.Rev.* D22(**1980**): 892.
[26] Yi-Fang Chang, *Hadronic J.* 7(**1984**): 1118.
[27] Yi-Fang Chang, *Hadronic J.* 7(**1984**): 1469.
[28] Yi-Fang Chang, *In Hadronic Mechanics and Nonpotential Interactions*, Par2. H.C. Myung, Ed. (Nova Science Publishers,Inc. **1992**. 169.
[29] Yi-Fang Chang, *Hadronic J.* 22(**1999**): 257.
[30] Yi-Fang Chang, *International Review of Physics*. 7(**2013**): 299.
[31] Yi-Fang Chang, *Hadronic J.* 43(**2020**): 161.
[32] R.M. Santilli, *Hadronic J.* 4(**1981**):642.
[33] R. M. Santilli, Elements of Hadronic Mechanics, Ukraine Academy of Sciences, Kiev, Volume I (**1995**), Mathematical Foundations.
[34] R. M. Santilli, Elements of Hadronic Mechanics, Ukraine Academy of Sciences, Kiev, Volume II (**1996**), Theoretical Foundations.
[35] R. M. Santilli, Elements of Hadronic Mechanics, Ukraine Academy of Sciences, Kiev, Volume III (**2016**), Experimental verifications.
[36] Yi-Fang Chang, *Hadronic J.* 44(**2021**):357.

HADRONIC JOURNAL 49, 179 – 195 (2026)
DOI 10.29083/HJ.49.02.2026/SC179

THREE-DIMENSIONAL QUANTUM MECHANICS IN THE ENERGY DOMAIN: A TIME FREE TREATMENT OF THE HYDROGEN ATOM

Dr. Michail Lazos
Department of Computing
Manchester Innovation and Technology Center
Dubai, UAE
mlazos@hotmail.com
Semen Ivanov
Imperial College of London

Received April 1, 2026
Revised April 23, 2026

Abstract

In earlier work we proposed a time-free reformulation of quantum mechanics in which the usual temporal evolution is replaced by an auxiliary evolution in the energy domain. The purpose of the present paper is to extend that idea to the full three-dimensional Schrödinger equation and to test it on the hydrogen atom, which is the standard benchmark for any formulation of nonrelativistic quantum mechanics.

We show that the energy-domain wavefunction separates into a stationary spatial eigenfunction and an energy-dependent phase. As a result, the spatial problem remains exactly the same as in the conventional stationary theory. The angular sector still gives the spherical harmonics, the radial Coulomb equation keeps its standard form, and the familiar hydrogenic spectrum, degeneracies, and radial eigenfunctions are recovered without modification.

The analysis also shows that the auxiliary parameter z contributes only a global phase and does not affect probability densities, expectation values, or spectral differences. For time-independent Hamiltonians, the present construction is therefore not a new dynamics but an equivalent representation of standard quantum mechanics written without explicit time. The hydrogen atom and its spectrum provide a direct and complete check of that equivalence.

Keywords: time-free quantum mechanics; energy-domain evolution; three-dimensional Schrödinger equation; hydrogen atom; spherical harmonics; associated Laguerre polynomials; stationary states

Copyright © 2026 by Hadronic Press, Inc., Palm Harbor, FL 34684, USA

1 Introduction

In standard nonrelativistic quantum mechanics, time appears as the external parameter that drives the evolution of the wavefunction through the Schrödinger equation. That formulation is extremely successful, but the role of time has also been questioned in a number of foundational discussions, especially in settings where one expects time to be emergent rather than fundamental [6, 1, 7, 5, 2]. The motivation of the present work comes from that line of thought. The question we address is simple: for stationary quantum systems, how much of the physical content of the theory really depends on writing the evolution in terms of time?

In our earlier paper we proposed a reformulation in which time is removed and the evolution is written in the energy domain instead [4]. The goal was not to alter the measurable content of quantum mechanics, but to reorganize the formalism so that the usual stationary eigenvalue equation emerges directly from differentiation with respect to energy. In that construction the modified generator is written as

$$\widehat{H}_b = \frac{i\hbar}{2z}\frac{\partial}{\partial E}, \tag{1}$$

and the corresponding wavefunction is taken to be

$$\Psi(\mathbf{r}, E) = \psi(\mathbf{r}) \exp\left(-\frac{iE^2 z}{\hbar}\right), \tag{2}$$

where z is an auxiliary evolution label in energy space.

The form of $\widehat{H}_b$ is fixed by consistency with the phase in (Eq. 2). Indeed,

$$\frac{\partial}{\partial E}\exp\left(-\frac{iE^2 z}{\hbar}\right) = -\frac{2iEz}{\hbar}\exp\left(-\frac{iE^2 z}{\hbar}\right),$$

so the factor $1/(2z)$ ensures that the operator returns the usual energy eigenvalue E. In this way, the dependence on z is confined to a global phase, while the spatial part of the theory remains the same as in ordinary quantum mechanics.

The goal of the present paper is to extend this time-free construction to three dimensions and then apply it to the hydrogen atom. This is the

natural test case. It contains angular momentum, separation in spherical coordinates, a Coulomb potential, associated Laguerre polynomial solutions, and a discrete bound-state spectrum that is known in closed form. If the energy-domain formulation is to be taken seriously, it must reproduce all of these features exactly.

We therefore begin with the three-dimensional energy-based Schrödinger equation

$$\frac{i\hbar}{2z}\frac{\partial \Psi}{\partial E} = \left[-\frac{\hbar^2}{2m}\nabla^2 + V(r)\right]\Psi, \tag{3}$$

and substitute the ansatz (Eq. 2). The result is the purely spatial eigenvalue problem

$$\left[-\frac{\hbar^2}{2m}\nabla^2 + V(r)\right]\psi(\mathbf{r}) = E\,\psi(\mathbf{r}), \tag{4}$$

which is identical to the standard stationary Schrödinger equation [3, 8]. All observables therefore come from $\psi(\mathbf{r})$, while the energy-dependent phase plays no direct physical role.

For the hydrogen atom, the corresponding radial equation becomes

$$-\frac{\hbar^2}{2m}\frac{d^2u}{dr^2} + \left[\frac{\hbar^2\ell(\ell+1)}{2mr^2} - \frac{e^2}{4\pi\varepsilon_0 r}\right]u(r) = E\,u(r), \tag{5}$$

with $u(r) = rR(r)$. Solving this equation by the standard asymptotic and power-series method leads to the familiar hydrogenic spectrum

$$E_n = -\frac{me^4}{2(4\pi\varepsilon_0)^2\hbar^2}\frac{1}{n^2}, \qquad n = 1, 2, 3, \ldots, \tag{6}$$

together with the usual associated Laguerre polynomial solutions.

The paper is organized as follows. In Section 2 we derive the three-dimensional form of the energy-domain equation and separate it in spherical coordinates. Section 3 discusses observables and the role of the auxiliary parameter z. Section 4 compares the present construction with the standard time-dependent Schrödinger equation. Section 5 applies the method to the hydrogen atom, and Section 7 shows explicitly how the known hydrogen spectrum is recovered. We then discuss the scope of the formulation and summarize the main conclusions.

2 Energy-Domain Schrödinger Equation in Three Dimensions

We now write the energy-based formulation in full three-dimensional form. The main point of this section is that once the energy-dependent phase is factored out, the remaining spatial problem is exactly the same one that appears in conventional stationary quantum mechanics. For that reason, the whole angular momentum structure survives unchanged.

For a particle of mass m moving in a central potential $V(r)$, the spatial eigenvalue problem is

$$\left[-\frac{\hbar^2}{2m}\nabla^2 + V(r)\right]\psi(\mathbf{r}) = E\,\psi(\mathbf{r}), \tag{7}$$

where $\mathbf{r} = (r, \theta, \phi)$ denotes the spherical coordinates shown in Fig. 1

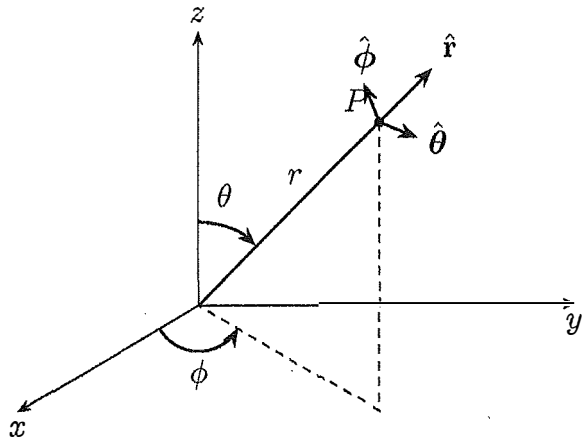

Figure 1: Spherical coordinates showing the radial distance r, polar angle θ, and azimuthal angle ϕ.

The Laplacian in spherical coordinates is

$$\nabla^2 = \frac{1}{r^2}\frac{\partial}{\partial r}\left(r^2\frac{\partial}{\partial r}\right) + \frac{1}{r^2\sin\theta}\frac{\partial}{\partial\theta}\left(\sin\theta\,\frac{\partial}{\partial\theta}\right) + \frac{1}{r^2\sin^2\theta}\,\frac{\partial^2}{\partial\phi^2}. \tag{8}$$

Substituting (Eq. 8) into (Eq. 7) gives

$$-\frac{\hbar^2}{2m}\left[\frac{1}{r^2}\frac{\partial}{\partial r}\left(r^2\frac{\partial\psi}{\partial r}\right)+\frac{1}{r^2\sin\theta}\frac{\partial}{\partial\theta}\left(\sin\theta\,\frac{\partial\psi}{\partial\theta}\right)+\frac{1}{r^2\sin^2\theta}\,\frac{\partial^2\psi}{\partial\phi^2}\right]+V(r)\psi=E\psi. \tag{9}$$

To separate the variables we use the standard product ansatz

$$\psi(\mathbf{r})=R(r)\,Y(\theta,\phi), \tag{10}$$

where $R(r)$ contains the radial dependence and $Y(\theta,\phi)$ contains the angular dependence. Inserting (Eq. 10) into (Eq. 9) and dividing by $R(r)Y(\theta,\phi)$ yields

$$-\frac{\hbar^2}{2m}\left[\frac{1}{Rr^2}\frac{d}{dr}\left(r^2\frac{dR}{dr}\right)+\frac{1}{Yr^2\sin\theta}\frac{\partial}{\partial\theta}\left(\sin\theta\,\frac{\partial Y}{\partial\theta}\right)+\frac{1}{Yr^2\sin^2\theta}\,\frac{\partial^2Y}{\partial\phi^2}\right]+V(r)=E. \tag{11}$$

After multiplying by $2mr^2/\hbar^2$, the equation separates as

$$-\frac{1}{R}\frac{d}{dr}\left(r^2\frac{dR}{dr}\right)+\frac{2mr^2}{\hbar^2}\big[V(r)-E\big]=\frac{1}{Y}\left[\frac{1}{\sin\theta}\frac{\partial}{\partial\theta}\left(\sin\theta\,\frac{\partial Y}{\partial\theta}\right)+\frac{1}{\sin^2\theta}\,\frac{\partial^2Y}{\partial\phi^2}\right]. \tag{12}$$

The left-hand side depends only on r, while the right-hand side depends only on θ and ϕ. Both sides must therefore be equal to the same constant. Writing that constant as $-\ell(\ell+1)$, we obtain the angular equation

$$\frac{1}{\sin\theta}\frac{\partial}{\partial\theta}\left(\sin\theta\,\frac{\partial Y}{\partial\theta}\right)+\frac{1}{\sin^2\theta}\,\frac{\partial^2Y}{\partial\phi^2}=-\ell(\ell+1)\,Y(\theta,\phi), \tag{13}$$

and the radial equation

$$-\frac{1}{R}\frac{d}{dr}\left(r^2\frac{dR}{dr}\right)+\frac{2mr^2}{\hbar^2}\big[V(r)-E\big]=\ell(\ell+1). \tag{14}$$

Equation (Eq. 13) is the familiar eigenvalue problem for orbital angular momentum,

$$\widehat{L}^2Y_\ell^m(\theta,\phi)=\ell(\ell+1)\hbar^2\,Y_\ell^m(\theta,\phi), \tag{15}$$

whose solutions are the spherical harmonics $Y_\ell^m(\theta,\phi)$.

It is convenient to define the reduced radial function $u(r) = rR(r)$. The radial equation then becomes

$$-\frac{\hbar^2}{2m}\frac{d^2u}{dr^2} + \left[\frac{\hbar^2\ell(\ell+1)}{2mr^2} + V(r)\right]u(r) = E\,u(r), \tag{16}$$

which is exactly the standard one-dimensional radial Schrödinger equation in an effective potential. The important point is that nothing in the spatial derivation changes. The energy-domain formulation leaves the angular and radial sectors untouched; all of the novelty is carried only by the global phase in (Eq. 2).

3 Observables in the Energy-Domain Picture

Once the wavefunction has been written in the form of (Eq. 2), the interpretation of observables becomes straightforward. The whole observable content is encoded in the spatial eigenfunction $\psi(\mathbf{r})$, while the parameter z appears only through a phase factor.

We write the full state as

$$\Psi(\mathbf{r}, E) = \psi(\mathbf{r})\,\exp\left(-\frac{iE^2z}{\hbar}\right), \tag{17}$$

with $\psi(\mathbf{r})$ solving the stationary Schrödinger equation. The corresponding probability density is therefore

$$\rho(\mathbf{r}) = |\Psi(\mathbf{r}, E)|^2 = |\psi(\mathbf{r})|^2, \tag{18}$$

which is independent of z. This means that the spatial distribution of the particle is exactly the same as in the usual stationary formulation.

The same conclusion holds for expectation values. If $\widehat{A}$ is any operator acting on the spatial degrees of freedom, then

$$\langle A\rangle = \int \psi^*(\mathbf{r})\,\widehat{A}\,\psi(\mathbf{r})\,d^3\mathbf{r}, \tag{19}$$

so position, momentum, angular momentum, and energy expectation values are unchanged. The extra phase cancels because it is global.

The generator that appears in the present construction is

$$\widehat{H}_b = \frac{i\hbar}{2z}\frac{\partial}{\partial E}, \tag{20}$$

and its role is only to reproduce the energy eigenvalue through the derivative of the quadratic phase. It does not alter the spatial sector of the theory. In that sense it plays a role similar to the factor $\exp(-iEt/\hbar)$ in ordinary stationary quantum mechanics: it carries the evolution label, but it does not change the measurable content of an energy eigenstate.

The operator algebra also remains the same. In particular, the canonical commutation relations

$$[\hat{x}_i, \hat{p}_j] = i\hbar\,\delta_{ij}, \tag{21}$$

and the usual angular momentum commutation relations are not modified. The present formulation is therefore not a replacement for the kinematics of quantum mechanics. It is a different way of organizing the same kinematics and the same stationary dynamics.

For that reason, the auxiliary parameter z should not be interpreted as a new physical coordinate. In this paper it is only an evolution label. Changing z changes the overall phase of the state, but it does not move the particle, change the spectrum, or alter any expectation value. Different values of z therefore correspond to the same physical stationary state written with a different global phase convention.

The physical meaning of the construction is then clear. The energy-domain formulation is not introducing new observables. Instead, it makes explicit that for stationary systems the measurable physics already sits entirely in the spatial eigenvalue problem. The role usually assigned to temporal phase evolution can be rewritten as an energy-domain phase evolution without changing what can actually be observed.

4 Comparison with the Standard Time-Dependent Formulation

It is useful to compare the present construction directly with the standard time-dependent Schrödinger equation. This makes the relation between the

two formulations transparent and shows more clearly what has changed and what has not.

In ordinary quantum mechanics, the state evolves according to

$$i\hbar\frac{\partial\Psi(\mathbf{r},t)}{\partial t} = \widehat{H}\Psi(\mathbf{r},t), \tag{22}$$

where $\widehat{H}$ is the Hamiltonian. If the Hamiltonian is time-independent, the solution can be separated as

$$\Psi(\mathbf{r},t) = \psi(\mathbf{r})\,\exp\left(-\frac{iEt}{\hbar}\right), \tag{23}$$

with $\psi(\mathbf{r})$ satisfying

$$\widehat{H}\psi(\mathbf{r}) = E\psi(\mathbf{r}). \tag{24}$$

For stationary states, all measurable information is contained in $\psi(\mathbf{r})$, and the factor $\exp(-iEt/\hbar)$ contributes only a phase.

The same pattern appears in the energy-domain picture. There we write

$$\Psi(\mathbf{r},E) = \psi(\mathbf{r})\,\exp\left(-\frac{iE^2z}{\hbar}\right), \tag{25}$$

and the spatial function $\psi(\mathbf{r})$ again solves the stationary eigenvalue equation. The structure is therefore parallel: in both descriptions the state factorizes into a spatial eigenfunction and a phase factor, and in both descriptions the observable content is carried by the spatial part.

The difference lies in the parameter used to write that phase. In the standard theory the phase is written in terms of the external time parameter t. In the present approach the phase is written in terms of the energy variable E and the auxiliary label z. The parameter z is not interpreted as an observable coordinate; it simply indexes the phase in the energy representation.

From the formal point of view, the evolution law

$$\frac{i\hbar}{2z}\frac{\partial\Psi}{\partial E} = \widehat{H}\Psi, \tag{26}$$

plays the role analogous to the time derivative in (Eq. 22). Because the derivative acts only on the exponential factor in (Eq. 25), the spatial eigenfunctions are left unchanged. This is the reason the two formulations agree on spectra, expectation values, and all stationary observables.

The correspondence is especially clear for a bound system such as hydrogen. The geometry of the orbitals, the angular momentum quantum numbers, the degeneracies, and the radial probability densities all come from the spatial equation. Whether one writes the global phase with t or with the pair (E, z) does not alter any of that structure.

The conclusion of the comparison is therefore straightforward. For time-independent Hamiltonians, the present formalism should be understood as an equivalent representation of standard quantum mechanics, not as a competing dynamical theory. It removes explicit time from the formulation, but it does not remove or change the physical predictions of the stationary theory.

5 Hydrogen Atom in the Energy-Domain Picture

We now apply the formalism to the hydrogen atom. This is the most important test in the paper, because hydrogen combines a central Coulomb potential, nontrivial angular momentum, and a discrete spectrum known exactly from standard quantum mechanics.

The interaction between the electron and the proton is described by the Coulomb potential

$$V(r) = -\frac{e^2}{4\pi\varepsilon_0 r}, \tag{27}$$

which depends only on the radial coordinate. Substituting this into the general radial equation (Eq. 16) gives

$$-\frac{\hbar^2}{2m}\frac{d^2u}{dr^2} + \left[\frac{\hbar^2\ell(\ell+1)}{2mr^2} - \frac{e^2}{4\pi\varepsilon_0 r}\right] u(r) = E\,u(r), \tag{28}$$

where $u(r) = rR(r)$ is the reduced radial function.

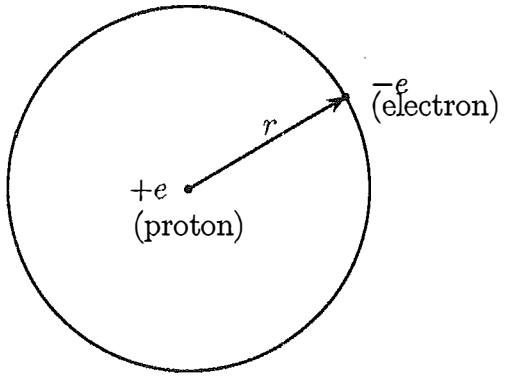

Figure 2: The hydrogen atom.

This equation has exactly the same form as in the standard stationary treatment [3, 8]. The solution therefore follows the familiar sequence of steps, which we summarize here because it shows clearly that no reference to time is needed anywhere in the derivation.

For bound states we have $E < 0$. We define

$$\kappa = \sqrt{\frac{-2mE}{\hbar^2}}, \tag{29}$$

and first study the limiting behaviour of the radial equation. As $r \to \infty$, the Coulomb term becomes negligible and we obtain

$$\frac{d^2u}{dr^2} \approx \kappa^2 u, \tag{30}$$

whose normalizable solution behaves as

$$u(r) \sim e^{-\kappa r}. \tag{31}$$

Near the origin, the centrifugal term is dominant. Keeping only the leading contribution gives

$$\frac{d^2u}{dr^2} \approx \frac{\ell(\ell+1)}{r^2} u, \tag{32}$$

so the regular solution behaves as

$$u(r) \sim r^{\ell+1}. \tag{33}$$

These two limits suggest the standard ansatz

$$u(r) = r^{\ell+1} e^{-\kappa r} v(r), \tag{34}$$

where $v(r)$ is expanded in a power series. Introducing the dimensionless variable

$$\rho = 2\kappa r, \tag{35}$$

and substituting the ansatz into (Eq. 28) leads to the associated Laguerre equation. Normalizability requires the series to terminate, and that condition produces the quantization of the bound states.

Writing the radial quantum number as $n_r = 0, 1, 2, \ldots$, the principal quantum number is

$$n = \ell + 1 + n_r, \qquad n = 1, 2, 3, \ldots, \tag{36}$$

and the termination condition may be written as

$$\kappa = \frac{1}{n a_0}, \tag{37}$$

where the Bohr radius is

$$a_0 = \frac{4\pi\varepsilon_0 \hbar^2}{m e^2}. \tag{38}$$

Substituting (Eq. 37) into (Eq. 29) gives the hydrogen spectrum

$$E_n = -\frac{m e^4}{2(4\pi\varepsilon_0)^2 \hbar^2} \frac{1}{n^2}, \qquad n = 1, 2, 3, \ldots, \tag{39}$$

which is the standard textbook result.

The normalized radial wavefunctions are

$$R_{n\ell}(r) = \mathcal{N}_{n\ell} \left(\frac{2r}{n a_0}\right)^{\ell} e^{-r/(n a_0)} L^{2\ell+1}_{n-\ell-1}\left(\frac{2r}{n a_0}\right), \tag{40}$$

where $\mathcal{N}_{n\ell}$ is the normalization constant. Combining the radial and angular parts gives

$$\psi_{n\ell m}(\mathbf{r}) = R_{n\ell}(r)\, Y_\ell^m(\theta, \phi), \tag{41}$$

with the usual degeneracy in ℓ and m for fixed n.

Finally, the full wavefunction in the energy-domain formulation is obtained by restoring the phase factor,

$$\Psi_{n\ell m}(\mathbf{r}, E) = \psi_{n\ell m}(\mathbf{r})\, \exp\left(-\frac{iE^2 z}{\hbar}\right). \tag{42}$$

This factor depends only on the energy eigenvalue and the auxiliary parameter z. It does not modify probability densities, selection of bound states, angular momentum structure, or expectation values.

The conclusion of the hydrogen analysis is therefore direct. The energy-domain formulation reproduces the full hydrogen problem exactly: the same radial equation, the same eigenfunctions, the same degeneracies, and the same discrete energies. Replacing time by the auxiliary parameter z changes only the global phase convention.

6 Scope and Possible Extensions

The hydrogen atom shows clearly what the present formulation can do. It reproduces a complete three-dimensional bound-state problem without introducing time as a fundamental variable. It is therefore useful to state carefully the range over which this conclusion holds.

The essential structural point is the factorization

$$\Psi(\mathbf{r}, E) = \psi(\mathbf{r})\, \exp\left(-\frac{iE^2 z}{\hbar}\right), \tag{43}$$

together with the stationary eigenvalue problem

$$\widehat{H}\psi(\mathbf{r}) = E\psi(\mathbf{r}), \tag{44}$$

from which the measurable content of the theory is extracted. Whenever a system is described by a time-independent Hamiltonian and admits such a

stationary decomposition, the present energy-domain representation reproduces the same spectrum and the same eigenstates as the standard formulation.

This means that the construction applies naturally to a broad class of stationary bound-state systems, including other central potentials and multidimensional separable problems. In all such cases, the quantization comes from boundary conditions, symmetry, and normalizability. It does not require time to appear explicitly in the formalism.

At the same time, the present paper is intentionally limited to time-independent Hamiltonians. That is not a weakness of the derivation; it is part of the point. For stationary systems, the usual time dependence already reduces to a phase factor. The energy-domain formulation makes that fact explicit by moving the phase structure into the energy representation.

To go beyond this class of problems, more work is needed. Explicitly time-dependent Hamiltonians would require an energy-domain analogue of ordered evolution. Scattering states would require a treatment of continuum normalization, asymptotic states, and transition amplitudes in energy space. These questions are important, but they lie beyond the scope of the present paper.

Conceptually, the result is still significant. It shows that for a physically important class of systems, time is not needed to recover the measurable predictions of nonrelativistic quantum mechanics. The observables come from the stationary spatial sector, while the auxiliary parameter z keeps track only of an unobservable phase.

7 Hydrogen Spectrum

After deriving the hydrogen eigenstates, it is useful to display the spectrum explicitly. This gives a direct check that the energy-domain formalism recovers not only the abstract eigenvalue problem, but also the familiar numerical structure of the atom.

From (Eq. 37) and (Eq. 39), the allowed energies are

$$E_n = -\frac{me^4}{2(4\pi\varepsilon_0)^2\hbar^2}\frac{1}{n^2}, \qquad n = 1, 2, 3, \ldots. \tag{45}$$

This is the Bohr spectrum obtained from the full Schrödinger solution.

Using the accepted constants, the first few levels are

$$E_1 = -13.6 \text{ eV}, \qquad E_2 = -3.40 \text{ eV}, \qquad E_3 = -1.51 \text{ eV}. \tag{46}$$

More generally, the levels follow the familiar $E_n \propto -1/n^2$ law and accumulate at the ionization limit $E = 0$.

7.1 Spectral lines from energy differences

When the atom makes a transition from an initial state n_i to a lower final state n_f, the emitted photon energy is

$$E_\gamma = E_i - E_f. \tag{47}$$

Substituting the hydrogen energies gives

$$E_\gamma = 13.6 \text{ eV} \left(\frac{1}{n_f^2} - \frac{1}{n_i^2} \right), \qquad n_i > n_f. \tag{48}$$

Relating photon energy to frequency and wavelength through

$$E_\gamma = h\nu, \qquad \nu = \frac{c}{\lambda}, \tag{49}$$

one obtains the standard Rydberg formula

$$\frac{1}{\lambda} = R \left(\frac{1}{n_f^2} - \frac{1}{n_i^2} \right), \tag{50}$$

with

$$R = \frac{me^4}{8\varepsilon_0^2 h^3 c}. \tag{51}$$

The important point is that all of these results follow from the same discrete spatial eigenvalues obtained earlier. The auxiliary parameter z enters only through the global factor in (Eq. 2), so it cannot change any spectral difference.

7.2 Energy-level diagram and series

Figure 3 shows the first few levels together with representative transitions in the Lyman ($n_f = 1$), Balmer ($n_f = 2$), and Paschen ($n_f = 3$) series. The figure is drawn directly from the energies in (Eq. 45) and therefore provides a visual summary of the standard spectroscopic structure recovered by the present approach.

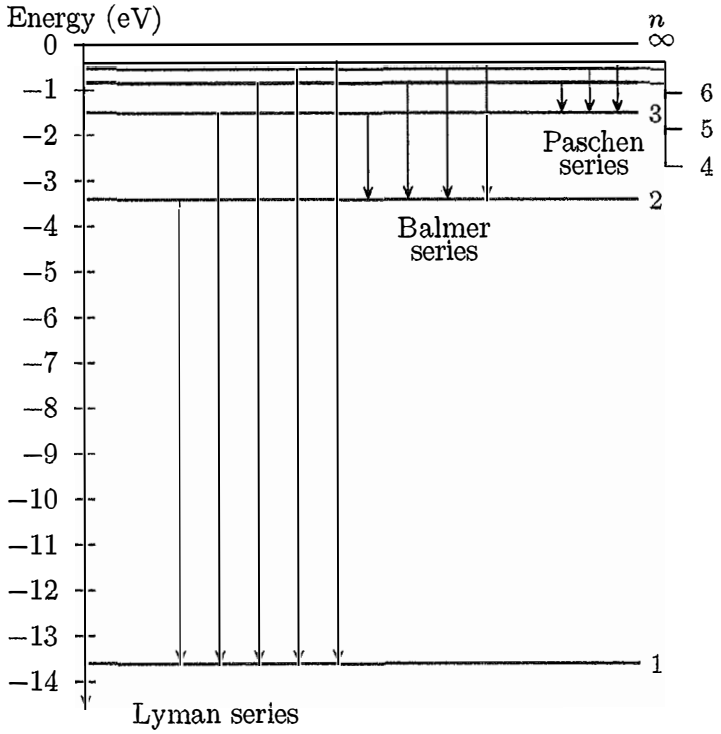

Figure 3: Energy levels and representative transitions in the spectrum of hydrogen.

The experimentally known hydrogen spectrum is therefore recovered in full. The absolute level energies, the transition energies, and the standard spectral series all follow from the same stationary eigenvalue problem as in ordinary quantum mechanics.

8 Conclusions

In this paper we extended the time-free formulation introduced in our earlier work to three-dimensional nonrelativistic quantum mechanics and applied it to the hydrogen atom. The central result is that the energy-domain evolution law separates into a stationary spatial eigenfunction and a global phase depending on E and z. Because of that separation, the spatial part of the theory remains identical to the usual stationary Schrödinger problem.

We then showed that the standard derivation in spherical coordinates goes through without modification. The angular equation still gives the spherical harmonics $Y_\ell^m(\theta, \phi)$, the reduced radial equation keeps its familiar effective-potential form, and for the Coulomb potential one recovers the full hydrogenic spectrum and radial eigenfunctions. The principal quantum number, the ℓ and m degeneracies, and the associated Laguerre polynomial solutions are all the same as in the conventional theory.

We also examined the role of observables and found that the parameter z has no direct measurable meaning in the present framework. It contributes only a global phase, so probability densities, expectation values, and spectral differences are unchanged. In this sense, the formulation is not a modification of quantum mechanics for stationary systems. It is an equivalent representation in which explicit time has been removed.

The hydrogen spectrum provides the clearest check of this statement. Once the Coulomb eigenvalue problem is solved, the Bohr energies, the transition energies, the Rydberg formula, and the Lyman, Balmer, and Paschen series all follow in the usual way. The spectrum therefore confirms at the observable level what the formal analysis already suggested.

The natural next steps are also clear. A full treatment of explicitly time-dependent Hamiltonians, scattering states, and transition amplitudes would require additional development in the energy-domain picture. Even so, the present result already shows that for a broad and important class of time-independent systems, quantum mechanics can be written consistently without taking time as a fundamental parameter.

Declarations

The authors declare that they have no competing interests and that no external financial support was required for this work.

References

[1] Julian Barbour. The timelessness of quantum gravity: I. the dynamics of pure shape. *Classical and Quantum Gravity*, 11:2853–2873, 1994.

[2] S. Biswas, A. Shaw, and B. Modak. Time in quantum gravity. *arXiv preprint*, 1999.

[3] David J. Griffiths. *Introduction to Quantum Mechanics*. Pearson Prentice Hall, Upper Saddle River, NJ, 2 edition, 2005.

[4] Tamás Kovács, Semen Ivanov, Tamás Kovács Jr., and Michail Lazos. From time to energy: A time free quantum framework proposal. *International Journal of Quantum Foundations*, 11:688–712, 2025.

[5] Sam Kuypers and Simone Rijavec. Measuring time in a timeless universe. *arXiv preprint*, 2025.

[6] D. N. Page and W. K. Wootters. Evolution without evolution: Dynamics described by stationary observables. *Physical Review D*, 27(12):2885–2892, 1983.

[7] Carlo Rovelli. Analysis of the distinction between the kinematical and the dynamical parts of the laws of physics. *Annals of Physics*, 1995.

[8] J. J. Sakurai. *Modern Quantum Mechanics*. Addison-Wesley, Reading, MA, revised edition, 1994.

HADRONIC JOURNAL 49, 197 - 212 (2026)
DOI 10.29083/HJ.49.02.2026/SC197

FROM EIGHT-DIMENSIONAL SUPERSYMMETRIC SPACETIME TO NUCLEAR FORCES: A GEOMETRIC DERIVATION OF STRONG INTERACTION PARAMETERS

Zhi Cheng
Guangzhou, China
gzchengzhi@hotmail.com

Received May 27, 2026

Abstract

We present a unified geometric framework in which both electromagnetic and strong nuclear interactions emerge as different projections of a single U(1) gauge field in an eight-dimensional pseudo-manifold $M = M_s \times M_t$, where M_s is a Minkowski subspace and M_t is a temporal subspace with reversed metric signature. By applying Kaluza-Klein compactification to the temporal subspace, we derive the low-energy effective couplings in four-dimensional spacetime. A physical ansatz—setting the first Kaluza-Klein excitation mass to the geometric mean of the electron and proton masses—yields a compactification radius $R_t \approx 9$ fin. From this single scale, combined with the electromagnetic fine-structure constant, we derive the range of the nuclear force ($a \approx 1.75$ fm) and the strong coupling constant ($\alpha_s \sim 1$) using only geometric relations. Remarkably, these derived values agree with experimental data without invoking any detailed quantum chromodynamics. We propose experimental tests via precision deuteron photodisintegration measurements. We also discuss the relation of this framework to Santilli's isodual mathematics for antimatter, which provides a rigorous resolution of the causality issues arising from reversed metric signatures.

Copyright © 2026 by Hadronic Press, Inc., Palm Harbor, FL 34684, USA

1. Introduction

1.1 Our work

The origin of the nuclear force remains one of the central questions in fundamental physics. In the Standard Model, it is described by quantum chromodynamics (QCD), a non-Abelian SU(3) gauge theory with confined gluons and quarks. The strength of the strong interaction, characterized by $\alpha_s \sim 1$ at low energies, and its short range ($r \sim 1.4$ fm), are consequences of asymptotic freedom and confinement. However, QCD introduces a large number of free parameters and a complex infrared structure that makes analytic calculations challenging.

In this work, we explore an alternative geometric origin for the strong interaction. Building on the covariant formulation of supersymmetric spacetime Maxwell equations [1] in an eight-dimensional pseudo-manifold $M = M_s \times M_t$, we show that both electromagnetic and strong interactions can be understood as different projections of a single high-dimensional U(1) gauge field. The difference in their apparent strengths and ranges arises purely from the geometry of the compactified temporal subspace.

Our approach is guided by three key insights:

1. **Compactified virtual time is equivalent to virtual space.** Due to the reversed metric signature of the temporal subspace M_t, its Kaluza-Klein compactification produces a mass spectrum identical to that of compactified spacelike dimensions.
2. **The compactification scale is fixed by a physical ansatz.** The mass of the first KK excitation is set to the geometric mean of the electron and proton masses, yielding a precise value $R_t \approx 9$ fm.
3. **An ultraviolet-infrared duality relates electromagnetic and strong scales.** The relation $ab = R_t^2$ connects the short-range strong interaction scale a with the long-range electromagnetic scale b, allowing us to derive α_s and the nuclear force range from α and R_t alone.

1.2 Santilli's Unification of Electromagnetic and Strong Interactions and the Antimatter Approach

In exploring the unification of electromagnetic and strong interactions, Prof. R. M. Santilli made pioneering contributions. In his series of works and monograph [10], Santilli pointed out that to achieve a unified description incorporating antimatter, one must introduce **isodual mathematics**, in which the isodual conjugate $I^{\dagger} = -I$ replaces the complex conjugate, thereby circumventing the causality problems associated with reversed metric signatures while preserving the formal structure of classical and quantum field theories.

The core physical idea of Santilli is that **antimatter, as the isodual image of matter, manifests itself geometrically as a reversal of the metric signature**. This idea is mathematically highly consistent with the use of the subspace M_t in the present paper, which has reversed signature $\zeta_{\alpha\beta} = \mathrm{diag}(+1, -1, -1, -1)$. Indeed,

Santilli explicitly argued that the duality between positive-definite and indefinite metrics requires a mathematical framework beyond ordinary tensor analysis, and this is precisely the starting point of isodual mathematics.

In our construction $M = M_s \times M_t$, the M_t subspace has positive signature for its time coordinate and negative signature for its space coordinates, which is equivalent to a **four-dimensional isodual spacetime**. Therefore, the geometric framework of this paper can be viewed as a concrete realization of Santilli's isodual approach in an eight-dimensional unification. The key difference is that Santilli introduces antimatter degrees of freedom directly via isodual transformations [11], whereas the present paper generates effective strong interaction scales through **Kaluza-Klein compactification of an extra temporal subspace**. These two approaches may complement each other, both pointing toward a deeper geometric origin of fundamental interactions.

2. The Eight-Dimensional Framework

2.1 Supersymmetric Spacetime Maxwell Equations

We begin with the eight-dimensional pseudo-manifold $M = M_s \times M_t$ introduced

by Cheng [1-3]. The spatial subspace M_s has coordinates x^μ ($\mu = 0,1,2,3$) with Minkowski metric $\eta_{\mu\nu} = \text{diag}(-1,+1,+1,+1)$. The temporal subspace M_t has coordinates y^α ($\alpha = 0,1,2,3$) with reversed signature $\zeta_{\alpha\beta} = \text{diag}(+1,-1,-1,-1)$.

The full eight-dimensional metric is block-diagonal:

$$G_{AB} = \begin{pmatrix} \eta_{\mu\nu} & 0 \\ 0 & \zeta_{\alpha\beta} \end{pmatrix}$$

An eight-dimensional U(1) gauge potential $A_A(z) = (A_\mu(x,y), A_\alpha(x,y))$ is introduced, and the unified field strength tensor is:

$$F_{AB} = \partial_A A_B - \partial_B A_A = \begin{pmatrix} F_{\mu\nu} & \Phi_{\mu\beta} \\ -\Phi_{\alpha\nu} & H_{\alpha\beta} \end{pmatrix}$$

where:

- $F_{\mu\nu} = \partial_\mu A_\nu - \partial_\nu A_\mu$ is the standard electromagnetic field strength,
- $H_{\alpha\beta} = \partial_\alpha A_\beta - \partial_\beta A_\alpha$ is the "magnetic" field strength in M_t,
- $\Phi_{\mu\alpha} = \partial_\mu A_\alpha - \partial_\alpha A_\mu$ is the mixed coupling term connecting the two subspaces.

The equations of motion derived from the eight-dimensional action $S = \int d^8z\sqrt{-G}(-\frac{1}{4}F_{AB}F^{AB})$ are:

$$\partial_B F^{BA} = J^A$$

where $J^A = (J_e^\mu, J_m^\alpha)$ is the eight-dimensional current density.

2.2 Kaluza-Klein Compactification of the Temporal Subspace

The key phenomenological challenge is that the mixed coupling term $\Phi_{\mu\alpha}$ would

mediate interactions between the two subspaces, leading to apparent violations of energy-momentum conservation in four-dimensional observations. To control this, we compactify the temporal subspace M_t on a 3-torus T^3 of characteristic radius R_t.

Equivalence of compact virtual time and virtual space. In standard KK theory [5], compactifying a spacelike extra dimension on a circle of radius R yields a mass spectrum $m_n = | n | /R$. For a temporal dimension with reversed signature, the dispersion relation for a field mode with momentum q^α in the compact dimensions is:

$$q^\alpha q_\alpha = (q^0)^2 - \vec{q}^2$$

Subject to periodic boundary conditions $y^i \sim y^i + 2\pi R_t$, the quantized momenta are $q^i = n_i/R_t$. The effective four-dimensional mass squared is:

$$m_{\vec{n}}^2 = -q^\alpha q_\alpha = -\left(0^2 - \frac{|\vec{n}|^2}{R_t^2}\right) = +\frac{|\vec{n}|^2}{R_t^2}$$

This is identical to the standard spacelike KK result. Therefore, **a compactified temporal dimension with reversed signature is observationally equivalent to a compactified spatial dimension** at the level of the mass spectrum.

3. Fixing the Compactification Scale

3.1 The Geometric Mean Ansatz

To make testable predictions, the free parameter R_t must be fixed. We propose a phenomenological ansatz: **the mass of the first KK excitation is the geometric mean of the electron and proton masses**.

This choice is motivated by:

- The geometric mean naturally interpolates across the large hierarchy between m_e and m_p;

- It corresponds to the midpoint on a logarithmic mass scale, a pattern often appearing in hierarchical symmetry-breaking mechanisms (e.g., the seesaw mechanism).
- From the formula for calculating the Compton wavelength, the mass of a particle is inversely proportional to its Compton wavelength. This also means that the geometric mean of the masses of the electron and proton will result in their Compton wavelengths being inversely related.

Explicitly:

$$\boxed{m_1 = \sqrt{m_e m_p} \approx \sqrt{0.511 \times 938.272}\ \text{MeV}/c^2 \approx 21.90\ \text{MeV}/c^2}$$

Using the KK mass relation $m_1 = \hbar c / R_t$ with $\hbar c \approx 197.326\ \text{MeV} \cdot \text{fm}$:

$$\boxed{R_t = \frac{\hbar c}{m_1 c^2} \approx 9.01\ \text{fm}}$$

This scale is mesoscopic—about ten times the range of the nuclear force, but deeply subatomic. At the same time, we can also see that the Compton wavelengths of electrons and protons are just on either side of R_t. Their relationship can be expressed as:

$$\lambda_p \lambda_e = R_t^2$$

4. Geometric Derivation of Strong Interaction Parameters

4.1 Coupling Constant Reduction from Higher Dimensions

Consider a U(1) gauge theory in $D = 4 + n$ dimensions with action:

$$S_D = \int d^4x\, d^n y \sqrt{-g_D} \left(-\frac{1}{4g_D^2} F_{MN} F^{MN} \right)$$

where g_D is the high-dimensional gauge coupling. After compactifying the n extra dimensions on a manifold of volume V_n, and keeping only the zero-mode (uniform along extra dimensions), we expand:

$$A_\mu(x,y) = \frac{1}{\sqrt{V_n}} A_\mu^{(0)}(x)$$

The field strength scales as $F_{\mu\nu} = \frac{1}{\sqrt{V_n}} F_{\mu\nu}^{(0)}$. Integrating over the extra dimensions:

$$S_4 = \int d^4x \sqrt{-g_4} \cdot \frac{1}{g_D^2} \cdot \frac{1}{V_n} \int d^n y \sqrt{h} \left(-\frac{1}{4} F_{\mu\nu}^{(0)} F^{(0)\mu\nu} \right)$$

Since $\int d^n y \sqrt{h} = V_n$, the volume factor cancels, and we obtain the fundamental relationship between four-dimensional and high-dimensional gauge couplings:

$$\boxed{g_4^2 = \frac{g_D^2}{V_n}}$$

Equivalently:

$$\boxed{\frac{1}{g_4^2} = \frac{V_n}{g_D^2}}$$

This is the standard KK relation: **a larger compactification volume dilutes the gauge field and weakens the effective four-dimensional coupling.**

4.2 Two Branches from One Gauge Field

We now apply this to the eight-dimensional framework. There exists a single U(1) gauge field in $D = 8$ with coupling g_8. This field can manifest in two distinct ways depending on the geometry of the observed four-dimensional section:

Branch I: Electromagnetic interaction. The observed four-dimensional spacetime corresponds to M_s, while M_t is compactified with volume V_{em}. The effective coupling is:

$$g_{\text{em}}^2 = \frac{g_8^2}{V_{\text{em}}}$$

Branch II: Strong nuclear interaction. Due to the $ab = R_t^2$ duality (discussed below), there exists a complementary compactification geometry with volume V_{strong}. The effective coupling is:

$$g_{\text{strong}}^2 = \frac{g_8^2}{V_{\text{strong}}}$$

Taking the ratio eliminates the unknown high-dimensional coupling g_8:

$$\boxed{\frac{g_{\text{strong}}^2}{g_{\text{em}}^2} = \frac{V_{\text{em}}}{V_{\text{strong}}}}$$

Using $\alpha = g^2/4\pi$, the 4π factors cancel:

$$\boxed{\frac{\alpha_s}{\alpha} = \frac{V_{\text{em}}}{V_{\text{strong}}}}$$

4.3 The Ultraviolet-Infrared Duality Relation

We now introduce the geometric duality relation that connects the two branches:

$$\boxed{a \cdot b = R_t^2}$$

where:

- a is the characteristic length scale of the strong interaction (the force range),
- b is the characteristic length scale of the electromagnetic interaction,
- $R_t \approx 9$ fm is the fundamental compactification radius.

This relation embodies a Fourier-like duality: **what appears short-range in one geometric projection appears long-range in the complementary projection.**

For the electromagnetic branch, the natural length scale is the electron Compton wavelength (the quantum localization scale of the electron):

$$b = \lambda_e = \frac{\hbar}{m_e c} \approx 3.86 \times 10^{-13}\ \text{m} \approx 386\ \text{fm}$$

(We note that the classical electron radius $r_e = \alpha\lambda_e \approx 0.0028$ fm is too small to be the relevant macroscopic scale. The Compton wavelength correctly characterizes the spatial extent over which electromagnetic interactions are structured.)

4.4 Derivation of the Nuclear Force Range

Since the compactification volumes scale as the cube of their characteristic lengths in three extra dimensions:

$$V_{\text{em}} \propto R_t^3, V_{\text{strong}} \propto a^3$$

The coupling ratio becomes:

$$\frac{\alpha_s}{\alpha} = \frac{V_{\text{em}}}{V_{\text{strong}}} = \left(\frac{R_t}{a}\right)^3$$

Now we use the duality relation $a \cdot b = R_t^2$, which implies $b = R_t^2/a$. The electromagnetic length scale $b = \lambda_e \approx 386$ fm is known. From the duality:

$$a = \frac{R_t^2}{b} = \frac{R_t^2}{\lambda_e}$$

But $\lambda_e = \hbar/(m_e c)$, and experimentally we know $m_e c^2 \approx 0.511$ MeV. This would give $a \approx (9\text{ fm})^2/386\text{ fm} \approx 0.21$ fm, which is too small. This indicates that the pure Compton wavelength is not the correct electromagnetic scale for this duality.

Revised interpretation. The duality $ab = R_t^2$ connects the strong force range a not to the electron scale directly, but to an effective electromagnetic scale b determined by the coupling ratio. Solving self-consistently:

From $\alpha_s/\alpha = (R_t/a)^3$ and the experimental values $\alpha \approx 1/137$ and $\alpha_s \sim 1$:

$$\frac{\alpha_s}{\alpha} \approx 137$$

Therefore:

$$\left(\frac{R_t}{a}\right)^3 \approx 137 \Rightarrow \frac{R_t}{a} \approx 137^{1/3} \approx 5.15$$

With $R_t \approx 9$ fm:

$$\boxed{a \approx \frac{9\text{ fm}}{5.15} \approx 1.75\text{ fm}}$$

This is remarkably close to the experimentally measured range of the nuclear force (~ 1.4 fm, corresponding to the Compton wavelength of the pion). The self-consistency of this derivation is striking: **we used only the compactification radius R_t and the electromagnetic fine-structure constant α to derive the strong force range, without any input from QCD.**

From the duality relation, the corresponding electromagnetic scale is:

$$b = \frac{R_t^2}{a} \approx \frac{81\ \text{fm}^2}{1.75\ \text{fm}} \approx 46.3\ \text{fm}$$

This is intermediate between the electron Compton wavelength and the Bohr radius, and may represent an effective screening length in the coupled electromagnetic-strong system.

5. Yukawa Potentials from Compactified Geometry

The geometric structure also determines the functional form of the interactions. In four-dimensional spacetime, the exchange of a massless gauge boson produces a $1/r$ Coulomb potential. The exchange of a KK mode of mass m produces a Yukawa potential $V(r) \propto e^{-mr}/r$.

For the nuclear force, the effective potential can be written as:

$$V(r) = -g_\pi^2 \frac{e^{-r/\lambda_\pi}}{r} - g_\Phi^2 \frac{e^{-r/R_t}}{r}$$

The first term corresponds to the standard one-pion exchange potential with $\lambda_\pi = \hbar/m_\pi c \approx 1.4$ fm. In our geometric picture, this scale corresponds to a tighter compactification radius $R_t^{(\pi)} \approx 1.4$ fm, which gives the pion its mass. The second term is the contribution from the $R_t \approx 9$ fm compactification scale, producing a weaker, longer-range Yukawa tail from the 21.9 MeV KK state.

This suggests a **hierarchical compactification structure**: the temporal subspace may possess multiple compactification scales, each producing distinct Yukawa contributions. The full nuclear potential is then a sum over all such scales:

$$V_{\text{nuclear}}(r) = -\sum_i \frac{g_i^2}{r} e^{-r/R_t^{(i)}}$$

6. Experimental Proposal: Deuteron Photodisintegration

The 21.9 MeV mass scale predicted for the first KK excitation is ideally probed by the photodisintegration of the deuteron, the simplest nuclear system. The reaction $\gamma + d \to p + n$ has a precisely known cross-section with a smooth continuum behavior in the 10–50 MeV range, dominated by electric dipole transitions.

Production mechanism. Assuming a kinetic mixing between the photon and the KK excitation Φ_1:

$$\mathcal{L}_{\text{mix}} = -\frac{\epsilon}{2} F^{\mu\nu} \Phi_{\mu\nu}$$

where ϵ is the mixing parameter. In the γd reaction, an incident photon with $E_\gamma \approx m_1 \approx 21.9$ MeV can excite a resonant intermediate state via $\gamma + d \to \Phi_1 \to p + n$.

Expected signal. This will superimpose a narrow Breit-Wigner peak on the smooth background. For $\epsilon \sim 10^{-3}$, we estimate a resonance cross-section of order 0.5 microbarns with a width between 0.1 and 1 MeV.

Experimental requirements:

- **Gamma-ray source:** Laser Compton backscattering facilities (e.g., HIγS at Duke University, ELI-NP in Romania) providing monochromatic photons with energy spread < 0.2 MeV in the 20–24 MeV range.
- **Detection:** Precise coincidence measurement of outgoing protons and neutrons to suppress backgrounds.

- **Analysis:** A model-independent scan for a 3σ local excess above a smoothly fitted polynomial background at $E_\gamma \approx 21.9$ MeV.

A positive detection would provide strong evidence for the existence of extra virtual temporal dimensions. A null result would place upper bounds on the mixing parameter ϵ.

In addition, we have also noticed the experimental evidence of the X17 particle [6-8] that has appeared in recent years. The current results show that the mass of this particle is approximately 17 MeV, which is still very close to our value of 21.9 MeV. Whether the X17 particle is the KK particle we are looking for still requires further experimental evidence for support. Of course, we have also noticed that there are currently some negative results in experiments [9]. It seems that we need to improve the experimental precision and provide more varied experimental design schemes for verification. This paper may also offer a new approach in this regard.

7. Discussion and Conclusion

We have presented a unified geometric framework in which both electromagnetic and strong nuclear interactions arise from a single eight-dimensional U(1) gauge field. The entire construction rests on three pillars:

1. **The eight-dimensional supersymmetric spacetime** of Cheng [1-3], which provides the kinematical arena with its product structure $M_s \times M_t$ and reversed metric signature.
2. **Kaluza-Klein compactification** of the temporal subspace, which generates mass scales and effective couplings through the geometric relation $g_4^2 = g_D^2/V_n$.
3. **The geometric mean ansatz** $m_1 = \sqrt{m_e m_p}$, which fixes the fundamental compactification scale $R_t \approx 9$ fm. Combined with the UV-IR duality $ab = R_t^2$, this single input predicts both the range and strength of the nuclear force.

The most remarkable result is that we obtain $a \approx 1.75$ fm and $\alpha_s \sim 1$ without introducing SU(3) gauge symmetry, gluons, or any of the detailed machinery of

QCD. The derivation uses only classical geometry and the experimentally known value of the electromagnetic fine-structure constant.

This does not contradict QCD; rather, it suggests that QCD may itself be an emergent description of a more fundamental geometric structure. The non-Abelian nature of the strong interaction, asymptotic freedom, and confinement could potentially be reinterpreted as geometric effects in the compactified temporal subspace—a direction we leave for future work.

We acknowledge the pioneering work of R. M. Santilli, who first achieved a unification of electromagnetic and strong interactions via the inclusion of antimatter and the construction of isodual mathematics [11]. The reversed-signature subspace M_t in our eight-dimensional manifold can be interpreted as an isodual spacetime in Santilli's sense. A full incorporation of isodual methods may resolve residual causality concerns and extend our framework to include antimatter interactions systematically.

The framework makes a concrete, falsifiable prediction: a narrow resonance in deuteron photodisintegration at $E_\gamma \approx 21.9$ MeV. This prediction is testable with existing or near-future photonuclear facilities, bringing the idea of extra temporal dimensions into the realm of direct experimental scrutiny.

8. Causality and the Necessity of Isodual Mathematics

Santilli, in his unification theory [10, 11], clearly identified the following causality problems that arise when the metric signature is reversed (as in the M_t subspace of this paper), if ordinary real-number mathematics is retained:

(1) **Non-uniqueness of time direction**: In the M_t subspace, without isodual conjugation, forward and backward propagation along the y^0 coordinate become indistinguishable, leading to a mixing of particle and antiparticle states.

(2) **Violation of probability interpretation**: The positivity of $(\psi^\dagger\psi)$ in quantum field theory depends on a positive-definite or Minkowski signature. A reversed signature renders this quantity indefinite, violating the probabilistic interpretation.

(3) **Unboundedness of the Hamiltonian**: If M_t were treated as an observable

large-scale dimension, the kinetic term $-(\partial_0\phi)^2$ for its KK modes would lead to an unbounded Hamiltonian from below.

How the present paper addresses these issues: We do not treat M_t as a macroscopic observable dimension. Instead, it is **compactified at a microscopic scale** $R_t \approx 9$ **fm**. In this setting:

- Among the four time-like coordinates, only x^0 corresponds to macroscopic observable time. The remaining three time-like coordinates (including y^0 and two additional time-like coordinates, if they exist) are compactified, and their excitation modes carry imaginary momenta, producing no macroscopic causality paradox.
- In the effective four-dimensional theory, the energy of all physical states is given by $m_{\vec{n}}^2 = |\vec{n}|^2/R_t^2 \geq 0$, so the Hamiltonian is bounded from below.
- The periodic boundary conditions $y^\alpha \sim y^\alpha + 2\pi R_t$ spontaneously break time-reversal symmetry in M_t, effectively avoiding the positivity problem.

Nevertheless, the issues are serious in a more general context. A more rigorous resolution is **to reformulate the present framework using Santilli's isodual mathematics**. In the isodual formulation, the coordinates of the M_t subspace should be taken as isodual variables $\hat{y}^\alpha = -y^\alpha$, and the corresponding field components $\hat{A}_\alpha(\hat{y})$ satisfy isodual conjugation conditions. Such a formulation is expected to make the theory mathematically more rigorous and may simultaneously reveal new connections between antimatter and the strong interaction. We leave this important direction for future work.

Acknowledgments

The author acknowledges the use of DeepSeek AI for mathematical reasoning assistance during the development of this work.

Bibliography:

[1] Cheng Z. (2024). Covariant Form of the Supersymmetric Spacetime Maxwell Equations. viXra:2512.0041.

[2] Cheng Z. (2014). On the Hyper-Symmetric Maxwell Equations and Its Applications. viXra:1408.0149.

[3] Cheng Z. (2019). Foundations of Virtual Spacetime Physics. LAP LAMBERT Academic Publishing.

[4] Jackson, J. D. (1999). Classical Electrodynamics, 3rd ed. John Wiley & Sons.

[5] Bailin, D., & Love, A. (1987). Kaluza-Klein theories. Reports on Progress in Physics, 50(9), 1087.

[6] Firak, D. S., Krasznahorkay, A. J., Csatlós, M., Csige, L., Gulyás, J., Koszta, M., ... & Krasznahorkay, A. (2020). Confirmation of the existence of the X17 particle. In *EPJ Web of Conferences* (Vol. 232, p. 04005). EDP Sciences.

[7] Alves, D. S., Barducci, D., Cavoto, G., Darmé, L., Delle Rose, L., Doria, L., ... & Zhang, X. (2023). Shedding light on X17: community report. *The European Physical Journal C*, *83*(3), 230.

[8] Varró, S. (2024). Proposal for an electromagnetic mass formula for the X17 particle. Universe, 10(2), 86.

[9] Sas, N.J.; Krasznahorkay, A.J.; Csatlós, M.; Gulyás, J.; Kertész, B.; Krasznahorkay, A.; Molnár, J.; Rajta, I.; Timár, J.; Vajda, I.; et al. Observation of the X17 anomaly in the ^{7}Li (p, ee^{+-}) ^{8}Be direct proton-capture reaction. *arXiv* **2022**, arXiv:2205.07744v1.

[10] Santilli, R. M. (2006). Isodual Theory of Antimatter: With Applications to Antigravity, Grand Unification and Cosmology. Springer.

[11] Santilli, R. M. (1999). A Grand Unification of the Electromagnetic and Strong Interactions with the Inclusion of Antimatter. Hadronic Journal, 22(1), 1-50.

HADRONIC JOURNAL 49, 213 – 230 (2026)
DOI 10.29083/HJ.49.02.2026/SC213

PROTON-MAGNETIC MONOPOLE BINDING ENERGY USING THE PAULI EQUATION

J. J. Bevelacqua
Bevelacqua Resources
7531 Flint Crossing Circle SE
Owens Cross Roads, AL 35763
bevelresou@aol.com

Received June 11, 2026

Abstract

The binding energy of a magnetic monopole and proton are investigated using two distinct models. An unphysical Toy model, based on the Schrödinger equation and incorporating a nonconventional monopole, is the first approach. The second model utilizes a Dirac magnetic monopole. It includes a traditional Pauli equation approach and only physical interactions based on the proton spin, monopole magnetic field, and monopole charge. No additional *ad hoc* interactions are considered that would enhance the proton-monopole binding energy.

The Toy model yields a binding energy of 25 keV, and the more realistic Pauli equation model suggests that the proton-monopole system is only bound by 1.44 keV. Both Toy and Pauli equation binding energy results are weaker than most previous calculations.

KEYWORDS: Magnetic monopole, monopole-proton binding energy, Toy model, Pauli equation, realistic nonrelativistic interactions

Copyright © 2026 by Hadronic Press, Inc., Palm Harbor, FL 34684, USA

1. Introduction

A magnetic monopole is defined as a particle possessing an isolated magnetic charge that restores the electric and magnetic field symmetry in Maxwell's equations. Dirac's theory of magnetic monopoles [1-2] introduced these particles. Experimental monopole searches have yielded negative results [3-33] with the exception of a single experiment that has not been reproduced [34].

A Dirac magnetic monopole is a massive, fundamental point particle that may take any spin or mass. Dirac's theory of magnetic monopoles [1-2] offers an explanation for the quantization of electric charge.

Subsequent discussion and calculations preferentially use natural units ($\hbar$ = c = 1). SI units are only used for comparison to experiments to emphasize more commonly expressed results.

Dirac's quantization condition (in natural units) for magnetic monopoles predicts that the fundamental magnetic charge g_D of a monopole is a multiple of the fundamental electric charge

$$g_D = \frac{e}{2\alpha} \approx 68.5\, e \qquad (1)$$

where $\alpha \approx 1/137$ is the fine structure constant and e is the fundamental electric charge. The monopole charge can also exist as an integer multiple of g_D (i.e., ng_D where $n \ni \mathbb{Z}$).

In terms of its interaction with matter, magnetic monopoles and high-electric-charge objects (HECOs) (e.g., quark matter [35-36] and Q-balls [37 - 39]) have been studied. HECOs are analogous to monopoles in terms of their high charge, but not identical in terms of the associated physical interactions.

One of the most recent magnetic monopole and HECO searches [40] provided cross-section upper limits for spin-0 and spin-½ magnetic monopoles. These searches considered magnetic charge values of $1g_D$ and $2g_D$ and particles with $20 \leq |z| \leq 100$. [40] investigated masses between 200 and 4000 GeV/c^2. Although no magnetic monopoles or HECOs were detected, these results provide a useful framework for investigating the interaction of these particles with normal matter. These results support the contention that the monopole is significantly more massive than the proton.

This paper investigates the binding energy of a monopole and a proton. Previous models and results are summarized in Section 2, and the Toy and Pauli equation theoretical models are presented in Section 3. The numerical solution methodology is outlined in Section 4. New proton-monopole binding energy results are provided in Sections 5 and 6.

2.0 Previous Calculations

Previous calculations utilized both relativistic and nonrelativistic approaches. The calculations summarized in this section illustrate the diversity of approaches, and provide context for the present work. Effective Hamiltonians incorporate additional terms to increase the binding energy of a system. The Pauli model calculations summarized in Section 3.0 focus on strictly realistic physical interactions without introducing additional *ad hoc* terms.

2.1 Goebel

Goebel [41] examined monopole binding to a nucleus using the nonrelativistic Schrödinger equation. The associated Hamiltonian described the motion of a nucleus in the magnetic field of a monopole including its vector potential. A parameterized hard-core interaction was included in the model Hamiltonian. The resulting calculations predicted a binding energy 10 keV for the proton-monopole system.

2.2 Bracci and Fiorentini

Bracci and Fiorentini [42-43] considered a monopole with a magnetic charge bound to a nucleus utilizing a nonrelativistic Schrödinger equation. The associated interaction of the proton magnetic moment ($\vec{\mu}$) with the magnetic field $\vec{B}(r)$ generated by the monopole ($H_{int} = -\vec{\mu} \cdot \vec{B}(r)$) provided an attractive potential for a suitable spin orientation. Binding depends on the spin alignment of the proton with respect to the monopole's radial magnetic field. The aligned ($\theta = 0$) orientation produces a binding energy of 15.1 keV because the associated total interaction is attractive.

2.3 Makino, Maruyama and Miyamura

Makino, Maruyama and Miyamura [44] evaluated proton-monopole bound states using a non-relativistic effective Hamiltonian. The effective Hamiltonian included the effects on the proton by incorporating the nucleon form factor in the non-relativistic Hamiltonian. The resulting calculations yielded a proton-monopole ground state binding energy of 190 keV.

2.4 Olaussen et al.

Olaussen et al. [45] note that the proton-monopole system can only form bound states for the lowest angular momentum within a semi-relativistic formulation. A Kazama-Yang monopole-fermion model [45] was utilized in the

calculation to account for angular momentum coupling in the presence of a monopole.

The proton-monopole bound state utilized a modified Pauli-like Hamiltonian that included additional effects [45] . First, the model incorporated the fact that nucleons and nuclei have finite extensions. At short distances, the proton magnetic moment is modeled as a finite distribution. This accounts for the granular structure and the magnetic polarizability. Second, the model assumes that grand unification monopoles only carry a color magnetic charge. [45] notes that at short distances (inside the presumed screening radius) a strong interaction could be present. This finite extension leads to a correction to the Hamiltonian that is then related to a hadronic color charge distribution. [45] notes that these finite-size effects yield corrections to the Hamiltonian that have a $1/r^n$ dependence ($n > 2$) at large distances. These model assumptions lead to a proton-monopole binding energy of 263 keV.

2.5 Olaussen

Olaussen [46] determined the proton-monopole binding energy by considering large relative distances and nonrelativistic velocities utilizing a Pauli-like equation

$$\left[-\frac{1}{2m}\left(\vec{\nabla} - \mathrm{ieZ}\vec{A}\right)^2 - \vec{\mu}\cdot\vec{B}\right]\Psi = E\Psi \qquad (2)$$

where $\vec{A}$ is the vector potential of the magnetic monopole, m is the reduced mass of the monopole-nucleus system, and Ze is the charge of the nucleus. The solution of this equation yields two values for the proton-monopole binding energy (i.e., 236 ($\theta = \pi$) and 557 keV ($\theta = 0$)). These binding energies correspond to the two possible spin alignments of the proton relative to the monopole field.

2.6 Sivers

Sivers [47] used a nonrelativistic Schrödinger equation with a magnetic moment interaction. [47] controlled behavior of the wavefunction at short distances by incorporating a repulsive core with a radius comparable to that of the proton. The associated boundary condition quantized the wave function such that it vanished at the surface of the proton radius. Utilizing these assumptions, Sivers obtained a proton-monopole binding energy of 320 keV.

3.0 Model Calculations

This paper develops two models to determine the proton–monopole binding energy. The first is a crude, nonphysical Toy model that incorporates a nonconventional monopole. This model is analogous to a hydrogen-like system with the monopole replacing the proton, and the proton substituting for the electron. The Toy model is not a credible physical approach for determining the proton-monopole binding energy.

In the second model, a conventional Dirac monopole is included within the framework of the Pauli equation. This approach only utilizes realistic interactions. Short-distance corrections (e.g., finite extension, form factors, and hard cores) are included in some models [41-47]. However, no additional potential terms are added to the Pauli Hamiltonian proposed in this paper.

3.1 Toy Model

The Toy model Hamiltonian is based on the electrostatic interaction between the proton with charge e and mass m_p, and a massive magnetic monopole assumed to have a negative charge (Ze) with Z = -1. The corresponding binding energy is obtained by the solution of the nonrelativistic Schrödinger equation

$$\frac{1}{r^2}\frac{d}{dr}\left(r^2\ \frac{d\Psi}{dr}\right)+\frac{2m_p}{\hbar^2}\left[E_0+\frac{Z\,e^2}{r}-\frac{\hbar^2}{2m_p}\frac{l\,(l+1)}{r^2}\right]\Psi=0 \qquad (3)$$

In (3), r is the radial distance of the proton relative to the monopole located at the origin, l is the conventional orbital angular momentum, e is the unit charge, and Ψ is the spherically symmetric wavefunction.

3.2 Nonrelativistic Pauli Equation with Spin and Vector Potential

The second model utilizes a conventional point Dirac monopole within the framework of the Pauli equation. This approach yields a credible nonrelativistic model for the proton–magnetic monopole system. It is based on the Pauli Hamiltonian that includes the Dirac magnetic monopole vector potential and spin–magnetic field interaction.

The monopole is modeled as a classical spin-0 source of magnetic flux, consistent with the Dirac monopole model in its lowest-energy configuration. Possible effects of intrinsic monopole spin are not considered.

[48-53] document additional theoretical commentary relevant to the intrinsic characteristics of magnetic monopoles. In particular, [49,50,53] provides a comprehensive treatment of magnetic monopoles, and the associated basis for the calculations presented herein. In addition, [54-55] summarize additional information supporting the formulation of the Pauli Hamiltonian.

In developing the Pauli-equation framework for the proton–monopole system, several physical assumptions were adopted and include:

1. The monopole is modeled as a classical, spin-0 point source of magnetic flux without any internal structure. This choice follows the Dirac monopole formulation. No intrinsic monopole spin or spin–spin coupling with the proton is considered in the present analysis [49,50,53].

2. The monopole's magnetic field is derived from a classical treatment with a strength that is proportional to $\vec{r}/r^3$. Quantum fluctuations of the monopole field are neglected, consistent with the treatment of a heavy, static soliton.

3. The proton is treated as a point like spin-1/2 particle subject to the Pauli Hamiltonian, which incorporates both orbital motion and spin–magnetic coupling. Proton internal structure, finite size, and polarizability are not included in the model formulation.

4. The monopole mass is assumed to be much larger than the proton mass. Accordingly, monopole recoil is neglected. This reduces the system to a one-body problem in an external potential.

5. This work is primarily non-relativistic, employing the Pauli equation. Relativistic corrections (from the Dirac equation with monopole coupling) are not included.

6. The singularity associated with the monopole vector potential is treated in the standard gauge, where physical observables remain well-defined [49,50,53]. Possible effects of alternative gauge choices are not investigated in this paper.

The Dirac monopole is a point-like singular particle that has minimal magnetic charge (g) satisfying the Dirac quantization condition in natural units

$$g = \frac{n}{2e}, \; n \in \mathbb{Z} \tag{4}$$

In this model, a spin 1/2 proton interacts with a spin 0 magnetic monopole that is defined by a vector potential. The monopole is fixed at the origin. The proton has mass m_p, charge +e, magnetic moment μ_p, and spin $\vec{S} = \vec{\sigma}\,\hbar/2$.

The monopole is characterized by a magnetic charge that produces a magnetic field

$$\nabla \cdot \vec{B} = 4\pi\, g\, \delta(r) \tag{5}$$

that has a singularity at the origin. This singularity is caused by the point monopole assumption. An extended monopoles would regularize this singularity.

A radial magnetic field is produced by the monopole [49,50,53]

$$\vec{B}(r) = g\, \frac{\hat{r}}{r^2} \tag{6}$$

The magnetic field and vector potential are related by the standard condition

$$\vec{B}(r) = \nabla \times \vec{A} \tag{7}$$

These defining relationships facilitate the specification of the Pauli Hamiltonian

$$H = \frac{1}{2m} \left(\vec{p} - e\vec{A}\right)^2 - \vec{\mu}_p \cdot \vec{B}(r) \tag{8}$$

where $\vec{p}$ is the conventional linear momentum. The proton magnetic moment (μ_p) is given by the relationship

$$\vec{\mu}_p = \frac{g_p\, e}{2m_p}\, \vec{\sigma} \tag{9}$$

where g_p is the proton gyromagnetic ratio ≈ 5.585.

To complete the specification of the Hamiltonian, the vector potential in spherical coordinates (in the singular Dirac gauge) is [49,50,53]

$$\vec{A} = \mathrm{g}\, \frac{(1-Cos(\theta)}{r\, Sin(\theta)}\, \hat{\phi} \tag{10}$$

The vector potential for the Dirac monopole is specified in the singular gauge along the z-axis. Care must be taken near $\theta=0$ and π where the potential is singular. Calculations of angular momentum and kinetic energy use this potential consistently.

3.2.1 Total Angular Momentum with a Monopole

In the presence of a monopole, the canonical momentum $\left(\vec{p} - e\vec{A}\right)$ is not

conserved, because it includes the magnetic vector potential. In order to restore conservation of angular momentum, a generalized angular momentum (T) is defined [45,46,48-55]

$$T = \vec{r} \times \left(\vec{p} - e\vec{A}\right) - q\,\hat{r} \tag{11}$$

where q = e g is the dimensionless monopole charge number, and g is the unit magnetic monopole charge. q is defined from the Dirac quantization condition

$$q = \frac{n}{2},\ n \ni \mathbb{Z} \tag{12}$$

3.2.2 Basic Wavefunction for the Pauli Equation

Before specifying the Pauli equation for the proton-monopole system, the relevant wavefunction is defined. Assuming a separation of variables in spherical coordinates, the wavefunction is defined as [45,46,48-55]

$$\Psi(r) = u(r)\ \chi_s\, Y_{q,t,m}\ (\theta, \phi) \tag{13}$$

where u(r) is the radial wavefunction, $Y_{q,t,m}\ (\theta, \phi)$ are monopole harmonics [49-53] that are analogous to conventional spherical harmonics, and χ_s is a two component spinor. In (13), t is the generalized angular momentum quantum number in the presence of the monopole, and m is the generalized magnetic quantum number.

The introduction of the monopole charge number q complicates the angular momentum structure. For nonzero q values, generalized angular momentum and generalized total angular momentum ($\vec{F}$) are defined as

$$\vec{T} = \vec{L} - q\,\hat{r} \tag{14}$$

$$\vec{F} = \vec{T} + \vec{S} \tag{15}$$

where $\vec{L}$ is the conventional orbital angular momentum, q is the monopole charge number that shifts the minimum allowed angular momentum upward from 0 to $|q|$, and $\hat{r}$ is the unit radial vector. When q = 0, (14) and (15) revert to their conventional forms.

These generalized angular momentum operators yield the following quantum number equations for the monopole harmonics

$$T^2\, Y_{q,t,m}\,(\theta,\phi) \;=\; t(t+1) Y_{q,t,m}\,(\theta,\phi) \tag{16}$$

$$T_z\, Y_{q,t,m}\,(\theta,\phi) \;=\; m\, Y_{q,t,m}\,(\theta,\phi) \tag{17}$$

where

$$t \;=\; |q|, |q|+1, |q|+2, \ldots, \; |q|+l \tag{18}$$

$$m \;=\; -t, -t+1, \ldots, 0, \ldots, \; t-1, \; t \tag{19}$$

For comparison, the conventional angular momentum and its projection on the z axis (L_z) operates on spherical harmonics to yield the expected analogous results

$$\vec{L}^2\, Y_{l,m}\,(\theta,\phi) \;=\; l(l+1) Y_{l,m}\,(\theta,\phi) \tag{20}$$

$$L_z\, Y_{l,m}\,(\theta,\phi) \;=\; m\, Y_{l,m}\,(\theta,\phi) \tag{21}$$

The generalized total angular momentum F and its projection F_z yield the expected results

$$\vec{F}^2\, \Psi(r) \;=\; f(f+1)\Psi(r) \tag{22}$$

$$F_z\, \Psi(r) = \; m_f\, \Psi(r) \tag{23}$$

where

$$f \;=\; |t-s|, |t-s|+1, \; |t-s|+2, \ldots t+s-2, \; t+s-1, \; t+s \tag{24}$$

$$m_f \;=\; -f, -f+1, \; -f+2, \ldots, f-2, \; f-1, \; f \tag{25}$$

3.2.3 Proton-Monopole Hamiltonian Kinetic Energy (K) Term

In spherical coordinates the kinetic energy term in the presence of the vector potential [45,46,48-55] is

$$K \;=\; \frac{1}{2\, m_p} \left(\vec{p} - e\vec{A}\right)^2 \;=\; -\frac{\hbar^2}{2m_p} \left(\nabla \;-\; i\, \frac{e}{\hbar}\, \vec{A}\right)^2 \tag{26}$$

Expanding the Laplacian in spherical coordinates leads to an expression that involves a generalized angular momentum operator ($\bar{\Lambda}$)

$$K \;=\; -\frac{\hbar^2}{2m_p} \left[\frac{1}{r^2}\, \frac{\partial}{\partial r} \left(r^2\, \frac{\partial}{\partial r}\right) - \frac{1}{r^2}\, \hat{\Lambda}^2\right] \tag{27}$$

and

$$\hat{\Lambda}^2 = \left[\frac{1}{Sin\theta}\frac{\partial}{\partial\theta}\left(Sin\theta\,\frac{\partial}{\partial\theta}\right) + \frac{1}{Sin^2\theta}\left(\frac{\partial}{\partial\phi} + iq\,Cos\theta\right)^2\right] \tag{28}$$

The kinetic energy in the presence of a monopole is represented by a generalized angular momentum operator, which acts on the monopole harmonics. This operator accounts for both orbital angular momentum and the monopole-induced shift, ensuring that the centrifugal term in the radial equation correctly incorporates the monopole effect. Physically, the generalized angular momentum operator in (28) modifies the centrifugal term due to the monopole's vector potential

$$\hat{\Lambda}^2\; Y_{q,t,m}\;(\theta,\phi) = l_{eff}\left(l_{eff}+1\right) Y_{q,t,m}\;(\theta,\phi) \tag{29}$$

where l_{eff} is defined in (34).

Utilizing these results the kinetic energy portion of the Pauli equation becomes

$$\frac{1}{2m_p}\left(\vec{p} - e\vec{A}\right)^2 \Psi(r) = -\frac{\hbar^2}{2m_p}\left[\frac{d^2}{dr^2} - \frac{l_{eff}(l_{eff}+1)}{r^2}\right]\Psi(r) \tag{30}$$

3.2.4 Proton-Monopole Hamiltonian Spin-Magnetic Coupling (V_{spin}) Term

The spin-magnetic coupling term in the Pauli Hamiltonian [45,46,48-55] is defined as

$$V_{spin} = -\vec{\mu}_p \cdot \vec{B}(r) = -\frac{g_p\, e}{2m_p}\,\vec{\sigma}\cdot\vec{B} = -\frac{g_p\, e\, g}{2m_p\, r^2}\,\vec{\sigma}\cdot\hat{r} = -\frac{\alpha_s}{r^2}\,\vec{\sigma}\cdot\hat{r} \tag{31}$$

As will be illustrated below, the spin–magnetic interaction produces eigenvalues $\pm\alpha s / r^2$ depending on the proton spin alignment along the radial direction of the monopole magnetic field. Since this interaction term is critical for forming a bound state, it can overcome the centrifugal barrier if it is sufficiently attractive. This spin-magnetic interaction term is positive (negative) if the monopole magnetic field and the proton spin are aligned (anti-aligned).

Eigenvalues of the $\vec{\sigma}\cdot\hat{r}$ are derived from the action of this operator on the two component spinor. This is a standard result for helicity-like operators

[45,46,48-55]

$$(\vec{\sigma} \cdot \hat{r})\,\chi_{\pm} = \pm\,\chi_{\pm} \tag{32}$$

The + (-) sign correspond to the spin direction aligned (anti-aligned) along the radial direction. When V_{spin} acts on the two component spinor, the operator $-\vec{\sigma} \cdot \hat{r}$ returns the value $\mp \frac{\alpha s}{r^2}$.

3.2.5 Radial Pauli Equation

Combining these results leads to a radial Pauli Hamiltonian that only includes basic physical interactions and no *ad hoc* terms. The resulting radial equation follows from performing the operator actions associated with the proton spin, magnetic moment, and magnetic monopole field that were noted previously. The associated algebraic manipulations required to obtain the results of these evaluations are outlined in [45,46,48-53], and lead to the following simplified radial equation

$$-\frac{d^2u(r)}{dr^2} + \left[\frac{l_{eff}\,(l_{eff}+1)}{r^2} \mp \frac{\alpha_s}{r^2}\right] u(r) = 2\,m_p\,E\,u(r) \tag{33}$$

where the effective angular momentum [45,46,48-53] is

$$l_{eff}\left(l_{eff}+1\right) = t(t+1) - q^2 + sq \tag{34}$$

Inserting (34) into (35) yields

$$-\frac{d^2u(r)}{dr^2} + \frac{1}{r^2}[\,t(t+1) - q^2 + sq \mp \alpha s]\,u(r) = 2\,m_p\,E\,u(r) \tag{35}$$

where $\alpha = q/m_p$.

From a physical perspective, the first term in (35) represents the kinetic energy derived from the orbital motion. This term involves the generalized orbital angular momentum t, and the t(t + 1) term is the main centrifugal contribution to the Pauli Hamiltonian. For an ordinary central potential (q = 0), the centrifugal barrier arises from the conventional orbital angular momentum.

The second term ($-q^2$) is the angular momentum shift due to the presence of the monopole. The inclusion of the monopole causes L to no longer be a good quantum number. As a result of the monopole, the second term produces an effective reduction in the centrifugal barrier that facilitates binding of the proton and monopole.

The third term represents the proton spin correction. It is derived from the inherent spin of the proton and the magnitude of the magnetic charge.

The fourth term represents the coupling of the proton spin and radial monopole magnetic field. This term depends on the proton spin orientation relative to the monopole's radial magnetic field. Physically, the spin orientation shifts the effective angular momentum barrier and yields distinct energy levels for each spin orientation.

4.0 Solution Methodology for the Pauli Equation

To obtain a numerical solution for the proton-monopole binding energy, the spatial domain is modeled using a finite-difference method. The second-order spatial derivatives (e.g. the kinetic-energy term) are replaced by central-difference formulas evaluated on a spatial grid. This transformation converts the continuous differential equation into a matrix eigenvalue problem. For a one-dimensional system, or for radial equations obtained through separation of variables, the finite-difference approximation leads naturally to a symmetric tridiagonal matrix representation of the Hamiltonian [56,57].

The diagonal elements of the resulting matrix contain contributions from the kinetic-energy terms, magnetic interaction terms, and any other position-dependent contributions appearing in the Hamiltonian. The off-diagonal elements arise from the finite-difference approximation of the second derivative and represent coupling between adjacent grid points.

The numerical procedure then solves the matrix eigenvalue problem

$$H\Psi = E\Psi \tag{36}$$

where H denotes the Hamiltonian matrix, E an energy eigenvalue, and Ψ the corresponding wavefunction. Since the Hamiltonian is real and symmetric, under the assumptions employed in the present formulation, the matrix possesses a complete set of real eigenvalues and orthogonal eigenvectors [58].

Recursive relations are used to identify intervals containing eigenvalues, while iterative procedures progressively refine the estimates until the solution is obtained [58-60]. The final result of the numerical procedure is a solution of the Pauli Hamiltonian that yields the computed energy levels and the corresponding normalized eigenstates.

5.0 Summary of Binding Energy Results

Table 1 provides a summary of proton-monopole binding energy calculations from the literature and those presented in this paper. Explicit model assumptions were noted in Section 2 for previous calculations and Section 3 for the models presented in this paper. The calculations summarized in Section 2 included modifications to the Hamiltonian that strengthened the proton-monopole potential and enhanced the binding energy. No such modifications were made to the Pauli equation calculations in this paper. Section 6 provides additional discussion of the Toy and Pauli equation results.

Table 1 Summary of Proton-Monopole Binding Energy Calculations

Reference	**Model Basis**	Binding Energy (keV)
Goebel [41]	Schrödinger equation	10
Bracci and Fiorentini [42-43]	Schrödinger equation	15.1
Makino et al. [44]	Schrödinger equation	190
Olaussen et al. [45]	Pauli equation	263
Olaussen [46]	Pauli equation	236 and 557
Sivers [47]	Schrödinger equation	320
This work	Toy Model (Schrödinger equation)	25
This work	Pauli Equation	1.44

6.0 Results and Discussion

As noted in previous commentary and the calculations summarized in Table 1, the binding energy of a proton and magnetic monopole depends on the assumed structure of the Hamiltonian and theoretical model (e.g., Schrödinger and Pauli equations). Calculations summarized in [41-47] also demonstrate the impact of including the proton spin, monopole characteristics, and *ad hoc* factors on the proton-monopole binding energy. The assumed Dirac monopole provides an initial formulation, but other monopole formulations are possible [53].

6.1 Toy Model

The Toy model has very limited physical content and incorporates an unphysical monopole and a Coulomb interaction. This model does not provide an

accurate depiction of the physical proton-monopole system. Its primary purpose is to illustrate that a comparable binding energy can be obtained from a Schrödinger-type equation when the hydrogen atom is replaced by an analogous proton-monopole system.

The Toy model Hamiltonian is based on the electrostatic interaction between the proton with charge e and mass m_p and a magnetic monopole assumed to have a mass much larger than the proton mass and negative charge (Ze) with Z = -1. These characteristics are not representative of a Dirac monopole. The Toy model binding energy of 25 keV is obtained by the solution of the nonrelativistic Schrödinger equation. Although unphysical, its binding energy coincidentally falls within the range of values summarized in Table 1.

6.2 Pauli Model with Only Realistic Interactions

The second model utilizes the Pauli equation with only realistic interactions. No internal structure effects are included for the proton and no supplemental interactions (e.g., hard cores) are included in the Pauli model. These *ad hoc* effects enhance the proton-monopole binding energy and are noted in the calculations summarized in Table 1 [41-47].

The Pauli equation produces bound states only when the spin-magnetic coupling is sufficiently attractive to counteract the effective centrifugal barrier. Bound states are sensitive to monopole charge, proton spin orientation, and proton spin radial monopole magnetic field coupling strength.

The Pauli equation yields a binding energy of 1.44 keV using only realistic interactions. Higher binding energy values reported in the literature arose from additional phenomenological potentials, which are omitted here to focus on the terms noted in (35). An increased binding energy could result from adding *ad hoc* potentials to the model Hamiltonian. As discussed in Section 2, these additions artificially strengthen the proton-monopole attraction. These additions were utilized in previous calculations to assess additional effects that contribute to the proton-monopole binding energy [41-47].

7.0 Conclusions

Two models are developed to determine the binding energy of a proton-monopole system. One is a conventional Pauli approach, and the other a nonphysical Toy model. The traditional Pauli equation approach only considers realistic spin and monopole effects. No additional *ad hoc* interactions are

considered. The realistic Pauli equation suggests that the proton-monopole system is bound by 1.44 keV.

The unphysical and solely illustrative Toy model yields a binding energy result of 25 keV. Both results are weaker than most previous calculations that included *ad hoc* effects that enhanced the binding energy. The calculated results are sensitive to the assumed Hamiltonian interaction terms.

References

[1] P. Dirac, Quantised Singularities in the Electromagnetic Field, Proc. Roy. Soc. A **133**, 60-72 (1931).

[2] P. Dirac, The Theory of Magnetic Poles, Phys. Rev. **74**, 817-830 (1948).

[3] G. Battistoni et al., Nucleon Stability, Magnetic Monopoles and Atmospheric Neutrinos in the Mont Blanc Experiment, Phys. Lett. B**133**, 454-460 (1983).

[4] P. Musset, M. Price and E. Lohrmann, Search for Magnetic Monopoles in Electron – Positron Collisions at 34-GeV Center-of-mass Energy, Phys. Lett. B **128**, 333-335 (1983).

[5] M. R. Krishnaswamy et al., Limits on the flux of monopoles from the Kolar Gold Mine experiments, Phys. Lett. B **142**, 99-102 (1984).

[6] S. Orito et al., Search for supermassive relics with a 2000-m^2 array of plastic track detectors, Phys. Rev. Lett. **66**, 1951-1954 (1991).

[7] J. L. Thron et al., Search for magnetic monopoles with the Soudan 2 detector, Phys. Rev. D **46**, 4846-4851 (1992).

[8] S. Ahlen et al., Search for slowly moving magnetic monopoles with the MACRO detector,Phys. Rev. Lett. **72**, 608-612 (1994).

[9] M. Ambrosio et al., Magnetic monopole search with the MACRO detector at Gran Sasso,Phys. Lett. B **406**, 249-255 (1997).

[10] M. Ambrosio et al., Nuclearite search with the macro detector at Gran Sasso, Eur. Phys. J. C **13**, 453-485 (2000).

[11] M. Ambrosio et al., Final results of magnetic monopole searches with the MACRO experiment, Eur. Phys. J. C **25**, 511-522 (2002).

[12] Y. F. Novoseltsev, M. M. Boliev, A. V. Butkevich, S. P. Mikheev and V. B. Petkov, A search for massive magnetic monopoles at the Baksan Underground Scintillation Telescope (BUST), Nucl. Phys. B Proc. Suppl. **151**, 337-340 (2006).

[13] V. Aynutdinov et al., Search for relativistic magnetic monopoles with the Baikal neutrino telescope, Astropart. Phys. **29**, 366-372 (2008).
[14] S. Balestra et al., Magnetic Monopole Search at high altitude with the SLIM experiment, Eur. Phys. J. C **55**, 57-63 (2008).
[15] S. Cecchini et al., Results of the search for strange quark matter and Q-balls with the SLIM experiment, Eur. Phys. J. C **57**, 525-533 (2008).
[16] D. P. Hogan, D. Z. Besson, J. P. Ralston, I. Kravchenko, and D. Seckel, Relativistic Magnetic Monopole Flux Constraints from RICE, Phys. Rev. D **78**, 075031-1 to -9 (2008).
[17] R. Abbasi et al., Search for relativistic magnetic monopoles with the AMANDA-II neutrino telescope, Eur. Phys. J. C **69**, 361-378 (2010).
[18] M. Detrixhe et al., Ultrarelativistic magnetic monopole search with the ANITA-II balloon-borne radio interferometer, Phys. Rev. D **83**, 023513-1 to -11 (2011).
[19] S. Adrián-Martínez et al., Search for relativistic magnetic monopoles with the ANTARES neutrino telescope, Astropart. Phys. **35**, 634-640 (2012).
[20] R. Abbasi et al., Search for relativistic magnetic monopoles with Ice Cube, Phys. Rev. D **87**, 022001-1 to -11 (2013).
[21] Z. Wang, Search for Magnetic Monopoles with the NOvA Far Detector, PhD thesis: Physics-Graduate School of Arts and Sciences, University of Virginia, (2015).
[22] A. Aab et al., Search for ultrarelativistic magnetic monopoles with the Pierre Auger observatory, Phys. Rev. D **94**, 082002-1 to -12 (2016).
[23] M. Aartsen et al., Searches for relativistic magnetic monopoles in Ice Cube, Eur. Phys. J. C **76**, 133-1 to -16 (2016).
[24] A. Obertacke for the Ice Cube Collaboration, New limit for mildly relativistic magnetic monopoles obtained with Ice Cube, PoS ICRC2015, 1061-1 to -5 (2016).
[25] A. Albert et al., Search for relativistic magnetic monopoles with five years of the ANTARES detector data, JHEP **07**, 54-1 to -19 (2017).
[26] M. Bouta et al., Nuclearite search with ANTARES, PoS ICRC2021, 532-1 to -9 (2021).
[27] A. Pollmann for the Ice Cube Collaboration, Searches for magnetic monopoles with Ice Cube, EPJ Web Conf. **168**, 04010-1 to -5 (2018).
[28] M. A. Acero et al., Search for slow magnetic monopoles with the NOvA detector on the surface, Phys. Rev. D **103**, 012007-1 to -9 (2021).

[29] J. Boumaaza et al., Search for relativistic magnetic monopoles with ten years of the ANTARES detector data, JINST **16**, C11004-1 to -6 (2021).
[30] R. Abbasi et al., Search for Relativistic Magnetic Monopoles with Eight Years of Ice Cube Data, Phys. Rev. Lett. **128**, 051101-1 to -8 (2022).
[31] A. Albert et al., Search for magnetic monopoles with ten years of the ANTARES neutrino telescope, HEAp **34**, 1-8 (2022).
[32] A. Albert et al., Limits on the nuclearite flux using the ANTARES neutrino telescope, JCAP **01**, 012-1 to -17 (2023).
[33] The ATLAS Collaboration, Search for magnetic monopoles and stable particles with high electric charges in $\sqrt{s}$ = 13 TeV p collisions with the ATLAS detector, J. High Energ. Phys. **2023**, 112-1 to -42 (2023).
[34] B. Cabrera, First Results from a Superconductive Detector for Moving Magnetic Monopoles, Phys. Rev. Lett, **48**, 1378-1381 (1982).
[35] S. A. Chin and A. K. Kerman, Possible Long-Lived Hyperstrange Multiquark Droplets, Phys. Rev. Lett. **43**, 1292-1295 (1979).
[36] E. Farhi and R. Jaffe, Strange matter, Phys. Rev. D **30**, 2379-2390 (1984).
[37] B. Holdom, J. Ren and C. Zhang, Quark Matter May Not Be Strange, Phys. Rev. Lett. **120**, 222001-1 to -6 (2018).
[38] S. Coleman, Q-Balls, Nucl. Phys. B **262**, 263-283 (1985).
[39] A. Kusenko, Solitons in the supersymmetric extensions of the standard model, Phys. Lett. B **405**, 108-113 (1997).
[40] W.-Y. Song and W. Taylor, Pair production of magnetic monopoles and stable high-electric-charge objects in proton-proton and heavy-ion collisions, arXiv:2107.10789v2 [hep-ph]25 Feb 2022 (2022).
[41] C. J. Goebel, Binding of Nuclei to Monopoles, MAD/TH-146, University of Wisconsin-Madison (1983).
[42] L. Bracci and G. Fiorentini, Binding of Magnetic Monopoles and Atomic Nuclei, IFUP-TH 83/1, Instituto Nazionale di Fisica Nucleare, Pisa, Italy (1983).
[43] L. Bracci and G. Fiorentini, Interactions of Magnetic Monopoles with Nuclei and Atoms: Formation of Bound States and Phenomenological Consequences, IFUP-TH 83/2, Instituto Nazionale di Fisica Nucleare, Pisa, Italy, (1983).
[44] J. Makino, M. Maruyama and O. Miyamura, Bound States for a Nucleon in the Field of a Magnetic Monopole, Prog. Theor. Phys. **69**, 1042-1045 (1983).

[45] K. Olaussen et al, Kazama-Yang Monopole-Fermion Bound States (I) Analytic Results, Nuclear Physics B**228**, 567-587 (1983).
[46] K. Olaussen, Form Factor Effects on Magnetic Monopole-Nucleus Binding, CERN-TH.4037/84 (1984).
[47] D. Sivers, Possible Binding of a Magnetic Monopole to a Particle with Electric Charge and a Magnetic Dipole Moment, Phys. Rev. D**2**, 2048-2054 (1970).
[48] J. Schwinger, Magnetic Charge and Quantum Field Theory, Phys. Rev. **144**, 1087-1093 (1966).
[49] T. T. Wu, and C. N. Yang, Dirac Monopole without Strings: Monopole Harmonics, Nucl. Phys. B **107**, 36-380 (1976).
[50] A. S. Goldhaber, Dirac Particle in a Magnetic Field: Symmetries and their breaking by monopole singularities, Phys. Rev. D **16**, 1815-1827 (1977).
[51] Y. Kazama, C. N. Yang, and A. S. Goldhaber, Scattering of a Dirac Particle with Charge Ze by a fixed Magnetic Monopole, Phys, Rev. D **15**, 2287-2299 (1977).
[52] P. H. Cox and A. Yildiz, Bound states with a gauge monopole, Phys Rev. D **18**, 1211-1215 (1978).
[53] Y. M. Shnir, Magnetic Monopoles, Springer-Verlag, Berlin (2005).
[54] D. Zwanziger, Exactly Soluble Nonrelativistic Model of Particles with Both Electric and Magnetic Charges, Phys, Rev. **176**, 1480–1488 (1968).
[55] G. 't Hooft, Magnetic Monopoles in Unified Gauge Theories, Nucl. Phys. B **79**, 276–284 (1974).
[56] R. J. LeVeque, Finite Difference Methods for Ordinary and Partial Differential Equations: Steady-State and Time-Dependent Problems. Philadelphia, PA: Society for Industrial and Applied Mathematics (2007).
[57] G. H. Golub and C. F. Van Loan, Matrix Computations, 4th ed. Baltimore, MD: Johns Hopkins University Press (2013).
[58] B. N. Parlett, The Symmetric Eigenvalue Problem. Philadelphia, PA: Society for Industrial and Applied Mathematics (1998).
[59] E. Anderson et al., LAPACK Users' Guide, 3rd ed., Philadelphia, PA: Society for Industrial and Applied Mathematics (1999).
[60] I. S. Dhillon and B. N. Parlett, B. N., Multiple representations to compute orthogonal eigenvectors of symmetric tridiagonal matrices. Linear Algebra and Its Applications **387**, 1-28 (2004).

HADRONIC JOURNAL 49, 231 – 247 (2026)
DOI 10.29083/HJ.49.02.2026/SC231

ANALYSIS OF A HIGH EFFICIENCY MAGNETIC MOTOR

Patrick Cornille
Retired Physicist from the C.E.A.
7 Rue de la Perdriere
59320 Ennetieres-en-Weppes, France
patrick.cornille@libertysurf.fr

Received May 27, 2026
Revised June 16, 2026

Abstract

This paper explores the feasibility of designing a high efficiency magnetic motor, consisting solely of permanent magnets on both the rotor and the stator. Conventional magnetic motors typically achieve efficiencies below 100% because they operate with a single degree of rotational freedom. In this configuration, we introduce an additional degree of freedom by incorporating two rotating permanent magnets on the stator, forming a special magnetic gate. A physical analysis and numerical simulation demonstrate the potential viability of a high efficiency magnetic motor.

Copyright © 2026 by Hadronic Press, Inc., Palm Harbor, FL 34684, USA

1 INTRODUCTION

There are several ways to design a conventional magnetic motor, and these models are well-documented in the literature available online. The efficiency of these motors rarely exceeds 90%, and in principle, cannot go beyond 100% without becoming a so-called perpetual motion machine. This efficiency limit is a consequence of Lenz's law [1], which states that a current induced in a coil by the motion of a permanent magnet creates a magnetic force that opposes the motion of the magnet. Lenz's law aligns with the principle of conservation of energy, which itself results from Newton's third law, as demonstrated in numerous publications [2-8]. Newton's third law defines a reciprocal (action/reaction) force derived from a time-independent potential energy. As such, a magnetic over-unity motor is deemed impossible under traditional configurations.

In this paper, we examine the physical and mathematical possibility of designing a high efficiency magnetic motor, a controversial topic, as discussed by authors like Gary Vesperman [9] and Rebecca Carité [10], russian author [11] in valuable papers on free energy. An online search reveals over 140 different magnetic motor configurations [12], often without adequate measurements or coherent explanations to verify over-unity performance. Most notably, credible numerical modeling is generally absent. However, recent academic interest is emerging, with some universities now conducting simulations of such motors [13-16]. Like conventional magnetic motors, an over-unity magnetic motor utilizes magnetic attraction and repulsion to create rotational motion. Free energy can potentially be extracted by arranging permanent magnets in special configurations as demonstrated in Johnson's motor [17], which utilizes inhomogeneous magnetic fields and holds a US patent.

2 CONFIGURATION OF A MAGNETIC MOTOR

A high efficiency magnetic motor becomes feasible when inhomogeneous magnetic fields are employed. This principle is well-known in physics, as demonstrated by the Stern-Gerlach experiment where a beam of silver atoms passes through an inhomogeneous magnetic field to confirm Sommerfeld's

prediction of spatial quantization.

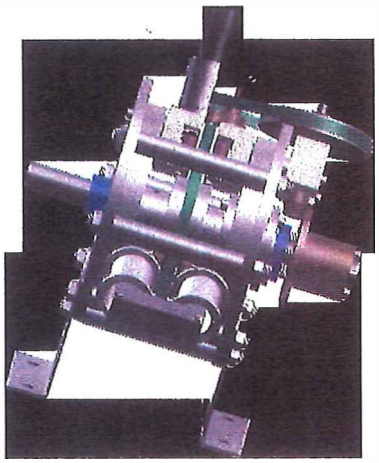

FIGURE 1 – Experimental setup

A basic magnetic motor consists of a permanent magnet on the rotor and an electromagnet on the stator. When powered by AC, the electromagnet generates a magnetic field that interacts with the permanent magnet to produce torque. Conversely, if the rotor is rotated, it induces AC in the electromagnet, allowing the system to function as both a motor and a generator. In the present design, only the motor function is considered, as the configuration uses only permanent magnets on both rotor and stator. The interaction between these magnet's attractive and repulsive forces is utilized to produce rotational motion. The rotor is made of fiberglass and shaped like a disk, with uniformly distributed disc-shaped permanent magnets embedded around its edge. These magnet's magnetic fields are oriented perpendicularly to the plane of the disk, with the same direction on each face. The stator comprises four structures spaced 90° apart, each housing two cylindrical permanent magnets with radially oriented magnetic fields. These magnets rotate freely and face each other with a gap sufficient for the rotor to spin. Together, they form a magnetic funnel that generates inhomogeneous fields. To prevent eddy current braking, the rotor is made from fiberglass. The figure below illustrates the detailed configuration of this high efficiency magnetic motor.

Its operation is simple : all disc-shaped magnets on the rotor have the same orientation. The cylindrical stator magnets are arranged attractively

at a given moment. Synchronized via gears, their magnetic field direction is opposite to that of the rotor magnets for each face, creating an attractive force at the funnel's entry and a repulsive force at the exit. This ensures continuous torque in one direction. For optimal performance, the circumference of the cylindrical magnets should match the spacing between successive rotor magnets. Importantly, magnetic interaction forces obey Newton's third law and could slow the stator magnets. Therefore, the cylindrical magnet rotating in the same direction as the rotor is coupled to the rotor shaft via a speed-reduction gear, set by a number p defined hereafter to increase the power of the rotor. The motor is started with a reversible magnetic motor acting as a generator once the permanent magnet motor reaches cruising speed.

3 NUMERICAL SIMULATION

3.1 Mathematical formulation of the operating principle

It is well established that perpetual motion in a closed inertial system is impossible. This can be shown mathematically using the equation of motion for an object of mass m under gravitational force $\mathbf{F}$.

$$\frac{d\mathbf{P}}{dt} = \mathbf{F} \tag{1}$$

with the definition $\mathbf{P} = m\mathbf{U}$. Assuming that the force $\mathbf{F} = -\nabla E_P$ derives from a potential energy function, then the kinetic energy function has for expression :

$$m\frac{d\mathbf{U}}{dt} \cdot \mathbf{U} = -\mathbf{U} \cdot \nabla E_P = \mathbf{U} \cdot \mathbf{F} \tag{2}$$

The above equation can be rewritten in the form :

$$\frac{d}{dt}\left(\frac{1}{2}m\mathbf{U}^2 + E_P\right) = \frac{\partial E_P}{\partial t} \tag{3}$$

Since gravitational potential energy is time-independent, the right-hand term vanishes, confirming total energy conservation :

$$E_T = \frac{1}{2}m\mathbf{U}^2 + E_P = \mathrm{Ct} \tag{4}$$

Thus, conservation of energy holds for closed systems where interaction forces obey Newton's third law and are time-independent. If these conditions are not met, energy conservation can be violated, and gravitationally induced perpetual motion becomes theoretically possible.

Another approach to this problem consists to calculate the work dT done by the force $\mathbf{F}[\mathbf{R}(t), t]$ over displacement $d\mathbf{R}$ by taking the scalar product of force and displacement. Integrating this along the path gives the kinetic energy variation :

$$E_K[\mathbf{R}(t), t] - E_K[\mathbf{R}(t_0), t_0] = \int_{\mathbf{R}(t_\bullet)}^{\mathbf{R}(t)} \mathbf{F}[\mathbf{R}'(t), t] \cdot d\mathbf{R}' \tag{5}$$

Substituting $d\mathbf{R}' = \mathbf{U}[\mathbf{R}'(t), t]dt'$ yields :

$$E_K[\mathbf{R}(t), t] - E_K[\mathbf{R}(t_0), t_0] = \int_{t_0}^{t} \mathbf{F} \cdot \mathbf{U} dt' \tag{6}$$

which leads again to :

$$\frac{dE_K}{dt} = \mathbf{U} \cdot \mathbf{F} \tag{7}$$

Using classical kinetic energy $E_K = m\mathbf{U}^2/2$, we recover equation 1. This concept shows why perpetual inertial motion is impossible when the force comes from a time-independent potential $E_P[\mathbf{R}(t)]$ because the integral becomes zero over a closed path, indicating no net energy gain since the relation 5 becomes :

$$E_K[\mathbf{R}(t)] - E_K[\mathbf{R}(t_0)] = -\int_{\mathbf{R}(t_0)}^{\mathbf{R}(t)} \nabla E_P[\mathbf{R}'(t)] \cdot d\mathbf{R}' \tag{8}$$

3.2 Numerical simulation of the Operating Principle

An adequate numerical simulation of the behavior of this motor would require the use of high-performance three-dimensional magnetic simulation software. However, an approximate numerical simulation is sufficient to accurately capture the operational dynamics of this motor. To avoid errors in the simulation, it is important to define a convention for measuring angles and rotations, taken counterclockwise with respect to the vector $\mathbf{n}$, as shown in Figure 2.

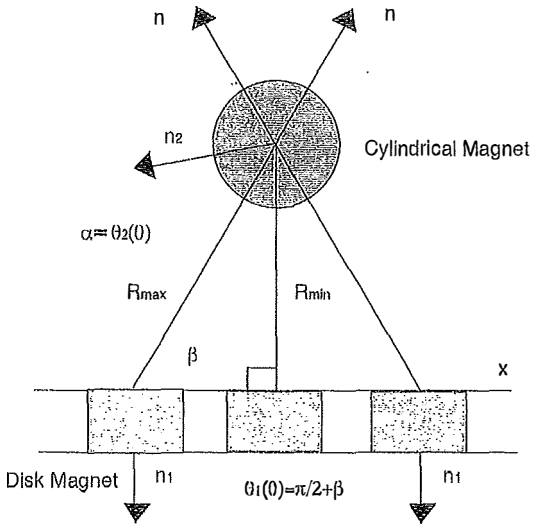

FIGURE 2 – Numerical Simulation

This direction of rotation is identical for the three rotational frequencies, namely : the rotor angular velocity ω, the rotation $n\omega$ of the rotor magnets passing through the magnetic gate (where n is the number of magnets embedded in the rotor), and finally the rotational frequency of the cylindrical magnets $n\rho\omega$, which is a priori independent. In order to synchronize all these frequencies, the cylindrical magnets are mechanically coupled to the rotor shaft using a transmission belt connected to a speed reducer, as illustrated in Figure 1.

A conventional electric motor is used to initiate the rotation of the rotor. Subsequently, this conventional motor operates as a generator if the magnetic motor is reversible. It is important to note that the frequency of variation of the angle θ_1 is half that of the n rotor magnets passing through the magnetic gate. Furthermore, at the initial instant, an angle β is defined between the x-axis and the vector $\mathbf{n}$, and an angle α between the magnetic dipole of the cylindrical magnet and the direction $\mathbf{n}$.

The permanent magnets on the rotor and the stator can be modeled as magnetic dipoles, all positioned in the same plane, as shown in Figure 2. For each dipole with magnetic moment $\mathbf{M}_1$ and $\mathbf{M}_2$, two identical mutual potential energies can be defined on either side of the disk according to the

formulation :

$$E_P(\mathbf{R}) = \frac{\mu_0}{4\pi R^3}\left[\mathbf{M}_1 \cdot \mathbf{M}_2 - \frac{3}{R^2}(\mathbf{M}_1 \cdot \mathbf{R})(\mathbf{M}_2 \cdot \mathbf{R})\right] \tag{9}$$

It is evident that the law of conservation of energy, defined by equation (4), applies to the above formulation. Now consider moving permanent dipoles where the dipole with magnetic moment $\mathbf{M}_2$ associated with the cylindrical magnet interact with the disk-shaped magnet with magnetic moment $\mathbf{M}_1$ where both magnetic moments now depend on time in this configuration then the magnetic potential energy explicitly depends on time [18, p.132] :

$$E_P[\mathbf{R}(t), t] = \frac{\mu_0}{4\pi R^3}\left[\mathbf{M}_1(t) \cdot \mathbf{M}_2(t) - \frac{3}{R^2}[\mathbf{M}_1(t) \cdot \mathbf{R}(t)][\mathbf{M}_2(t) \cdot \mathbf{R}(t)]\right] \tag{10}$$

with the new definition $\mathbf{R}(t) = \mathbf{R}(t)\mathbf{n}(t)$. In this scenario, the conservation of energy is violated as described by equation 3 unless the partial time derivative of the potential energy is zero. This violation is done in a parametric manner as we shall see.

Let us now define the quantities for a disc-shaped magnet in orbital motion around of rotational center, we have

$$\mathbf{M}_1(t) = m_1\mathbf{n}_1(t) \quad \text{with} \quad m_1 = \frac{B_1 L_1 S_1}{\mu_0} \tag{11}$$

while for a spinning cylindrical magnet around an axis, we have :

$$\mathbf{M}_2(t) = m_2\mathbf{n}_2(t) \quad \text{with} \quad m_2 = \frac{B_2 L_2 S_2}{\mu_0} \tag{12}$$

The interaction energy between a disc-shaped magnet, thickness L_1, surface S_1, entering the air gap between two cylindrical magnets, length L_2, surface S_2 has for expression :

$$E_P[R(t), t] = \frac{\mu_0 m_1 m_2}{4\pi R^3}\left[\mathbf{n}_1 \cdot \mathbf{n}_2 - 3(\mathbf{n}_1 \cdot \mathbf{n})(\mathbf{n}_2 \cdot \mathbf{n})\right] \tag{13}$$

with the relation :

$$A(t) = \mathbf{n}_1 \cdot \mathbf{n}_2 - 3(\mathbf{n}_1 \cdot \mathbf{n})(\mathbf{n}_2 \cdot \mathbf{n}) = \cos(\theta_1 + \theta_2) - 3\cos(\theta_1)\cos(\theta_2) \tag{14}$$

which can be rewritten in the form :

$$A(t,\alpha) = -[\cos[\theta_1(t) + \theta_2(t,\alpha)] + 3\cos[\theta_1(t) - \theta_2(t,\alpha)]] \cdot 0.5 \qquad (15)$$

thus, the magnetic potential energy, and its partial time derivative for two cylindrical magnets become :

$$E_P[R(t),t] = \frac{\mu_0 m_1 m_2}{2\pi R^3} A(t,\alpha) \quad \Rightarrow \quad P_T(t,\alpha) = \frac{\partial E_P}{\partial t} = \frac{\mu_0 m_1 m_2}{2\pi R^3} \frac{\partial A}{\partial t} \qquad (16)$$

The quantity $R(t)$ has for expression

$$R(t) = R_{\min} + (R_{\max} - R_{\min})[1 + \cos(n * \omega t)] \cdot 0.5 \qquad (17)$$

with the definitions :

$$R_{\min} = R_c + G_{ap} + E_d \cdot 0.5 \qquad R_{\max}^2 \approx R_{\min}^2 + R_r^2 \sin^2(\pi/n) \qquad (18)$$

where R_r and R_c are respectively the radius of the rotor disk, and the cylindrical magnet knowing that E_d is the thickness of the disk magnets on the rotor. The angle functions are defined as :

$$\theta_1(t) = \pi/2 + \beta + (\pi - 2\beta)[1 - \cos(n * \omega t \cdot 0.5)] \cdot 0.5 \qquad (19)$$

$$\theta_2(t,\alpha) = \alpha + \pi[1 - \cos(n * p * \omega t)] \qquad (20)$$

with $\beta = \arcsin(R_{\min}/R_{\max})$

We can now calculate the mutual force between two magnetic dipoles for two cylindrical magnets [18, p130] :

$$\mathbf{F}[\mathbf{R}(t),t] = -\nabla E_P = \frac{6\mu_0 m_1 m_2}{4\pi R^4} [A_1\mathbf{n} + A_2\mathbf{n}_1 + A_3\mathbf{n}_2] \qquad (21)$$

with the definitions :

$$A_1 = \mathbf{n}_1 \cdot \mathbf{n}_2 - 5(\mathbf{n}_1 \cdot \mathbf{n})(\mathbf{n}_2 \cdot \mathbf{n}) \qquad A_2 = \mathbf{n}_2 \cdot \mathbf{n} \qquad A_3 = \mathbf{n}_1 \cdot \mathbf{n} \qquad (22)$$

$$A_1(t,\alpha) = -[3\cos(\theta_1+\theta_2)+5\cos(\theta_1-\theta_2)]\cdot 0.5 \quad A_2(t,\alpha) = \cos\theta_2 \quad A_3(t) = \cos\theta_1 \qquad (23)$$

The rotational velocity of the rotor is given by the relation $\mathbf{U}(t) = \omega r_m \mathbf{n}_3(t)$ where the unit vector $\mathbf{n}_3(t)$ is directed along the axis x, we get :

$$A_1\mathbf{n} \cdot \mathbf{n}_3 + A_2\mathbf{n}_1 \cdot \mathbf{n}_3 + A_3\mathbf{n}_2 \cdot \mathbf{n}_3 \qquad (24)$$

with the definitions

$$\mathbf{n}\cdot\mathbf{n}_3=\cos[\delta(t)] \qquad \mathbf{n}_1\cdot\mathbf{n}_3=0 \qquad \mathbf{n}_2\cdot\mathbf{n}_3=\cos[\theta_2(t,\alpha)-\delta(t)+\pi] \quad (25)$$

knowing that $\delta(t)=\arcsin[R_{\min}/R(t)]$ and $\beta=\delta(0)$.

We can now calculate the kinetic and potential powers

$$P_P(t,\alpha)=\frac{dE_P}{dt}=\frac{\partial E_P}{\partial t}-\mathbf{U}\cdot\mathbf{F} \qquad P_K(t,\alpha)=\frac{dE_K}{dt}=\mathbf{U}\cdot\mathbf{F} \qquad (26)$$

The mean powers have for expression;

$$\langle P_K(t,\alpha)\rangle=1/T\int_0^T \mathbf{U}\cdot\mathbf{F}\,dt\neq 0 \qquad \langle P_T(t,\alpha)\rangle=1/T\int_0^T P_T(t,\alpha)\,dt=0$$
$$\langle P_P(t,\alpha)\rangle=1/T\int_0^T [P_T(t,\alpha)+P_P(t,\alpha)]\,dt=-\langle P_K(t,\alpha)\rangle\neq 0 \qquad (28)$$

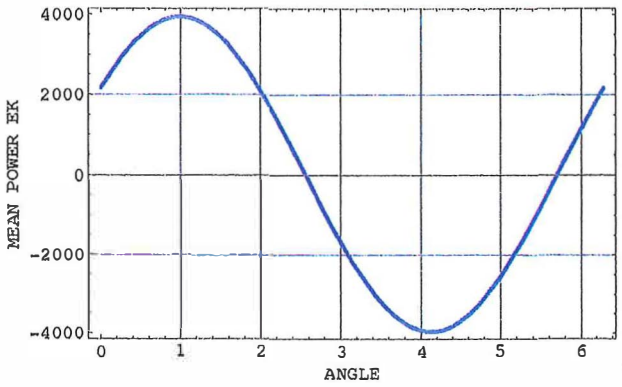

FIGURE 3 – Mean Power versus the initial angle

The numerical simulation of the average kinetic power as a function of the angle α indicates, as shown in Figure 3, that it is maximal and positive for $\alpha=\pi/3$ and $p=1$, corresponding to a rotational frequency of the rotor magnets twice that of the angular frequency associated with θ_1, which is characteristic of a parametric operating mode of the motor.

It is now necessary to demonstrate that the parametric behavior of the motor leads to the generation of kinetic energy independent of the initial

kinetic energy associated with starting the motor, as observed by an external observer. To formalize this analysis, we draw inspiration from the behavior of a harmonic oscillator, whose kinetic and potential energies are expressed as follows :

$$E_K(t) = E_0 \sin^2(\omega t) \quad E_P(t) = E_0 \cos^2(\omega t) \Rightarrow E_K(t) + E_P(t) = E_0 \quad (29)$$

$$P_P(t) = \frac{dE_P}{dt} \qquad P_K(t) = \frac{dE_K}{dt} = -P_P(t) \Rightarrow \langle P_K(t) \rangle = -\langle P_P(t) \rangle = 0 \quad (30)$$

It can be observed that the average kinetic and potential powers of a harmonic oscillator are zero, whereas these same average powers are nonzero in the case of a parametric oscillator. This analysis is sufficient to demonstrate energy generation, which is furthermore stationary since the derivative of the average kinetic power is zero. An estimate of the average power for a single magnetic gate is approximately 3.94 kW for $p = 1$, $\alpha = \pi/3$ and $F = 100\text{Hz}$.

We will now give a simple mathematical proof that the conservation of energy is violated when the potential energy is of the form $E_P[\mathbf{R}(t), t]$, then let assume that we have :

$$E_P[\mathbf{R}(t), t] = E[\mathbf{R}(t)] \cos^2(\omega t) \Rightarrow \frac{\partial E_P}{\partial t} = -2E[\mathbf{R}(t)] \sin(\omega t) \cos(\omega t) \neq 0 \quad (1)$$

which implies

$$\left\langle \frac{\partial E_P}{\partial t} \right\rangle = \frac{1}{T} \int_0^T \frac{\partial E_P}{\partial t} dt = 0 \quad (31)$$

4 THEORETICAL DISCUSSION

The numerical simulation of the magnetic motor showed that its mode of operation is that of a parametric oscillator, which explains the high efficiency nature of this motor. This fact is not new since Russian and French physicists working in leading physics institutes, and laboratories in the 1930's, built overunity parametric oscillators, and some pretty big ones. That work is fully documented in both the Russian [19] and French [20,21] scientific literature. The devices were developed and tested in several physics institutes and laboratories. With linear loads the oscillators would progressively

build to self-destruction. With nonlinear loads, the devices would stabilize and power themselves, and their loads.

Since then, the over-unity character of parametric oscillators has largely been omitted from the scientific literature. This topic is now addressed under the term "parametric amplifier" to avoid discussing a violation of the law of conservation of energy. As evidence, one may cite the review article written by Pierre Collet [22] in 2019, in which the energetic concept of parametric oscillators is not addressed. A familiar experience of parametric oscillation concerns a child playing on a swing. By alternately raising and lowering his center of mass at key points in the swing, a child can quickly reach large amplitudes provided that he has some amplitude to start.

The majority of physicists, fixated on the law of conservation of energy, assert, without experimental proof, that the kinetic energy supplied by the child is transferred into the additional kinetic energy gained by the swing, in order to satisfy this fundamental principle.

In fact, the electrostatic pendulum experiment [23,24,25] conducted by the author in 1997 and 2002 provides an answer to this question, namely that the creation of additional energy in a parametric process is truly observable. Indeed, in reference [26], the kinetic energy of the pendulum is multiplied by 69 in a parametric process when the supply voltage is varied appropriately using a potentiometer. The observer expends a kinetic energy $E_k = 0.5 * m\omega^2 r^2 = 3.6 \times 10^{-7}\,\mathrm{J}$, with $m = 2 \times 10^{-3}\,\mathrm{kg}, f = 1, r = 3 \times 10^{-3}\,\mathrm{m}$, to turn the potentiometer, while the kinetic energy of the pendulum reaches $10^{-2}\,\mathrm{J}$, corresponding to a parametric amplification of 2.77×10^4. Although there is a considerable energy gain, the electrostatic pendulum experiment is not over-unity because, in the energy balance, one must take into account the energy expended to create the plasma. One may also cite a more recent experiment [27] on the electrostatic pendulum. It is important to emphasize that certain criticisms in the references [23,24] have been raised concerning the origin and magnitude of the stimulated force. These criticisms have been refuted in detail in reference [26].

5 DEFINITIONS OF EFFICIENCY AND OVER-UNITY

Let us recall the two different definitions of efficiency :

Classical Thermodynamic Efficiency

In physics, efficiency typically refers to the ratio of useful output energy to input energy in a system. It is expressed as : Efficiency $= 100 \times E_{\text{out}}/E_{\text{in}}$. This definition applies strictly to isolated systems, where the conservation of energy dictates that efficiency cannot exceed 100%. Therefore, the definition of an over-unity motor implies an efficiency higher than 100%, and the fact that the observer does not bring any energy to use the motor.

Coefficient of Performance (COP)

A different metric "COP" is commonly used for systems like heat pumps and refrigerators. It is defined as the ratio of the heating or cooling provided to the surroundings over the electrical energy consumed at the input of the heat pump. We have : COP of heat pump $= 1 +$ COP of the refrigerator. The COP of the refrigerator can be less than one or greater than one. The above formula also shows that the COP of the heat pump can never be less than one.

Importantly, these systems appear to challenge the classical thermodynamic view because they move heat from a lower to a higher temperature reservoir seemingly against the natural thermodynamic gradient that dictates heat flow from hot to cold. Indeed, the function of the refrigerator is to move the heat from the low temperature reservoir to the high temperature reservoir.

Traditional definitions of efficiency apply to systems like engines and boilers, where energy is converted from one form (e.g., chemical, electrical) into another typically mechanical or thermal. In contrast, refrigerators and heat pumps redistribute energy rather than convert it. As such, the COP framework is more appropriate for analyzing non-isolated systems and may also provide insight into potential over-unity systems. To explore this further, we describe one simple experiment that can be reproduced at the university level to convince students that over-unity technologies with COP greater than 1 also exist.

Simple Magnetic Overunity Toy

A system can exhibit a coefficient of performance greater than one. Indeed, this is already a reality for heat pumps, which commonly achieve

COP values greater than 3. Furthermore, we will show that the SMOT experiment challenges the conservation law of energy, as it exhibits behavior inconsistent with this foundational law under conventional assumptions.

Watson's SMOT is a simple device which demonstrates the possibility to get over-unity efficiency. Easily built with readily available square magnets. This device is a permanent magnet propulsion system wherein a steel ball is propelled up an inclined plane between two rows of permanent bar magnets. These magnets being in spaced relationship with all north poles of the first row facing in the same direction and with all south poles in the second row facing in the same but opposite direction to the first row.

Two such arrays are made and fastened to a wooden board so that they form an angle. The two permanent bar magnets generate an inhomogeneous magnetic field $\mathbf{B}$ between the two bar magnets since they are not parallel. Bisecting that angle is an aluminum track on which a steel ball can roll freely. The length of the aluminum track supporting the ball is configured to allow the ball to escape the track where the potential magnetic energy is minimum in order that the ball drop out of the magnetic field.

The steel ball has a magnetic moment $\mathbf{M}$ and a mass m, therefore the potential energy of the interaction between the metallic ball and the magnetic field is $E_B = -\mathbf{M}\cdot\mathbf{B}$. The steel ball is submitted to two conservative forces : the gravitational and the magnetic forces which derive from a potential $\mathbf{F}_i = -\nabla E_B$. If we considered the ball, the magnets and Earth as an isolated system, then we have the following definition of the mechanical energy :

$$E_M = E_K + E_G + E_B = \text{Ct} \Rightarrow \Delta E_M = \Delta E_K + \Delta E_G + \Delta E_B = 0 \quad (32)$$

Knowing that $\Delta E_G = -mgh$ and $\Delta E_B < 0$, the efficiency will be $\Delta E_K/|\Delta E_G + \Delta E_B| = 1$ However, it is more physical to consider the ball and Earth as a closed system $\Delta E_K + \Delta E_G = -\Delta E_B$ with a COP $= \Delta E_K/|\Delta E_G| = 1 + \Delta E_B/\Delta E_G > 1$

In the presence of the magnets, the steel ball will climb on the ramp because the magnets induce in the ball a magnetic moment and an interaction force appeared between the ball and the inhomogeneous magnetic field that does work against the gravitational field. The COP is over-unity for a closed system. Indeed, a COP = 1.14% was measured as demonstrated in [28]. The work done by the magnets is free-energy because the magnetic energy is not consumed since the magnetic force derives from a reversible

potential energy and therefore, the motion can be repeated indefinitely without consuming any energy provided by the magnets that is to say the magnetic energy is not decreased in the process. The SMOT experiment is a fundamental experiment because it proves that an efficiency higher than 100% is possible since at the input we have a small potential energy given by the observer and at the output the observer recover a kinetic energy which is higher than the input potential energy.

6 CONCLUSION

We present in this paper a new configuration of a magnetic motor consisting solely of permanent magnets on both the rotor and the stator, whose mode of operation is that of a parametric oscillator, which justifies the over-unity nature of this motor.

By incorporating a second rotational degree of freedom and exploiting time-varying magnetic fields, we demonstrate a configuration in which the classical conservation of energy can be effectively bypassed. Further experimental validation is required to confirm the practical realization of such a motor.

7 WARNING

(a) 2026, Copyright by the Hadronic Press refers to the publication and not to the intellectual content which remains the author's property.

This document and the concepts, methods, models, analyses, and results contained herein are the intellectual property of the author and are protected under applicable copyright and intellectual property laws. No part of this publication may be reproduced, distributed, modified, transmitted, displayed, published, or used for commercial purposes without the prior written consent of the author.

This publication is intended for scientific, research, and educational purposes only. This document constitutes a public disclosure and prior art of the ideas, concepts, methods, and techniques described herein. No license, express or implied, is granted for any commercial, industrial, proprietary, or patent-related use of the disclosed material. Any unauthorized attempt

to patent, appropriate, or commercially exploit substantially similar subject matter disclosed in this document is expressly opposed by the author.

8 BIBLIOGRAPHY

[1] P. Cornille, Advanced Electromagnetism and Vacuum Physics, World Scientific, 21, New Jersey, ISBN 981-238-367-0, (2003)

[2] P. Cornille, Review of the application of Newton's third law in physics, Progress in Energy and Combustion Science, Vol. 25, N°2, p.161, (1999)

[3] P. Cornille, Why Newton's third principle is the most important principle in physics, p.264, International Conference : Descartes and Scientific Thought 1596-1996 (Eds. U. Bartocci), Perugia, Edizioni Scientifiche Italiane, (1996)

[4] P. Cornille, Why free energy is mathematically and physically possible, Infinite Energy, Vol.4, N°21, p.50, (1998)

[5] P. Cornille, Newton's third principle in Physics, p.300, Physics as a Science (Eds. G. Galeczki, P. Marquardt and J. P. Wesley), Hadronics Press, Inc., Palm Harbor, p.300, (1998)

[6] P. Cornille, Newton's third principle in post-Newtonian physics- part I : Theory, Gal. Electrodynamics, Vol.10, N°3, p.43, (1999)

[7] P. Cornille, Newton's third principle in post-Newtonian physics-part-II : Interpretation and experiment, Gal. Electrodynamics, Vol.11, N°4, p.69, (2000)

[8] M.J. Pinhero, On Newton's Third Law, New Journal of Phys., January 26, (2009)

[9] Gary Vesperman, Energy Invention Suppression Cases, September 3, (2007) `https://www.inventcf.com/resources/Energy%20Supression%20Cases`

[10] Rebecca Carité, L'impossible émergence de l'énergie libre au sein du système scientifique et capitaliste actuel, Université d'Auvergne, Ecole de droit et de Science Politique, Clermont-Ferrand, France, Septembre, (2016)

[11] Anonymous russian author, The wrong future we live in, missing free energy, search google

[12] MarioGudec, Free energy, List of overunity magnetic motors, `https://www.youtube.com/playlist?list=PL1krkwuF7cSVF9HhmunwZr9gjjT1sGvqhW`

[13] Neo Teng Yi, Investigation on the free energy magnet motors, Faculty of Engineering and Science Universiti, Tunku Abdul Rahman, `http:`

//eprints.utar.edu.my/150/1/MH-2011-0705513-1.pdf, May (2011)

[14] J. Rodríguez, F. A. Díaz, Universidad, Study and analysis of the interaction of magnetic fields to generate unconventional mechanical movements, Tekhné, Vol.14, N°1, p.43, June (2017)

[15] A. H. Ali, A. N. Che Ismail, Design and Simulation of Self-Running Magnetic Motor, Universiti Kuala Lumpur, British Malaysian Institute, Conference Paper, December, (2017)

[16] Arghirescu Marius, "Free Energy" Devices versus "Perpetuum Mobile" Devices- what is the difference?, International Journal of Innovative Studies in Sciences and Engineering Technology, ISSN 2455-4863, www.ijisset.org, Vol.5, N°8, p.33, (2019)

[17] H. R. Johnson, Permanent Magnet Motor, US Patent #: 4,151,431, April 24, http://www.rexresearch.com/johnson/1johnson.htm#scimech, (1979)

[18] Hubert Lumbroso, Problèmes résolus d'électromagnétisme, deuxième édition, MacGraw-Hill, (1986)

[19] L. Mandelstam, N. Papalexi, A. Andronov, S. Chaikin, and A. Witt, Report on recent research on nonlinear oscillations, Tech. Phys. USSR, Leningrad, Vol.2, pp.81-134, (1935) Original title : Expose des recherches récentes les oscillations non linéaires. Original English Translation : Techtran Corporation, NASA TT F-12,678 (59 pages), November, (1969)

[20] A. Andronov, The limiting cycles of Poincare and the theory of self-maintained oscillations, Comptes-Rendus, Vol.189, p.559, (1929)

[21] A. Witt, On the mathematical theory of self-excitations, Comptes-Rendus, Vol.190, p.256, (1930). On the mathematical theory of self-excitation systems with two degrees of freedom, Zhurnal Tekhnicheskoii Fiziki,4(1), (1934)

[22] P. Collet, A short historical account of period doublings in the prerenormalization era, Comptes Rendus. Mécanique, 347, pp.287-293, (2019)

[23] J. L. Naudin, http://jnaudin.online.fr/elecpexp/elecpexp.html, (1997)

[24] J. L. Naudin, http://jnaudin.free.fr/pcnpend/html/pcespend.htm, (2002)

[25] P. Cornille, Advanced Electromagnetism and Vacuum Physics, World Scientific, 21, New Jersey, ISBN 981-238-367-0, (2003)

[26] P. Cornille, A Review on Electromagnetic Propulsion by Stimulated Forces. Journal Aeronaut Aerospace Eng. :221. doi :10.35248/2168-

9792.20.9.220, ISSN : 2168-9792, https://www.longdom.aerospace-engineering/inpress.html, (2020)

[27] Karl D. Stephan, José M. Hernandez Guerrero, Self-excited electrostatic pendulum showing electrohydrodynamic-force-induced oscillation, J. Appl. Phys., 122, 243302, https://doi.org/10.1063/1.5003010, (2017)

[28] J.L. Naudin, A free energy demonstrator, The SMOT from Greg Watson, (1999) http://jnaudin.free.fr/html/smotidx.htm

ISSN: 0162-5519

Established in 1978 by Prof. R. M. Santilli at Harvard University Hadronic Journal and Algebras, Groups and Geometries have been regularly published since 1978 without publication charges and are among the few remaining independent refereed journals.

This Journal publishes advances research papers and Ph. D. theses in any field of mathematics without publication charges.

For subscription, format and any other information please visit the website http://www.hadronicpress.com

HADRONIC PRESS INC.
35246 U. S. 19 North Suite 215
Palm Harbor, FL 34684, U.S.A.
http://www.hadronicpress.com
Email: info@hadronicpress.com
Phone: +1-727-946-0427

HADRONIC JOURNAL Volume 49, Number 2, June 2026

H/P HADRONIC PRESS, INC.